Study of the Usefulness of Transcriptomics in Research and Development of Drugs

（医薬品の研究開発におけるトランスクリプトーム解析の有用性に関する研究）

Kotaro TAMURA

田村　幸太朗

TABLE OF CONTENTS

General Introduction

Continuous investment in biomedical research led to the completion of the human genome draft sequencing in 2001 (Baltimore, 2001; Venter *et al*., 2001), thereby offering prospects of the arrival of a new age in disease prevention and treatment. However, to date, not much development has been made. On the contrary, productivity of new medical products has continued to decline, causing an urgent issue that confronts nations and pharmaceutical industries. Along with the human genome sequencing study, analytical technologies of gene expression have dramatically advanced. Use of technologies such as microarray allows us to simultaneously determine expression levels of tens of thousands genes. Analysis of the whole transcripts (transcriptome analysis) using technologies including microarray is applied to various stage of drug development, offering prospects of improvement in research and development (R&D) productivity of medical products. However, the achievement has not yet emerged. Currently, improvement of productivity in the medical product R&D has been the focus of research. Here, I would like to mention the general process of medical product R&D, issues and their solutions in pharmaceutical industries (reduced productivity in new medical product R&D), and current utilization of transcriptome analysis in medical product R&D. This is followed by a description of the objectives and positioning of the present study.

General process of medical product R&D

In this paragraph, I would like to explain the general process of medical product R&D in four stages: target search, screening of candidate compounds, non-clinical trial, and clinical trial (Fig. GI-1). In the target search stage, target molecules of a novel drug are discovered through various analyses, such as genome and proteome analysis. In the compound screening stage, compounds with the desired physiological activity are obtained from a compound library using techniques such as high-throughput screening. Then, the screened compounds are modified to improve

their efficacy, selectivity, safety, and pharmacokinetic properties. Next, promising compounds are subjected to non-clinical trial in which pharmacological studies on drug efficacy, pharmacokinetic studies, safety pharmacological studies, and toxicological studies are conducted using experimental animals and cultured cells. Propriety to proceed to clinical trial is judged from the standpoint of mainly efficacy and safety. In the clinical trial stage, safety including adverse reactions is first examined in Phase I study using a small number of healthy subjects, followed by Phase II study in which effective and safe dose and other factors, such as administration route, are determined using a small number of patients. In Phase III study, the efficacy and safety of the new drug are confirmed in comparison with existing drugs in "double-blind test" etc. using a large number of patients.

Issues of pharmaceutical industry (decline of productivity in new medical product R&D)

Conventionally, the pharmaceutical industry uses a strategy in which a large amount of money is invested in several compounds to raise them to blockbusters through large-scale promotion. However, productivity in R&D of new medical products has rapidly declined due to a shift of the target of R&D from diseases that are rather general and easy to treat to diseases that are complicated or rare. Genome-based drug discovery utilizing the achievement of the human genome sequencing began being used in medical product R&D. In addition, new technologies such as combinatorial chemistry, a technique to synthesize a large number of compound libraries at a time, and high-throughput screening, a technology to screen compounds with activity on target molecules out of a huge compound library using an automated robotic system, etc., also started being adopted in the development. However, the low productivity of medical product R&D has not improved. The new molecular entities and biological license application approved by Food and Drug Administration (FDA)

have declined since the peak of 56 approvals in 1996 to record the lowest 18 cases in 2007 followed by almost steady numbers in 2010 (Mullard, 2011) (Fig. GI-2). The average cost per novel approved compound increased from 2.2 to 4.9 billion USD in 2001–2010 (PricewaterhouseCoopers, 2012). Failure of drug development in and after non-clinical trial raises the cost required for the medical product development. A report stated that 44% of hampered drug development in non-clinical studies was because of toxicities of the drugs (Suter *et al*., 2004). However, as the phase of clinical trial proceeds, problem in efficacy that drug efficacy confirmed in disease model animals is not reproduced in humans becomes leading cause of attrition (52% and 72% in Phases II and III trials, respectively) (Suter *et al*, 2004). A 10% improvement in predicting failures before clinical trials is reported to save 100 million USD cost per drug required for development (U.S Department of Health and Human Services, FDA, 2003).

Solutions for reduced productivity in medical product R&D

It is widely recognized that a significant change in medical product R&D are required to improve its reduced productivity. In March 2004, FDA addressed an action plan named Critical Path Initiative (U.S. Department of Health and Human Services, FDA, 2004). In FDA's view, the applied sciences used in the process of medical product development have not kept pace with the recent tremendous advances in basic sciences, contributing to the reduced productivity. In March 2006, FDA issued the Critical Path Opportunities List (U.S. Department of Health and Human Services, FDA, 2006). This list includes 76 specific items that would improve efficiency, predictability, and productivity of novel medical product development if conducted. These items are roughly summarized in the six following topics: 1. Better evaluation tools, 2. Streaming clinical trials, 3. Harnessing bioinformatics, 4. Moving manufacturing into the 21th century, 5. Developing products to address urgent public health needs, and 6.

Specific at-risk population—Pediatrics. The FDA has been widely asking external opinions, which has resulted in specification of Better evaluation tools (Developing New Biomarkers and Disease Models to Improve Clinical Trials and Medical Therapy) as a most important topic for improving the medical product development. Novel biomarkers which sensitively predict safety help us to understand safety issue of new drug before clinical trials or placing them on market. Moreover, new biomarkers for drug efficacy facilitate the development of a new type of clinical trial, allowing us to obtain better efficacy data more promptly than we do currently. In addition, use of disease model animals accurately reflecting the human diseases in evaluation of drug efficacy is expected to improve extrapolation of drug efficacy to humans.

For reduced productivity in medical product R&D, in addition to the technical solutions shown by FDA in Critical Path Initiative, an approach called Drug Repositioning, which aims at the efficient use of existing resources, is also an effective solution. Several pharmaceutical industries have begun to discover new effectiveness of existing drugs for novel indications (so-called 'drug repositioning') (Chong and Sullivan, 2007). To develop an existing drug for a new indication, Phase II trial normally requiring 2 years and 17 million USD (DiMasi *et al*., 2003) can be conducted in a simplified form and shorter period because the safety and pharmacokinetics in humans were already studied. In addition, majority of the toxicity and metabolism studies required by regulatory agencies for the medical product development can be omitted, allowing us to reduce 40% of overall cost (DiMasi *et al*., 2003). Based on this approach, at least 17 existing drugs are subjected to clinical trials and animal experiments for new usages as of 2007 (Chong and Sullivan, 2007). This Drug Repositioning approach targets not only medical products currently on market but also the products that were previously on market but withdrawn due to adverse reactions and also compounds that were confirmed to be safe in clinical trials but showed insufficient pharmacological activity. The successful examples include the cases of

Viagra that was developed as an antihypertensive but placed on market as a drug for erectile dysfunction, and thalidomide that withdrew from market due to the its teratogenicity but was later approved as a drug for Hansen's disease and multiple myeloma (Ashburn and Thor, 2004).

Transcriptomic technologies in medical product R&D

One of the most important matters in medical product R&D is selection of target molecules for the disease that the drug is developed against. Transcriptome analysis such as microarray and serial analysis of gene expression (SAGE) that was developed along with the human genome project have transformed techniques for searching novel drug target molecules (Ruan *et al*., 2004). Technologies for comprehensive mRNA expression analysis, such as a chip spotted with high density short DNA oligonucleotides capable of identifying individual genes (GeneChip®, Affymetrix) and a cDNA array spotted with high density PCR fragments of cDNA clones, were developed and began being used one after another for searching targets of medical product R&D since mid-1990s. Based on the hypothesis "differentially expressed genes between sick and normal conditions can be the targets of drug development," such novel genes have been discovered by comparison of diseased organs between patients and normal subjects, and by chronological comparison in disease model animals. Adiponectin, currently gaining attention as a target molecule of metabolic syndrome, was discovered by transcriptome analysis (Maeda *et al*., 1996).

In recent years, transcriptomic technologies including microarray have been applied not only to the search for target molecules, but also to various stages of medical product R&D. For example, in prediction of compound toxicity, toxicogenomics is introduced in the non-clinical stage. Toxicogenomics is a new field of science, which combines toxicology with transcriptomics. Toxicogenomics elucidates the mechanism of toxicity and predicts toxicity through transcriptome

analysis. In Japan, a large scale and good quality toxicogenomics database (TG-GATEs) was constructed and published by a collaborative project (Toxicogenomics Project, TGP, http://toxico.bibio.go.jp/) by the National Institute of Health Sciences, the National Institute of Biomedical Innovation, and 15 pharmaceutical companies. This database collected toxicity information and transcriptomic data obtained from rat liver and kidney, and rat and human hepatocytes treated with 150 compounds, mainly medicinal compounds (43 compounds for rat kidney) (Urushidani and Nagao, 2005). Effective utilization of this database is expected to enable early exclusion of compounds with potential toxicity from development candidates. In addition, in the development of new biomarkers, the most important issue taken up by Critical Path Opportunities List (U.S. Department of Health and Human Services, FDA, 2006), Omics technologies including transcriptomic technologies have become essential in searching for the markers. Kidney injury molecule-1 (Kim-1) gaining attention as a novel nephrotoxicity marker in recent years was discovered by transcriptome analysis (Ichimura *et al*., 1998).

Objectives of the present study

As mentioned above, in recent years, transcriptome analysis is used in various stages of medical product R&D. However, its achievement has not emerged in the productivity of the R&D. Transcriptome analysis has higher throughput of data acquisition than other comprehensive studies such as proteomics and metabolomics. For example, while using GeneChip® by Affymetrix, we can obtain expression data of tens of thousands genes per sample for 50 samples in one week. In addition, as indicated by the current presence of over 70 transcriptomic databases (Fernandex-Suarez and Galperin, 2013), transcriptomic data are suitable for database compilation. Successful and sufficient utilization of the potential of transcriptome analysis is expected to significantly improve productivity in medical product R&D. In

addition, I consider that there is much room for technical improvement to transcriptome analysis of kidney since in this organ the physiological functions, including gene expression, differ between the anatomical regions (papilla, medulla, and cortex). Under such circumstance, I studied techniques and usage of transcriptome analysis for improving the productivity of medical product R&D aiming to develop drugs for kidney diseases.

In chapter 1, I analyzed transcriptomic data of rat liver (*vivo*) and rat primary hepatocytes (*vitro*) treated with peroxisome proliferator-activated receptor α (PPARα) agonist using the toxicogenomics database (TG-GATEs). PPARα agonist, an antihyperlipidemic drug, has been recently reported to possess kidney-protecting activity and to potentially become a drug for chronic kidney disease (Kamijo *et al*., 2007a; Kamijo *et al*., 2007b; Kamijo *et al*., 2002; Kono *et al*., 2009). I clarified common points and differences between the gene expression profiles of *in vivo* and *in vitro* treated with PPARα agonists, and demonstrated how to extract PPARα agonist-like compounds from the database. In chapter 2, as a basis of transcriptome analysis of kidneys, I compared gene expression profiles in papilla, medulla, cortex of kidneys, and a whole slice containing all of the three regions to clarify the characteristics of gene expression profiles of each region. Through this analysis, I also clarified problems and solutions in comparative analysis among the regions. In chapter 3, I evaluated progress of nephrotic syndrome in ICR-derived glomerulonephritis (ICGN) mice, a model animal of the disease, with clinical chemistry, urinary and histopathological examination and histochemical quantification of collagen throughout their lifetime before transcriptome analysis of these mice (chapter 4). Additonally, I histologically evaluated changes in the cell-surface carbohydrate structures using 24 types of lectins. In chapter 4, I attempted to search for causative genes and diagnostic biomarkers for nephrotic syndrome in ICGN mice through transcriptome analysis.

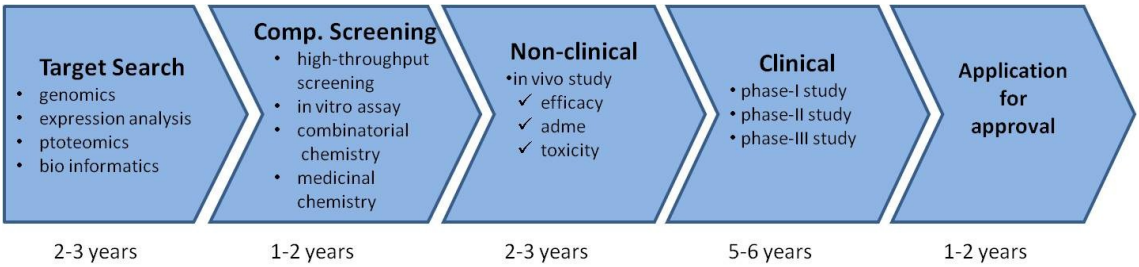

Fig. GI-1.

General process of medical product R&D. Comp: compound, adme: absorption, distribution, metabolism and excretion

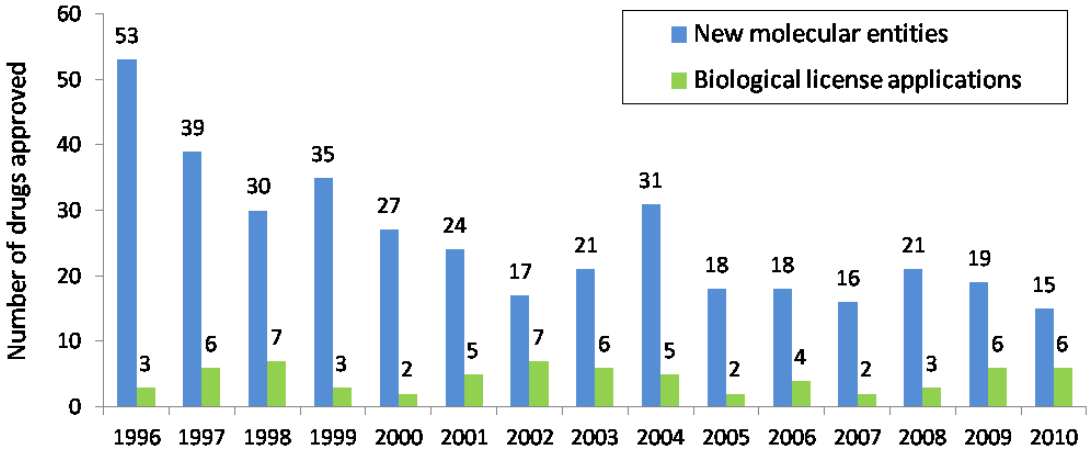

Fig. GI-2.

FDA drug approvals since 1996. New molecular entities and biologics license application approved by US Food and Drug Administration's (FDA's) Center for Drug Evaluation and Research, by year.

Source: Mullard, 2011

Chapter 1

Profiling of Gene Expression in Rat Liver and Rat Primary Cultured Hepatocytes Treated with Peroxisome Proliferators

Abstract

The Toxicogenomics project in Japan constructed a large-scale database of about 150 compounds exposed to rat (single dose, 3, 6, 9, 24 hrs and repeated dose for 3, 7, 14 28 days with 3 dose levels) and rat hepatocytes (2, 8, 24 hrs with 3 concentrations) and data of transcriptome in liver using GeneChip, and the related toxicological measures are accumulated. In the present study, I analyzed the data of three ligands of peroxisome proliferator activated receptor α (PPARα), i.e., clofibrate, WY-14643 and gemfibrozil in our database. Many of the β-oxidation-related genes were commonly induced *in vivo* and *in vitro*, whereas expression changes in genes related to cell proliferation, apoptosis, were detected *in vivo* (single and repeated dose) but not *in vitro*. Changes in those related to the immune response, coagulation and the stress response were also detectable exclusively *in vivo*. Using the genes mobilized in two or three PPARα agonists, hierarchical clustering was performed on 32 compounds stored in our database. In the profiling of an *in vivo* single dose, benzbromarone and aspirin were located in the same cluster of the three PPARα agonists. The clustering of *in vitro* data revealed that benzbromarone, three NSAIDs (aspirin, indomethacin and diclofenac sodium) and valproic acid belonged to the same cluster of PPARα agonists, supporting the reports that benzbromarone, valproic acid and some NSAIDs were reported to be PPARα agonists. Using the genes commonly up-regulated both *in vivo* and *in vitro*, principal component analysis was performed in 32 compounds, and principal component 1 was found to be the convenient parameter to extract PPARα agonist-like compounds from the database.

PPARα agonist has been recently reported to possess kidney-protecting activity. Therefore, the compounds which were indicated to be PPARα agonist in the present transcriptome analysis potentially become a drug for chronic kidney disease as well as known PPARα agonists become it.

Introduction

The Toxicogenomics Project is a 5-year collaborative project by the National Institute of Health Sciences (NIHS) and 17 pharmaceutical companies in Japan which started in 2002 (Urushidani and Nagao, 2005). In April 2005, some rearrangements were made and then the project was conducted by NIHS, the National Institute of Biomedical Innovation, and 15 pharmaceutical companies. Its aim was to construct a large-scale toxicology database of transcriptome for prediction of toxicity of new chemical entities in the early stage of drug development. I participated in this project and was engaged mainly in transcriptome data synthesis and its quality control. About 150 chemicals, mainly medicinal compounds, were selected, and the following were examined for each. The *in vivo* test using rat consists of a single administration test (3, 6, 9 and 24 h with 4 dose levels including vehicle control) as well as a repeated administration test (3, 7, 14 and 28 days with 4 dose levels including vehicle control) and the data of body weight, general symptoms, histopathological examination of liver and kidney, and blood biochemistry are obtained from each animal. The gene expression in liver (kidney in some cases) is comprehensively analyzed using Affymetrix GeneChip. An *in vitro* test using rat and human hepatocytes is also carried out to accomplish the bridging between the species. By the time the present study was performed, the whole data set of 32 compounds had been stored in the database ready for analysis. I started the analysis with three fibric acids in the database, i.e., clofibrate, WY-14643 and gemfibrozil (ligands of peroxisome proliferator activated receptor α, PPARα). They had been extensively studied regarding their mechanism of toxicity and had been reported to possess kidney-protecting activity (Kamijo *et al*., 2002). Therefore, I considered them excellent model cases for evaluating the quality of our database and for the theme of my study.

Materials and Methods

Compounds

All compounds were of the highest grade obtainable from the suppliers listed in Table 1-1.

In vivo studies

Male Sprague-Dawley rats were purchased from Charles River Japan Inc., (Kanagawa, Japan) at 5-weeks of age. After a 7-day quarantine and acclimatization period, the animals were divided into groups of 5 animals using a computerized stratified random grouping method based on body weight for each age. The animals were individually housed in stainless-steel cages on a 12 hr light/dark cycle. Each animal was allowed free access to water and pellet food (CRF-1, sterilized by radiation, Oriental Yeast Co., Japan). The test compounds were suspended in 0.5 % methylcellulose solution or corn oil. Animals were orally administered daily at three dose levels for 1, 3, 7, 14 and 28 days. The highest dose level for each was determined in a 1-week dose finding study (data not shown), and 1/3 and 1/10 of that were set as middle and low doses, respectively. The dose levels are given in Table 1-1.

Blood samples were taken at 3, 6, 9, and 24 hr after single dosing and 24 hr after repeated dosing with a needle and a heparinized syringe from the abdominal artery of animals under ether anesthesia. Plasma biochemical assessments were conducted by using COBAS MIRA plus autoanalyzer (Roche Diagnostics, Basel, SZ). After collecting the blood, the animals were euthanized by exsanguination from the abdominal veins and arteries under ether anesthesia. Livers were collected from each animal and weighed, and then a portion (about 30 mg) of each left lateral lobe was put into RNAlater® (Ambion, Austin, TX, USA) for expression profiling. The remaining liver samples were fixed in 10% buffered formalin solution for routine histological

processing. Paraffin sections were stained with hematoxylin and eosin for histopathological examination. The experimental protocols were reviewed and approved by the Ethics Review Committee for Animal Experimentation of the National Institute of Health Sciences.

In vitro studies

Hepatocytes were isolated from 6-week-old male Sprague-Dawley rats under sodium pentobarbital (120 mg/kg, ip) by a modified two-step collagenase perfusion method. The liver was perfused via the portal vein for 10 min with divalent cation-free EGTA (0.5 mM)-supplemented HEPES buffered Hank's balanced salt solution followed by a 10-min perfusion with HEPES-buffered normal Hank's balanced salt solution containing soybean trypsin inhibitor (Sigma, T-2011, 0.05 g/L) and collagenase (WAKO 034-10533, 0.5 g/L) at a flow rate of 10 - 30 ml/min. Isolated cells were washed three times by 50 g for 1min to obtain a parenchymal cell-enriched pellet. Hepatocytes were not used when their viability assessed by trypan blue exclusion was lower than 70%. The cells were seeded into collagen-coated six-well plates (BD BioCoat® Collagen I Cellware, BD Bioscience) at a density of 1 x 10^6 cells/well in 2 ml HMC Bulletkit medium (CAMBREX) supplemented with 10% fetal bovine serum. Following an attachment period of 3 hr, the medium was replaced and kept overnight before drug exposure at 37˚C in an atmosphere of 5% CO_2. The test compounds were added to the medium directly or as a 1,000 x stock solution in dimethylsulfoxide. The highest concentration of each compound was determined in a pilot test based on cytotoxicity (ca. 20% release of lactate dehydrogenase) and 1/5 and 1/25 of that were set as middle and lowest concentrations (data not shown). After 2, 8 and 24 hr-exposure, the cells were dissolved with RLT buffer (Qiagen) and collected for expression profiling. GeneChip® analysis was performed in a duplicated manner for each time and concentration point.

Expression profiling

The livers were homogenized using Mill Mixer (Qiagen) and zirconium beads. Total RNA was isolated from the liver homogenate or the hepatocyte lysate using RNeasy kit. Purity of the RNA was checked by gel electrophoresis, and the OD260/280 nm ratio was between 2.0-2.2. Microarray analysis was conducted on 3 out of 5 samples for each group by using GeneChip®RAE230A probe arrays (Affymetrix, Santa Clara, CA, USA), containing 15923 probe sets. The procedure was conducted basically according to the manufacturer's instructions using Superscript Choice System (Invitrogen, Carlsbad, CA, USA) and T7-(dT)24-oligonucleotide primer (Affymetrix) for cDNA synthesis, cDNA Cleanup Module (Affymetrix) for purification, and BioArray High yield RNA Transcript Labeling Kit (Enzo Diagnostics, Farmingdale, NY, USA) for synthesis of biotin-labeled cRNA. Twenty μg of the fragmented cRNA was hybridized to a RAE230A probe array for 18 hr at 45˚C at 60 rpm, after which the array was washed and stained by streptavidin-phycoerythrin using Fluidics Station 400 (Affymetrix) and then scanned by Gene Array Scanner (Affymetrix). The data were analyzed by using GeneSpring® version 6.1 (Silicon Genetics, Santa Clara, CA, USA). Expression data were normalized using the mean value (global normalization). Filtering of the data was performed by flags (present or marginal call) in at least half of the samples, as well as the fold change, over the concurrent control value.

Principal components analysis

To test whether profiling on *in vivo* effects of compounds can be estimated from *in vitro* transcriptome data, principal component analysis (PCA) on the data of three time points (24h after *in vivo* single dose, 29d after *in vivo* repeated dose, and 24h after *in vitro* exposure) was independently conducted using the expression of 41 genes which changed to the same direction both *in vitro* and *in vivo* (single or repeated

dose). The method of gene selection is described in the results section.

For calculation, I took the mean signals from three (*in vivo*) or two (*in vitro*) samples from each dose group and calculated the ratio for each respective control, and subsequently the values were transformed to log ratio to create a matrix. Each row corresponds to a different gene, and each column corresponds to a different condition including three different dose groups of 32 compounds. To compute the principal components, the eigenvalues and their corresponding eigenvectors were calculated from the correlation matrix of conditions. The calculations were done using the R version 2.2.0 (www.r-project.org) statistical environment.

Results

Pathology

Toxicological changes observed in repeated administration of three peroxisome proliferators are summarized in Fig. 1-1. All three chemicals showed a significant increase in the relative liver to body weight after 4 days or later of administration (Fig. 1-1A). They also showed a significant decrease in triglyceride after the 4th day of administration, known to be directly related to their activity of PPARα agonist (Fig. 1-1B). Signs of hepatotoxicity and an increase in ALT activity were observed in the 4th day of WY-14643- and the 29th day of gemfibrozil-treated groups (Fig. 1-1C). In pathological examinations, granular degeneration of hepatocytes was noted in all compounds. Furthermore, an increase in hepatocyte proliferation was observed in WY-14643 and gemfibrozil. Treatment with WY-14643 also induced necrosis of hepatocyte and hypertrophy of the bile duct (data not shown).

Analysis of mRNA expression profile

Differentially expressed genes in liver treated with clofibrate, WY-14643 and gemfibrozil were extracted as follows. For *in vivo* study, genes with present call in at least 3 out of 6 samples for each experimental set (3 each from control and treated group) were selected and used for further analysis. In the case of the *in vitro* study, genes with present call in at least 2 out of 4 samples in each experimental set (2 each from control and treated) were selected. Genes showing at least a 1.5 fold increase (or 1/1.5 fold decrease) both in middle and high dose vs. control at $p<0.05$ by Student's t-test were extracted for each time point. In the case of *in vitro* study, the same procedure without use of t-test was employed. In the next step, the common genes selected in at least 2 out of three peroxisome proliferators for single, repeated, and *in vitro* experiments were extracted. The numbers of genes extracted as above were as

follows: the up-regulated genes, 115/195/89 for *in vivo*-single/*in vivo*-repeated/ *in vitro*, respectively; and the down-regulated genes, 181/221/38, for *in vivo*-single/*in vivo*-repeated/ *in vitro*, respectively. The overlapping of these genes is depicted in a Venn diagram in Fig. 1-2.

Comparing the extracted genes between the protocols, 71, 29, and 37 up-regulated genes were in common between the single and repeated administration, between single administration and *in vitro*, and between repeated administration and *in vitro*, respectively. For down-regulated genes, 44 genes were in common between single and repeated administration, whereas no common genes were present between *in vivo* and *in vitro*. These genes are listed in Table 1-2 (up-regulated) and Table 1-3 (down-regulated).

Most of the genes categorized in β-oxidation and fatty acid and cholesterol synthesis, and the peroxisomal protein, were commonly changed both *in vivo* and *in vitro*. In general, genes related to lipid metabolism were commonly up-regulated *in vivo* and *in vitro* except that apolipoprotein A-IV, apolipoprotein M, and lipoprotein-binding protein were down-regulated only *in vivo* (mainly repeated dose). As for genes related to lipid metabolism other than that listed above, most of the up-regulated ones were common between *in vivo* and *in vitro*, whereas the down-regulated ones were only observed *in vivo* (single and repeated dose).

Of the genes related to carbohydrate metabolism, elevation of pyruvate dehydrogenase kinase 4 was observed both *in vivo* (single and repeated dose) and *in vitro*, whereas reduction of "pyruvate kinase liver and RBC" was observed only *in vivo* (mainly repeated dose) and others were increased *in vivo* (single and repeated dose).

The genes classified as cell proliferation were up- or down-regulated only *in vivo* (single and repeated dose). Some genes, including cyclin D1, showed more marked changes in single dose than in repeated dose. The changes of genes categorized in apoptosis were only detectable *in vivo* and their changes were also more prominent

in single dose than in repeated dose.

Obvious changes were noted in the genes related to "drug and xenobiotic metabolism" and most of them occurred exclusively *in vivo* (single and repeated dose). The only observable changes in growth factor-related genes were a reduction of the *in vivo* repeated dose. Changes in the expression of genes related to "cellular morphogenesis" as well as the "stress response" were mainly noted *in vivo* (single and repeated dose). Many other genes categorized to "transcription activation and repression", "transporter", "cell adhesion", "immune response", "blood coagulation", "regulation of blood pressure" were found to be down-regulated *in vivo* without any changes *in vitro*.

Hierarchical cluster analysis

Hierarchical clustering (complete linkage method, Euclidean distance) was performed in the 32 compounds stored in our database (the number at that stage of our analysis) using the data of gene expression *in vivo* or *in vitro* (24 hr after middle and high dose). The probe sets used for analysis of *in vivo* data were 36 (up-regulated) and 35 (down-regulated) which showed a more than 1.5 fold change with $p<0.05$ by Student's t-test both in middle and high dose of more than 2 compounds out of clofibrate, WY-14643 and gemfibrozil. The probe sets used for analysis of *in vitro* data were 49 (up-regulated) and 6 (down-regulated) which showed a more than 1.5 fold change with $p<0.05$ by Student's t-test both in the middle and the high doses of more than 2 out of the three compounds. In clusters of single dose experiments, benzbromarone and aspirin were classified into the same cluster of the three peroxisome proliferators (Fig. 1-3). In clusters of the *in vitro* experiments, benzbromarone, three non-steroidal anti-inflammatory drugs (aspirin, indomethacin, and diclofenac sodium), valproic acid, and ANIT were classified into the same cluster of the three peroxisome proliferators (Fig. 1-4).

PCA based estimation of PPARα activity

As previously shown in Fig. 1-2, no common down-regulated genes existed between *in vivo* and *in vitro*, whereas 41 up-regulated genes were found to be common genes (between *in vivo* and *in vitro*) by PPARα agonist treatment. I expected that these genes could be useful for prediction of *in vivo* effects from *in vitro* effects, so PCA analysis was conducted on the 32 compounds using these 41 genes.

A projection on the first two principal components for each condition, together with the contribution rate of the first three components, is shown in Fig. 1-5. It was obvious from the figure that the first principal component score (PC1) with high contribution (about 60%) for all three experimental sets, was negatively correlated to the dose levels of these PPARα ligands. Therefore, I reasoned that this negative PC1 score could be used to estimate the PPARα activity in general.

Fig. 1-6 shows the plotting of negative PC1 values from the 32 compounds examined *in vivo* and *in vitro*. In this figure, a clearer comparison of putative PPARα activity between the compounds can be performed. All the PPARα agonists showed high scores both *in vivo* and *in vitro*. Benzbromarone, aspirin and valproic acid again showed high scores both *in vivo* and *in vitro*. It was also easy to pick up the compounds that showed high scores *in vitro* rather than *in vivo*, such as diclofenac and indomethacin.

Discussion

In the present study, analysis of gene expression in rat liver was done with three peroxisome proliferators, clofibrate, WY-14643 and gemfibrozil, stored in our database. The changes of gene expression by these compounds observed *in vivo* (single and repeated) were largely in accordance with the report by Kramer *et al*.(2003), in which the effect of clofibrate on the gene expression profile in rat liver was analyzed. Among the genes whose expression was affected, a large number of genes were overlapped between *in vivo* and *in vitro*, both in up- and down-regulated ones. Between *in vivo* and *in vitro* experiments, however, there were many common genes in up-regulated ones but none in down-regulated ones.

A large number of genes related to β-oxidation were up-regulated by a single dose, and similar changes were also noted for *in vitro* experiments. The genes that possess PPRE sequence in their promoter regions, e.g., acyl-CoA oxidase (Tugwood *et al*., 1992), carnitine palmitoyl transferase I(Brandt *et al*., 1998), carnitine palmitoyl transferase II (Barrero *et al*., 2003) and fatty acid desaturase 2 (Tang *et al*., 2003) were found to be up-regulated both *in vivo* and *in vitro*. An exception was that malic enzyme (Castelein *et al*., 1994), whose promoter region contains PPRE, was induced *in vivo* but not *in vitro*. On the other hand, there were many genes whose promoter regions had no PPRE sequence showing common induction for *in vivo* and *in vitro*. For example, CD36, a fatty acid transporter, and CYP4A14, involved in fatty acid hydroxylation, were up-regulated both *in vivo* and *in vitro*, but there has been no report that their promoter regions contain functional PPRE. Apart from their mechanism, the genes that show common changes *in vivo* and *in vitro* (as listed by the present study) are considered to be useful to assess pharmacological and toxicological effects *in vivo* from *in vitro* experiments. This will be discussed later.

There were also data suggesting the limitations of *in vitro* experiments.

Among the genes modulated by administration of fibrates *in vivo*, those related to the functions of proliferation, apoptosis, immune response, transcription activation and repression, transporter, cell adhesion, blood coagulation and regulation of blood pressure, did not show any changes *in vitro*. It is well known that peroxisome proliferators are non-genotoxic carcinogens for rodents and their most convincing mechanism is presently considered to be the activation of proliferation in addition to attenuation of apoptosis (Boitier *et al*., 2003; Michalik *et al*., 2004). In the present study, many of the genes related to proliferation and apoptosis were mobilized by fibrates *in vivo* but not at all *in vitro*. There have been many reports describing the fact that stimulation of proliferation by peroxisome proliferators requires Kupffer cell or TNFα produced by the cell. Rose *et al*. (1997) reported that acceleration of proliferation in rat hepatocytes by WY-14643 was attenuated by the reduction of TNFα via inactivation of Kupffer cells. It was also reported that WY-14643 failed to cause cell proliferation in hepatic parenchymal cells cultured under the condition where non-parenchymal cells had been eliminated, and that its proliferative effect was recovered when Kupffer cells were added to the culture (Parzefall *et al*., 2001). As for the attenuation of apoptosis, it was reported that a high concentration of TNFα inhibited spontaneous TGFβ1-induced apoptosis in primary cultured hepatocytes (Rolfe *et al*., 1997). These reports suggest that Kupffer cell secreting TNF α, IL-1, IL-2 and IL-6 (Decker, 1990) plays an important role in hepatocyte proliferation stimulated by peroxisome proliferators. The present results that the expression changes of genes related to proliferation or apoptosis were rarely observed for the *in vitro* system could be due to the fact that the numbers of non-parenchymal cells (including Kupffer cells) in the culture were much less than that for *in vivo* liver. The present results also support the aforementioned concept that Kupffer cell (or its production of TNFα) is essential for the increase of proliferation and attenuation of apoptosis caused by peroxisome proliferators.

Many genes related to cellular morphogenesis, including extracellular matrix (ECM), were down-regulated exclusively *in vivo*. Ogata *et al*. (2002, 2004) reported that the increase in mRNA of collagen type I and type III in pressure-overloaded rat heart was reduced by the administration of fenofibrate and that the proliferation of cardiac fibroblast induced by endothelin-1 was inhibited by fenofibrate. It was also reported that ETYA, a PPARα agonist, reduced the mRNA contents of elastin, tropoelastin and α-smooth muscle actin in neonatal rat lung fibroblast (McGowan *et al*., 1997). It appears that peroxisome proliferators also act on non-parenchymal cells other than Kupffer cell, and that they reduce the production of ECM in fibroblasts. Stellate cell, a hepatic non-parenchymal cell, possesses both of the characteristics of lipocyte and fibroblast, and its ability to produce ECM was found to be increased in liver fibrosis (Tanaka *et al*., 1991). It is possible that production of ECM in stellate cells could be stimulated by peroxisome proliferators. Based on these ideas, it would be reasonable to conclude that the reduction of expression of genes related to ECM and cytoskeletons by peroxisome proliferators observed *in vivo* were not reproduced in the *in vitro* system, considering that these changes were a reflection of those occurring in non-parenchymal cells in liver. In the present study, relative liver weight was increased by a factor of two in peroxisome proliferators. The expression changes in genes classified to cell adhesion and cellular morphogenesis should have been associated with this obvious hypertrophy of the liver.

In the present study, down-regulation of genes classified to the immune response and coagulation was also *in vivo* specific. PPARα is known to function as an inhibitory factor for inflammation, and PPARα agonists were reported to inhibit the expression of mRNA of fibrinogen, an acute phase protein (Corton *et al*., 1998; Kockx *et al*., 1999), and induction of fibrinogen gene by IL-6 (Gervois *et al*., 2001). Moreover, it was also reported that WY-14643 inhibits induction of IL-6 and cyclooxygenase-2 by IL-1 in human aortic smooth muscle cells through inhibition of the translocation of

NF-κB from the cytosol to the nucleus. It is thus expected that inhibition of the inflammatory response by PPARα agonists not only affects the hepatic parenchymal cell (producing acute phase proteins) but also affects the mechanism relating to non-parenchymal cells (including Kupffer cell) that releases inflammatory cytokines. It would be reasonable to conclude that the reason down-regulation of genes classified to the immune response and coagulation was observed *in vivo* but not *in vitro* was again due to the involvement of non-parenchymal cells. However, it might be due simply to the fact that the basal level of the mRNAs of these genes was down-regulated during our culture condition, since there was a report that PPARα agonist could inhibit the expression of fibrinogen mRNA by IL-6, using human hepatocyte culture (Gervois *et al*., 2001).

As discussed above, the profiling of *in vivo* data represents gene expression in multiple cellular populations, whereas the profiling of *in vitro* data is focused on gene expression of hepatic parenchymal cells. The advantage of the *in vitro* system is that the direct effects of chemicals on hepatic parenchymal cells can be assessed, and in certain cases, the sensitivity and specificity of the test can be improved by eliminating noise due to gene expression of non-parenchymal cells. On the other hand, the *in vitro* system has an apparent disadvantage when indirect toxicity to parenchymal cells via non-parenchymal cells is involved or direct toxicity to non-parenchymal cells is involved.

In hierarchical clustering analysis of the *in vivo* data stored in our database, benzbromarone and aspirin were classified into the same cluster of the three peroxisome proliferators. It has been long known that benzbromarone is a PPARα ligand (Bichet *et al*., 1990). As for aspirin, some NSAIDs including indomethacin, ibuprofen and fenoprofen, were reported to activate PPARα (Lehmann *et al*., 1997), Suggesting that aspirin belongs to PPARα agonists as well. In the hierarchical clustering of the *in vitro* data, two NSAIDs (indomethacin and diclofenac) and valproic

acid were additionally located to the same cluster that included the three fibrates, and benzbromarone and aspirin. It has been reported that valproic acid induced the increase of liver weight and the activation of β-oxidation in rodents, suggesting that the drug has some PPARα agonist-like activity (Horie and Suga, 1985). Although the middle dose of ANIT belonged to the same cluster, its high dose showed a quite different profile. There is no report suggesting a relationship between ANIT and PPARα so far. One possibility is that ANIT is a potential PPARα agonist, and inconsistent results at high concentrations showed that cytotoxicity overwhelmed the inducing effects. At the middle dose of ANIT, various genes related to lipid metabolism (including β-oxidation), e.g., Acaa1, Acaa2, Cpt1a, Cpt1b, Pdk4, Ehhadh, Hmgcs2, Mte1, Cyp4a14, Cyp4b1, Cyp8b1, and Angptl4 were up-regulated more than twice of control *in vitro*. It would be interesting to examine the direct effect of ANIT on PPARα. It should be considered that any expression changes in β-oxidation-related genes do not necessarily mean the direct involvement of PPARα.

The reason why in the vitro system was more sensitive than that of *in vivo* for detecting PPARα agonist-like activity is the high concentration of the drugs *in vitro*. In the standard protocol in our project, the maximal dose of the drugs *in vivo* is set to the level at which the animals can tolerate for 28 days of repeated administration, while that for *in vitro* is independently determined according to the direct cytotoxicity of the cultured hepatocytes. Therefore, in the case of chemicals causing severe toxicity to organs other than the liver, the practical concentration around the hepatocyte becomes much lower *in vivo* than *in vitro*. Since the main lethal cause in the case of NSAIDs is intestinal perforation, the doses employed were relatively low compared with that needed to elicit PPARα activation *in vivo*, and actually, a reduction of plasma lipid was barely observed. The PPARα activity of aspirin could possibly have been detected because its ulcerogenicity to intestine is much lower than that of the other NSAIDs.

One of the aims of the present project is the prediction of *in vivo* effects from

in vitro experiments that have the advantages of saving chemicals, cost, and time. In the case of PPARα agonists, I could not find any common genes in down-regulated ones between *in vivo* and *in vitro*. On the other hand, 41 genes up-regulated *in vitro* were also up-regulated *in vivo*. I considered these as useful markers to predict PPARα activity *in vivo* from *in vitro*, and applied them to PCA. As shown in Fig. 1-5, PC1 appeared to have a PPARα agonist-like attribute, and 32 chemicals were aligned by this parameter in Fig. 1-6. This presentation conveniently identifies potential PPARα agonists both *in vivo* and *in vitro*.

In conclusion, our database efficiently works to classify a certain category of drugs (PPARα agonist in the present case) based on gene expression profiling. For these data, the gene expression profile *in vitro* is useful and sensitive to the direct toxicological and pharmacological effects of the chemicals in hepatic parenchymal cells, whereas indirect toxicities mediated by other cells or secondary toxicity due to pathophysiological changes such as blood pressure or inflammation in other organs might be overlooked. In order to predict *in vivo* effects from the *in vitro* system, it is important to identify genes commonly mobilized *in vivo* and *in vitro*. The scoring system (using the principal component that largely contributes the target effect) in the present study appeared to be quite useful and convenient to identify compounds with target activity among the ones stored in our database. PPARα agonist has been recently reported to possess kidney-protecting activity (Kamijo *et al*., 2007a; Kamijo *et al*., 2007b; Kamijo *et al*., 2002; Kono *et al*., 2009). Therefore, the compounds indicated to be PPARα agonist in the present transcriptome analysis are potentially become a drug for chronic kidney disease as well as known PPARα agonists become it.

Table 1-1.

Compound	Abbreviation	*in vivo*		*in vitro*		Supplier
		Dose (mg/kg)	Vehicle	Concentration (μM)	Vehicle	
acetaminophen	APAP	300, 600, 1000	MC	300, 1000, 3000	Medium	Sigma
allopurinol	APL	15, 50, 150	MC	5.6, 28, 140	DMSO	Sigma
allyl alcohol	AA	3, 10, 30	OIL	4, 20	Medium	Tokyo kasei
alpha-naphthyl-isothiocyanate	ANIT	1.5, 5, 15	OIL	8, 40, 200	DMSO	Kanto chemical
aspirin	ASA	45, 150, 450	MC	120, 600, 3000	DMSO	Wako
benzbromarone	BBr	20, 60, 200	MC	0.6, 3, 15	DMSO	Sigma
bromobenzene	BBZ	30, 100, 300	OIL	8, 40, 200	DMSO	Tokyo kasei
carbamazepine	CBZ	30, 100, 300	MC	12, 60, 300	DMSO	Sigma
carbon tetrachloride	CCL4	10, 30, 100	OIL	300, 1000, 3000	DMSO	Wako
chlorpromazine	CPZ	4.5, 15, 45	MC	0.8, 4, 20	DMSO	Wako
clofibrate	CFB	30, 100, 300	OIL	12, 60, 300	DMSO	Wako
coumarin	CMA	15, 50, 150	OIL	12, 60, 300	DMSO	Tokyo kasei
cyclophosphamide	CPA	1.5, 5, 15	MC	8, 40, 200	Medium	Ardrich
diazepam	DZP	25, 75, 250	MC	5, 25, 125	DMSO	Wako
diclofenac sodium	DFNa	1, 3, 10	MC	16, 80, 400	DMSO	Tokyo kasei
ethionine	ET	25, 80, 250	MC	400, 2000, 10000	Medium	Tokyo kasei
gemfibrozil	GFZ	30, 100, 300	OIL	4, 20, 100	DMSO	Sigma
hexachlorobenzene	HCB	30, 100, 300	OIL	0.6, 3, 15	DMSO	Tokyo kasei
indomethacin	IM	0.5, 1.6, 5	MC	12, 60, 300	DMSO	Sigma
isoniazid	INAH	10, 50, 100	MC	400, 2000, 10000	Medium	Sigma
methapyrilene hydrochloride	MP	10, 30, 100	MC	0.6, 3, 15	Medium	Sigma
methotrexate	MTX	10, 30, 100 (Single) 0.1, 0.3, 1 (Repeated)	MC	20, 100, 500	Medium	Wako
nitrofurantoin	NFT	10, 30, 100	MC	5, 25, 125	DMSO	ICN
omeprazole	OPZ	100, 300, 1000	MC	4.8, 24, 120	DMSO	Wako
phenobarbital	PB	10, 30, 100	MC	300, 1000, 3000	Medium	Sigma
phenylbutazone	PhB	20, 60, 200	MC	16, 80, 400	DMSO	Sigma
phenytoin	PHE	60, 200, 600	MC	2.4, 12, 60	DMSO	Tokyo kasei
propylthiouracil	PTU	10, 30, 100	MC	160, 800, 4000	Medium	Tokyo kasei
rifampicin	RIF	20, 60, 200	MC	2.8, 14, 70	DMSO	Wako
thioacetamide	TAA	4.5, 15, 45	MC	400, 2000, 10000	Medium	Ardrich
valproate sodium	VPA	45, 150, 450	MC	400, 2000, 10000	Medium	Sigma
Wy-14,643	WY	10, 30, 100	OIL	8, 40, 200	DMSO	Tokyo kasei

Supplier information: Wako; Wako pure chemical industries, Osaka, Japan, Tokyo kasei; Tokyo kasei kogyo, Tokyo, Japan. ICN; ICN Biomedical Inc., Aurora, OH, USA, Sigma (St. Louis, MO, USA), Aldrich (St. Louis, MO, USA), Kanto chemical (Tokyo, Japan)

Table 1-2. Up-regulated genes that are discussed in the text.

	ProbeID	GeneName	Gene Symbol	Vivo		Vitro[c)]
				Single[a)]	Repeated[b)]	
	ß-oxidation					
*	1387783_a_at	acetyl-Coenzyme A acyltransferase 1	Acaa1	3.9	5.8	8.4
	1367735_at	acetyl-Coenzyme A dehydrogenase, long-chain	Acadl	1.6	2.0	1.8
*	1367897_at	acyl-Coenzyme A dehydrogenase, very long chain	Acadvl	2.2	2.6	2.8
	1367680_at	acyl-Coenzyme A oxidase 1, palmitoyl	Acox1	2.7	3.1	4.3
*	1367836_at	Carnitine palmitoyltransferase 1 liver	Cpt1a	5.3	7.4	6.6
*	1386946_at	carnitine palmitoyltransferase 1, liver	Cpt1a	4.3	4.6	8.5
*	1386927_at	carnitine palmitoyltransferase 2	Cpt2	5.5	6.2	3.0
*	1367659_s_at	dodecenoyl-coenzyme A delta isomerase	Dci	6.4	7.0	3.6
*	1367777_at	2,4-dienoyl CoA reductase 1, mitochondrial	Decr1	2.4	3.3	3.0
*	1370818_at	2-4-dienoyl-Coenzyme A reductase 2 peroxisomal	Decr2	3.5	3.5	2.5
*	1386885_at	enoyl coenzyme A hydratase 1, peroxisomal	Ech1	8.9	11.6	4.6
*	1368283_at	enoyl-Coenzyme A, hydratase/3-hydroxyacyl Coenzyme A dehydrogenase	Ehhadh	7.1	8.4	83.0
	1370164_at	Hydroxyacyl-Coenzyme A dehydrogenase alpha subunit	Hadha	3.1	4.2	1.9
	1367694_at	hydroxyacyl-Coenzyme A dehydrogenase beta subunit	Hadhb	3.1	3.2	1.5
*	1388210_at	Mitochondrial acyl-CoA thioesterase 1	Mte1	24.1	32.1	3.9
*	1388211_s_at	Mitochondrial acyl-CoA thioesterase 1	Mte1	162.8	175.5	7.6
	Lipid mobilization					
	1370024_at	fatty acid binding protein 7, brain	Fabp7	2.4	3.0	1.5
*	1368150_at	solute carrier family 27 (fatty acid transporter), member 2	Slc27a2	1.7	1.9	3.3
	1398249_at	solute carrier family 25 member 20	Slc25a20	3.7	3.7	2.4
*	1367950_at	solute carrier family 22 member 5	Slc22a5	4.1	5.5	3.1
*	1367689_a_at	Cd36 antigen	Cd36	5.8	16.4	3.7
*	1386901_at	cd36 antigen	Cd36	5.2	9.6	3.8
*	1375247_at	Monoglyceride lipase	Mgll	3.2	7.4	3.3
*	1370831_at	Monoglyceride lipase	Mgll	4.2	7.4	3.5
*	1388644_at	Monoglyceride lipase	Mgll	7.2	9.4	3.9
	1368317_at	aquaporin 7	Aqp7	3.4	22.0	1.3
	Fatty acid and cholesterol synthesis					
	1367857_at	fatty acid desaturase 1	Fads1	1.5	1.8	1.2
	1368453_at	fatty acid desaturase 2	Fads2	2.4	3.8	1.3
*	1370355_at	Stearoyl-Coenzyme A desaturase 1	Scd1	1.6	2.6	2.2
	1372318_at	ELOVL family member 6 elongation of long chain fatty acids yeast	rELO2	4.6	7.2	1.5
*	1388108_at	ELOVL family member 6 elongation of long chain fatty acids yeast	rELO2	5.4	9.6	2.1
	1367767_at	3-hydroxy-3-methylglutaryl CoA lyase	Hmgcl	1.9	3.4	1.5
*	1370310_at	3-hydroxy-3-methylglutaryl-Coenzyme A synthase 2	Hmgcs2	1.9	1.9	11.5
	Ohter lipid methabolism related					
*	1386880_at	acetyl-Coenzyme A acyltransferase 2	Acaa2	2.0	2.5	4.3
	1373778_at	Acetyl-Coenzyme A carboxylase beta	Acacb	2.0	3.6	1.4
	1367763_at	Acetyl-coenzyme A acetyltransferase 1	Acat1	2.2	3.4	2.1
	1368177_at	acyl-CoA synthetase long-chain family member 3	Acsl3	2.4	5.8	3.6
*	1371886_at	Carnitine acetyltransferase	Crat	9.7	17.4	2.5
	1368426_at	carnitine O-octanoyltransferase	Crot	2.8	3.1	2.0
	1387183_at	Carnitine O-octanoyltransferase	Crot	6.4	6.4	3.6
*	1398250_at	cytosolic acyl-CoA thioesterase 1	Cte1	537.8	971.5	1906.3
	1368206_at	peroxisomal acyl-CoA thioesterase 1	Pte1	3.6	5.8	1.5
	1369485_at	cytoplasmic acetyl-CoA hydrolase	rACH	2.3	2.9	2.7

Table 1-2. Up-regulated genes that are discussed in the text. (continued)

	ProbeID	GeneName	Gene Symbol	Vivo		Vitro[c)]
				Single[a)]	Repeated[b)]	
*	1388924_at	Angiopoietin-like protein 4	Angptl4	5.3	5.6	5.5
	Peroxisomal Protein					
*	1379361_at	Peroxisomal biogenesis factor 11A	Pex11a	16.5	12.1	4.9
*	1387740_at	peroxisomal biogenesis factor 11A	Pex11a	14.8	13.3	7.4
	Carbohydrate methabolism					
*	1369150_at	pyruvate dehydrogenase kinase, isoenzyme 4	Pdk4	9.7	17.9	15.9
	1370509_at	Pyruvate dehydrogenase phosphatase isoenzyme 2	Pdp2	2.3	1.9	1.3
	1369560_at	glycerol-3-phosphate dehydrogenase 1 (soluble)	Gpd1	3.3	3.6	2.8
	1371363_at	Glycerol-3-phosphate dehydrogenase 1 soluble	Gpd1	2.4	2.3	2.2
	1387670_at	Glycerol-3-phosphate dehydrogenase 2	Gpd2	6.2	7.5	1.5
	1370870_at	Malic enzyme 1	Me1	5.0	15.0	1.2
	1370067_at	malic enzyme 1	Me1	5.1	12.0	1.1
	Proliferation					
	1371150_at	Cyclin D1	Ccnd1	2.2	1.7	1.1
	1383075_at	Cyclin D1	Ccnd1	3.7	1.6	1.1
	1368947_at	growth arrest and DNA-damage-inducible 45 alpha	Gadd45a	3.6	4.0	1.3
	1368308_at	myelocytomatosis viral oncogene homolog (avian)	Myc	2.2	5.7	1.2
	1373473_a_at	Nucleosome assembly protein 1-like 1	Nap1l1	3.3	3.9	1.2
	1370826_at	Nucleosome assembly protein 1-like 1	Nap1l1	2.0	2.2	1.1
	1387977_at	Nibrin	Nbn	3.3	2.3	1.3
	1387062_a_at	checkpoint kinase 1 homolog (S. pombe)	Chek1	2.8	2.7	1.3
	1371352_at	High mobility group protein 17	Hmgn2	1.8	1.9	1.5
	1370334_at	Evectin-1	Plekhb1	3.4	2.2	1.4
	1370413_at	Pregnancy specific beta-1-glycoprotein 4	Psg4	1.8	1.7	1.2
	1389403_at	Bone morphogenetic protein 7	Bmp7	1.7	1.9	1.2
	1368143_at	Annexin A7	Anxa7	2.3	3.5	1.0
	Growth factor					
	1369608_at	fibroblast growth factor 16	Fgf16	1.8	1.8	1.2
	Apoptosis					
	1368888_a_at	Reticulon 4	Rtn4	2.5	8.9	1.1
	1388027_a_at	Reticulon 4	Rtn4	3.5	13.3	1.1
	1387521_at	programmed cell death 4	Pdcd4	1.3	2.3	1.2
	Cellular morphogenesis					
*	1368475_at	collagen-like tail subunit of asymmetric acetylcholinesterase	Colq	7.8	7.7	2.4
	1368355_at	myosin 5B	Myo5b	4.2	7.0	1.1
	1398281_at	occludin	Ocln	2.7	3.0	1.1
	1367655_at	thymosin, beta 10	Tmsb10	2.4	5.0	1.9
	Drug and xenobiotic methabolism					
	1387296_at	cytochrome P450, family 2, subfamily J, polypeptide 4	Cyp2j4	2.8	4.6	1.6
	1370706_a_at	Cytochrome P450 family 2 subfamily j polypeptide 9	Cyp2j9	1.1	2.0	1.1
*	1370397_at	Cytochrome P450 family 4 subfamily a polypeptide 14	Cyp4a14	3.4	3.3	21.9
*	1368934_at	cytochrome P450, family 4, subfamily b, polypeptide 1	Cyp4b1	6.6	6.1	9.9
	1368738_at	Cytochrome P450 subfamily 11B polypeptide 1	Cyp11b1	2.2	2.4	3.5
	1387123_at	cytochrome P450, family 17, subfamily a, polypeptide 1	Cyp17a1	5.8	8.7	4.2

Table 1-2. Up-regulated genes that are discussed in the text. (continued)

	ProbeID	GeneName	Gene Symbol	Vivo		Vitro[c)]
				Single[a)]	Repeated[b)]	
	1369111_at	alcohol dehydrogenase 4 (class II), pi polypeptide	Adh4	1.4	1.2	10.7
	1370313_at	alcohol dehydrogenase 7 (class IV), mu or sigma polypeptide	Adh7	3.3	4.6	2.8
	1370613_s_at	UDP glycosyltransferase 1 family polypeptide A6	Ugt1a6	1.4	2.0	1.2
	1387759_s_at	UDP glycosyltransferase 1 family polypeptide A6	Ugt1a6	2.1	2.5	1.2
	Stress response					
	1367577_at	heat shock 27kDa protein 1	Hspb1	4.7	8.7	1.2
	1374105_at	Hypoxia induced gene 1	Hig1	2.4	1.9	1.7
	1387636_a_at	P11 protein	Cdtw1	3.3	3.6	1.3
	1368552_at	GrpE-like 1, mitochondrial	Grpel1	1.9	2.3	1.2
	1387023_at	glutathione S-transferase, mu type 3 (Yb3)	Gstm3	1.3	2.1	2.0
	1375357_at	Dystonia 1 torsion autosomal dominant torsin A	Dyt1	1.6	1.6	1.1
	Other probes which were used in PCA analysis					
*	1374265_at	NA	NA	4.7	5.6	2.6
*	1374556_at	Similar to spermine oxidase	NA	2.1	3.0	2.8
*	1376076_at	Transcribed locus strongly similar to NP_076005.1 RIKEN cDNA 2310016C08 gene Mus musculus	NA	5.8	5.9	4.4
*	1377037_at	Similar to peroxisomal acyl-CoA thioesterase 2B likely ortholog of mouse peroxisomal acyl-CoA thioesterase 2B	NA	17.5	10.6	7.9
*	1377867_at	Similar to Glutaminyl-peptide cyclotransferase precursor QC Glutaminyl-tRNA cyclotransferase Glutaminyl cyclase	NA	10.5	43.2	6.1
*	1383205_at	Similar to dapper2	NA	3.5	4.2	1.9
*	1388756_at	Similar to RIKEN cDNA 6330579B17 gene	NA	2.5	2.5	2.7
*	1389253_at	Vanin 1	Vnn1	14.7	29.9	5.6
*	1390383_at	Adipose differentiation-related protein	ADRP	4.7	2.4	2.0

a): The largest fold change among the single dose studies of CFB, WY and GFZ is shown. b): The largest fold change among the repeated dose studies of CFB, WY and GFZ is shown. c): The largest fold change among *in vitro* studies of CFB, WY and GFZ is shown. The columns are shaded when the corresponding probe sets appear in Fig. 1-2. *: Probes which were used in the PCA analysis.

Table 1-3. Down-regulated genes that are discussed in the text.

Probe ID	Gene Name	Gene Symbol	Vivo		Vitro[c)]
			Single[a)]	Repeated[b)]	
Lipid mobilization					
1368520_at	apolipoprotein A-IV	Apoa4	-4.0	-255.0	-1.2
1386980_at	apolipoprotein M	Apom	-1.4	-5.3	-1.1
1398859_at	Lipoprotein-binding protein	Hdlbp	-1.8	-1.9	-1.1
Other lipid Methabolism related					
1387959_at	Lysophospholipase	LOC246266	-2.2	-3.4	-2.3
1370530_a_at	Phospholipase D1	Pld1	-2.0	-1.8	-1.4
1369526_at	acyl-Coenzyme A dehydrogenase, short/branched chain	Acadsb	-2.0	-2.9	-1.8
Carbohydrate methabolism					
1368651_at	Pyruvate kinase liver and RBC	Pklr	-6.1	-5.8	-1.4
1387263_at	pyruvate kinase, liver and RBC	Pklr	-11.1	-15.7	-3.1
Proliferation					
1387129_at	X-ray repair complementing defective repair in Chinese hamster cells 1	Xrcc1	-1.9	-1.4	-1.2
1372863_at	MYC binding protein 2	Mycbp2	-2.3	-3.0	-1.2
1373291_at	Deleted in liver cancer 1	Dlc1	-2.0	-2.7	-1.3
1373332_at	Casein kinase 1 delta	Csnk1d	-1.9	-1.7	-1.1
1398273_at	ephrin A1	Efna1	-2.1	-1.6	-1.3
Transcription activation and repression					
1371202_a_at	Nuclear factor I B	Nfib	-2.6	-3.2	-1.3
1388167_at	Nuclear factor I B	Nfib	-2.5	-2.8	-1.4
1370946_at	Nuclear factor I X	Nfix	-2.5	-4.1	-1.3
1368221_at	nuclear receptor subfamily 3, group C, member 1	Nr3c1	-2.3	-2.5	-1.3
1369244_at	aryl hydrocarbon receptor nuclear translocator	Arnt	-1.8	-2.2	-1.3
1372601_at	Activating transcription factor 5	Atf5	-1.9	-2.8	-1.1
1367601_at	Cbp/p300-interacting transactivator, with Glu/Asp-rich carboxy-terminal domain, 2	Cited2	-3.1	-2.2	-1.3
1367602_at	Cbp p300-interacting transactivator with Glu Asp-rich carboxy-terminal domain 2	Cited2	-3.0	-2.3	-1.1
1387165_at	v-maf musculoaponeurotic fibrosarcoma (avian) oncogene homolog (c-maf)	Maf	-2.0	-3.7	-1.9
1371781_at	Signal transducer and activator of transcription 3	Stat3	-2.2	-2.6	-1.1
Growth factor					
1370830_at	Epidermal growth factor receptor	Egfr	-5.9	-3.8	-1.3
1373829_at	Fibroblast growth factor receptor 2	Fgfr2	-1.6	-2.5	-1.3
1370941_at	Platelet derived growth factor receptor alpha polypeptide	Pdgfra	-1.5	-2.7	-1.3
1367652_at	insulin-like growth factor binding protein 3	Igfbp3	-1.6	-2.6	-1.3
Apoptosis					
1369941_at	death-associated protein	Dap	-2.0	-2.8	-1.1
1369902_at	Bcl2 modifying factor	Bmf	-12.3	-22.2	-3.4
1370512_at	Androgen receptor-related apoptosis-associated protein CBL27	Cbl27	-2.9	-3.1	-1.3
1371491_at	Notch gene homolog 1 Drosophila	Notch1	-1.9	-1.9	-1.4
1398362_at	Notch gene homolog 2 Drosophila	Notch2	-3.5	-5.5	-1.2
1370243_a_at	Prothymosin alpha	Ptma	-1.5	-2.5	-1.0
Cell adhesion					
1386947_at	cadherin 1	Cdh1	-2.9	-2.1	-1.2
1369224_at	cadherin 17	Cdh17	-4.5	-10.1	-1.5
1368642_at	cadherin 2	Cdh2	-2.2	-3.3	-1.2
1387259_at	Cadherin 2	Cdh2	-2.2	-2.3	-1.1

Table 1-3. Down-regulated genes that are discussed in the text. (continued)

Probe ID	Gene Name	Gene Symbol	Vivo		Vitro[c)]
			Single[a)]	Repeated[b)]	
1369854_a_at	CEA-related cell adhesion molecule 1	Ceacam1	-2.0	-2.8	-1.4
1370371_a_at	CEA-related cell adhesion molecule 10	Ceacam10	-1.7	-2.2	-1.2
1370234_at	Fibronectin 1	Fn1	-2.7	-3.0	-1.1
1382027_at	Integrin beta 3 Cd61	Itgb3	-2.3	-3.5	-1.7
1372002_at	Gap junction membrane channel protein alpha 1	Gja1	-1.5	-2.2	-1.1
1367849_at	syndecan 1	Sdc1	-1.6	-2.1	-1.1
1370043_at	activated leukocyte cell adhesion molecule	Alcam	-2.4	-3.4	-1.3
1374432_at	Activated leukocyte cell adhesion molecule	Alcam	-2.1	-5.0	-1.6
1370108_a_at	Lin-7 homolog a C. elegans	Veli1	-2.5	-3.9	-3.7
1373027_at	Afadin	Af6	-1.9	-2.3	-1.2
Cellular morphogenesis					
1388459_at	Collagen type XVIII alpha 1	Col18a1	-3.0	-3.6	-1.2
1370959_at	Collagen type III alpha 1	Col3a1	-1.9	-2.6	-1.6
1376099_at	Collagen type V alpha 1	Col5a1	-2.2	-3.2	-1.4
1370895_at	Collagen type V alpha 2	Col5a2	-1.5	-2.1	-1.2
1371725_at	Myosin heavy polypeptide 9	Myh9	-2.7	-2.9	-1.2
1387402_at	myosin, heavy polypeptide 9	Myh9	-2.4	-3.3	-1.1
1369720_at	myosin Ib	Myo1b	-2.1	-2.9	-1.1
1386941_at	plectin	Plec1	-2.6	-2.7	-1.2
1370993_at	Laminin gamma 1	Lamc1	-2.2	-2.7	-1.2
1386956_at	scavenger receptor class B, member 1	Scarb1	-1.4	-3.3	-1.2
Immune response					
1371926_at	Interleukin 6 signal transducer	Il6st	-2.2	-1.9	-1.1
1368280_at	cathepsin C	Ctsc	-2.1	-3.2	-1.3
1387005_at	cathepsin S	Ctss	-1.3	-2.4	-1.1
1387893_at	Complement component 1 s subcomponent	C1s	-2.3	-13.6	-1.3
1370892_at	Complement component 4a	C4a	-2.3	-3.6	-1.1
1368558_s_at	allograft inflammatory factor 1	Aif1	-1.7	-3.3	-1.7
1370479_x_at	Alpha-2u globulin PGCL4	Obp3	-2.9	-81.0	-1.2
1387985_a_at	Alpha-2u globulin PGCL4	Obp3	-2.6	-207.5	-1.1
Coagulation					
1374320_at	Coagulation factor 5	F5	-2.5	-3.8	-1.6
1387351_at	fibrillin-1	Fbn1	-1.9	-3.2	-1.4
1371258_at	Fibrinogen alpha polypeptide	Fga	-2.1	-1.8	-1.5
1387323_at	kallikrein B, plasma 1	Klk3	-2.6	-2.7	-2.4
1369225_at	kininogen 1	Kng1	-1.8	-2.5	-1.1
Drug and xenobiotic methabolism					
1387243_at	Cytochrome P450 family 1 subfamily a polypeptide 2	Cyp1a2	-2.2	-8.1	-1.2
1387913_at	Cytochrome P450 family 2 subfamily d polypeptide 22	Cyp2d22	-2.6	-4.0	-1.6
1368608_at	cytochrome P450, family 2, subfamily f, polypeptide 2	Cyp2f2	-2.0	-3.0	-1.3
1368265_at	cytochrome P450 monooxygenase CYP2T1	Cyp2t1	-2.2	-3.7	-1.3
1370387_at	Cytochrome P450 family 3 subfamily a polypeptide 13	Cyp3a13	-3.6	-50.2	-1.7
1368467_at	cytochrome P450, family 4, subfamily F, polypeptide 2	Cyp4f2	-1.7	-2.3	-1.4
1367979_s_at	cytochrome P450, subfamily 51	Cyp51	-2.1	-1.4	-1.0
1389218_at	UDP-glucose ceramide glucosyltransferase-like 1	Ugcgl1	-2.9	-2.1	-1.3
1367938_at	UDP-glucose dehydrogenase	Ugdh	-2.4	-1.9	-1.2
1388410_at	UDP-glucose pyrophosphorylase 2	Ugp2	-3.0	-4.4	-1.2
Transport					
1370465_at	ATP-binding cassette sub-family B MDR TAP member 4	Abcb1	-5.5	-10.8	-1.3

Table 1-3. Down-regulated genes that are discussed in the text. (continued)

Probe ID	Gene Name	Gene Symbol	Vivo		Vitro[c)]
			Single[a)]	Repeated[b)]	
1368497_at	ATP-binding cassette, sub-family C (CFTR/MRP), member 2	Abcc2	-4.4	-2.5	-1.4
1369455_at	ATP-binding cassette, sub-family G (WHITE), member 5	Abcg5	-1.6	-3.1	-1.9
1369440_at	ATP-binding cassette, sub-family G (WHITE), member 8	Abcg8	-2.4	-5.6	-3.9
1398862_at	ATPase Ca transporting cardiac muscle slow twitch 2	Atp2a2	-2.6	-3.9	-1.2
1368698_at	ATPase Ca transporting plasma membrane 2	Atp2b2	-2.3	-3.4	-1.9
1387285_at	ATPase, Ca++ transporting, plasma membrane 2	Atp2b2	-2.1	-2.1	-1.7
1368621_at	aquaporin 9	Aqp9	-1.9	-8.4	-1.4
1390591_at	Na Pi cotransporter 4	Slc17a3	-1.8	-4.9	-1.5
1369746_a_at	Solute carrier family 21 member 10	Slc21a10	-1.8	-3.5	-1.6
1368461_at	solute carrier family 22 (organic anion transporter), member 8	Slc22a8	-2.0	-3.1	-1.2
1369169_at	solute carrier family 23 (nucleobase transporters), member 1	Slc23a1	-1.9	-2.6	-1.3
1368600_at	solute carrier family 26 (sulfate transporter), member 1	Slc26a1	-2.0	-2.5	-1.3
1369099_at	solute carrier family 30 (zinc transporter), member 1	Slc30a1	-1.6	-4.4	-1.3
1386960_at	solute carrier family 37 (glycerol-6-phosphate transporter), member 4	Slc37a4	-2.2	-2.3	-1.2
1368296_at	Solute carrier organic anion transporter family member 2b1	Slco2b1	-2.1	-2.4	-1.3
Stress response					
1371442_at	Hypoxia up-regulated 1	Hyou1	-2.9	-3.9	-1.6
1370665_at	Hypoxia up-regulated 1	Hyou1	-2.2	-3.3	-1.2
Regulation of blood pressure					
1387811_at	angiotensinogen	Agt	-2.2	-2.1	-1.1
1369664_at	arginine vasopressin receptor 1A	Avpr1a	-3.0	-2.7	-1.4
1367801_at	endothelin converting enzyme 1	Ece1	-1.9	-2.2	-1.2
1386953_at	hydroxysteroid 11-beta dehydrogenase 1	Hsd11b1	-2.2	-4.6	-1.1
1368102_at	hydroxysteroid 11-beta dehydrogenase 2	Hsd11b2	-1.8	-3.6	-1.9
1387994_at	Hydroxysteroid 17-beta dehydrogenase 9	Hsd17b9	-1.6	-1.8	-1.3
Others					
1368490_at	CD14 antigen	Cd14	-2.1	-5.1	-1.3
1370891_at	CD48 antigen	Cd48	-1.3	-2.1	-1.2
1367709_at	CD63 antigen	Cd63	-1.4	-2.9	-1.1

a): The smallest ratio to control value observed in single dose studies of CFB, WY and GFZ is shown. Negative figure means the reciprocal number of ratio; e.g., -3.0 means that one of the drugs reduced the gene expression to 1/3 of corresponding control. b): The smallest ratio to control value observed in repeated dose studies of CFB, WY and GFZ is shown. c): The smallest ratio to control value observed *in vitro* studies of CFB, WY and GFZ is shown. The columns are shaded when the corresponding probe sets appear in Fig. 1-2.

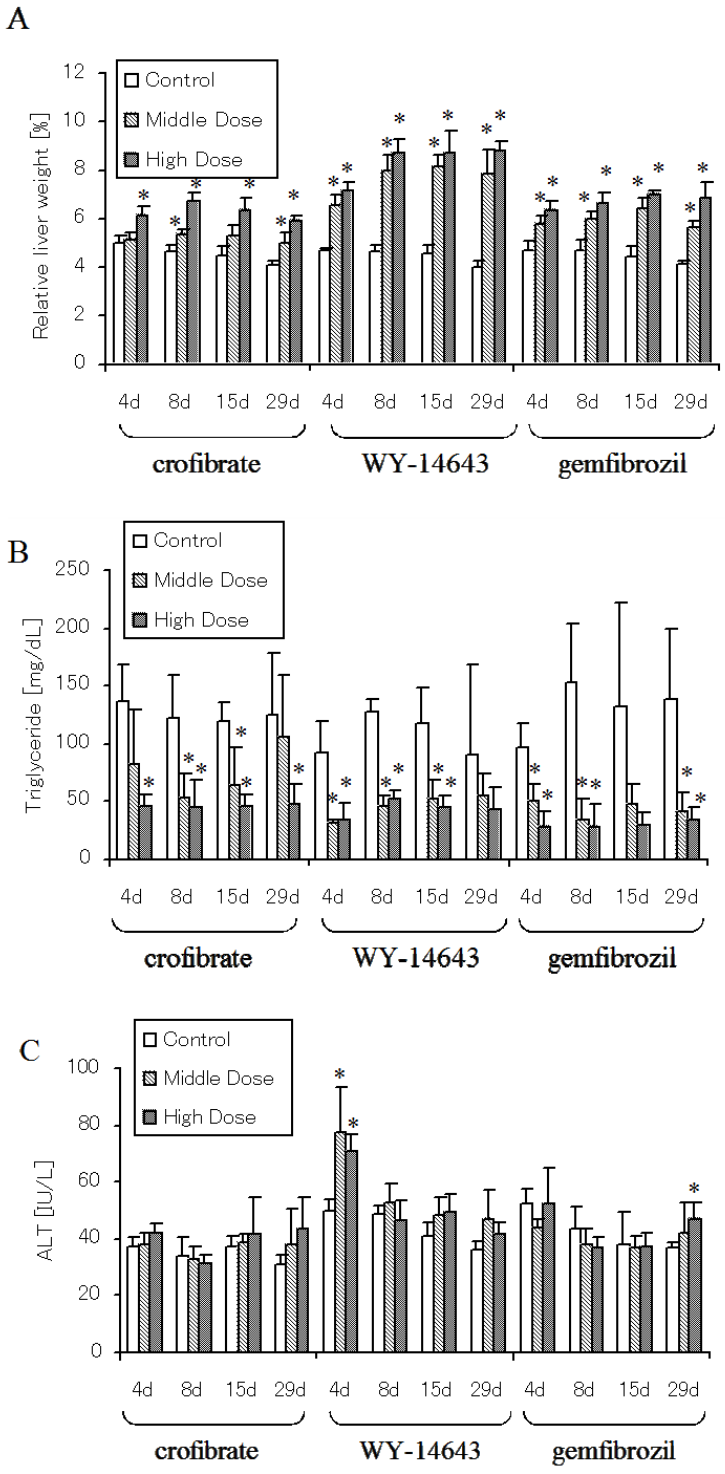

Fig. 1-1.

Effects of clofibrate, WY-14643 and gemfibrozil on relative liver weight (A), plasma triglyceride (B) and plasma alanine amino transferase (ALT; C). Values were obtained 24 hr after repeated administration of each drug for 3, 7, 14, and 28 days. Middle and high dose was 100 and 300mg/kg for clofibrate, 30 and 100 mg/kg for WY-14643, and 100 and 300mg/kg for gemfibrozil, respectively. For simplicity, data of the low dose was omitted. *Significantly different from control ($P<0.05$, Student's t-test, N=5)

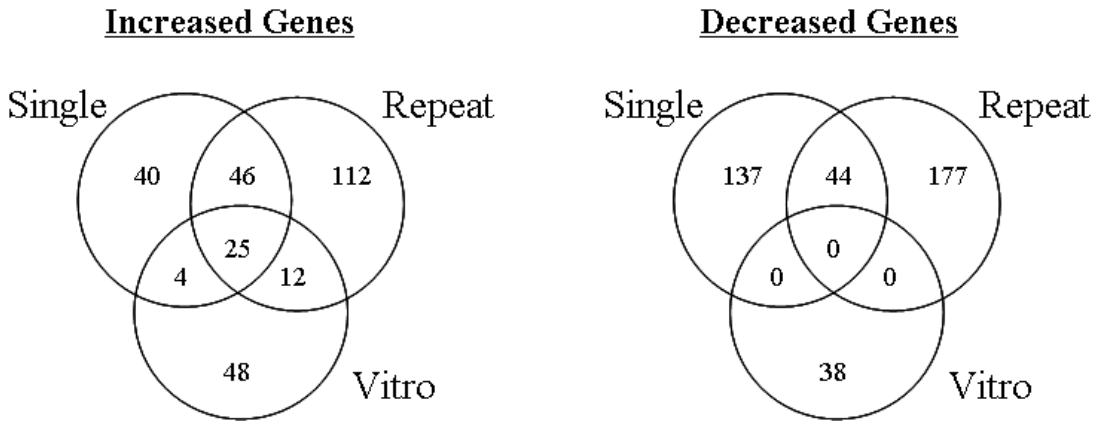

Fig. 1-2.

Venn diagram of extracted genes. Differentially expressed genes in liver treated with clofibrate, WY-14643 and gemfibrozil were extracted as follows. For *in vivo* study (single and repeated) genes with present call in at least 3 out of 6 samples in each experimental set that show at least a 1.5 fold increase (or 1/1.5 fold decrease) for both middle and high dose vs. control (at $p<0.05$ by Student's t-test) were extracted for each time point. For the *in vitro* study, genes with present call at least 2 out of 4 samples in each experimental set showing the same criteria as *in vivo* (without using t-test) were extracted. The numbers in the diagram show the numbers of extracted genes in each category.

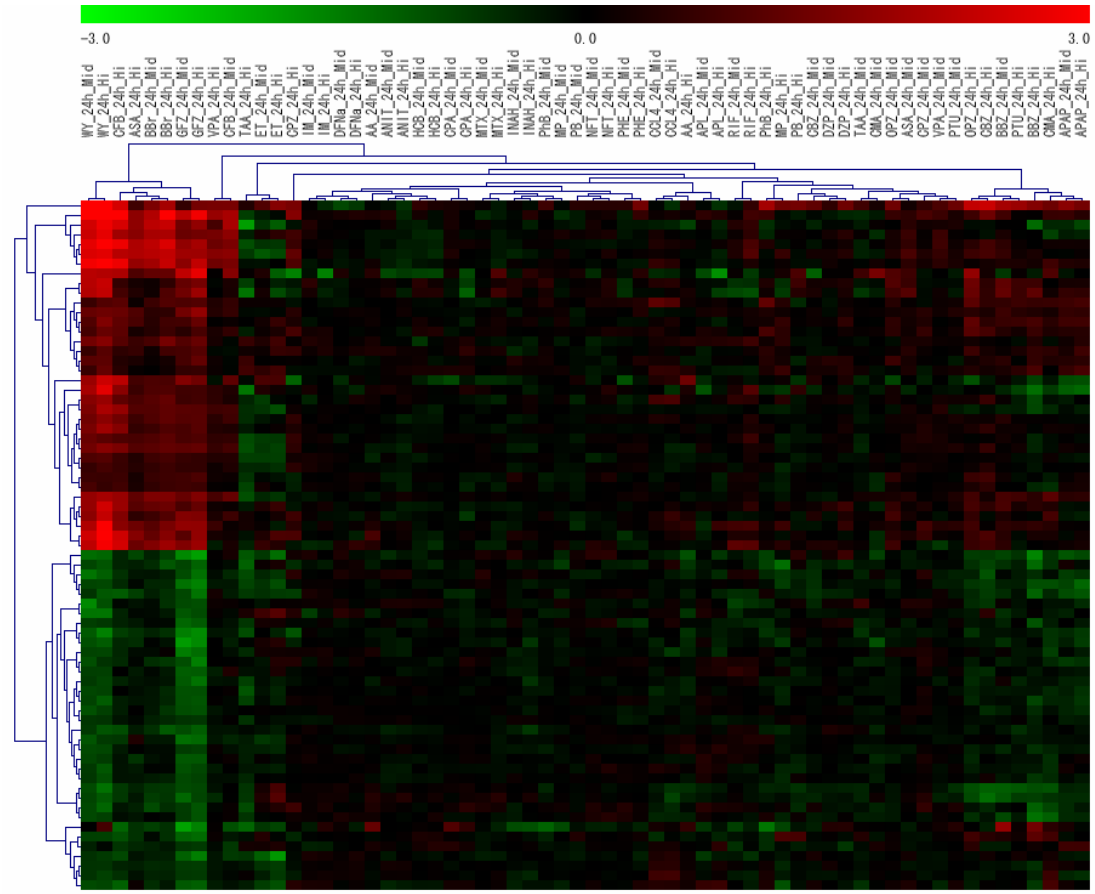

Fig. 1-3.

A heat map view of the gene expression profile for the 32 compounds *in vivo*. Hierarchical clustering analysis of the compounds (middle and high dose, 24 hours after a single dose) was conducted using the genes that were increased (1398296_at, 1398249_at, 1390851_at, 1389551_at, 1389253_at, 1388924_at, 1388891_at, 1388756_at, 1388223_at, 1387977_at, 1387783_a_at, 1387740_at, 1387636_a_at, 1387183_at, 1387022_at, 1386927_at, 1386885_at, 1386880_at, 1379361_at, 1375845_at, 1374475_at, 1373784_at, 1373564_at, 1372134_at, 1371976_at, 1371379_at, 1370870_at, 1370818_at, 1370397_at, 1370067_at, 1368934_at, 1368283_at, 1367937_at, 1367777_at, 1367694_at, 1367659_s_at) or decreased (1398362_at, 1391485_at, 1390172_at, 1390165_at, 1390115_at, 1389218_at, 1388742_at, 1388459_at, 1387913_at, 1382944_at, 1377375_at, 1376746_at, 1376709_at, 1376593_at, 1376140_at, 1375205_at, 1374493_at, 1374320_at, 1374266_at, 1373797_at, 1372308_at, 1371368_at, 1371202_a_at, 1370043_at, 1369973_at, 1369868_at, 1368698_at, 1368642_at, 1368497_at, 1368428_at, 1368304_at, 1368036_at, 1367905_at, 1367602_at, 1367601_at) 24 hours after a single dose (complete linkage method, Euclidean distance). A cluster consisting of 3 fibrates (CFB, WY, GFZ), benzbromarone (BBr) and aspirin (ASA) was identified on the left side.

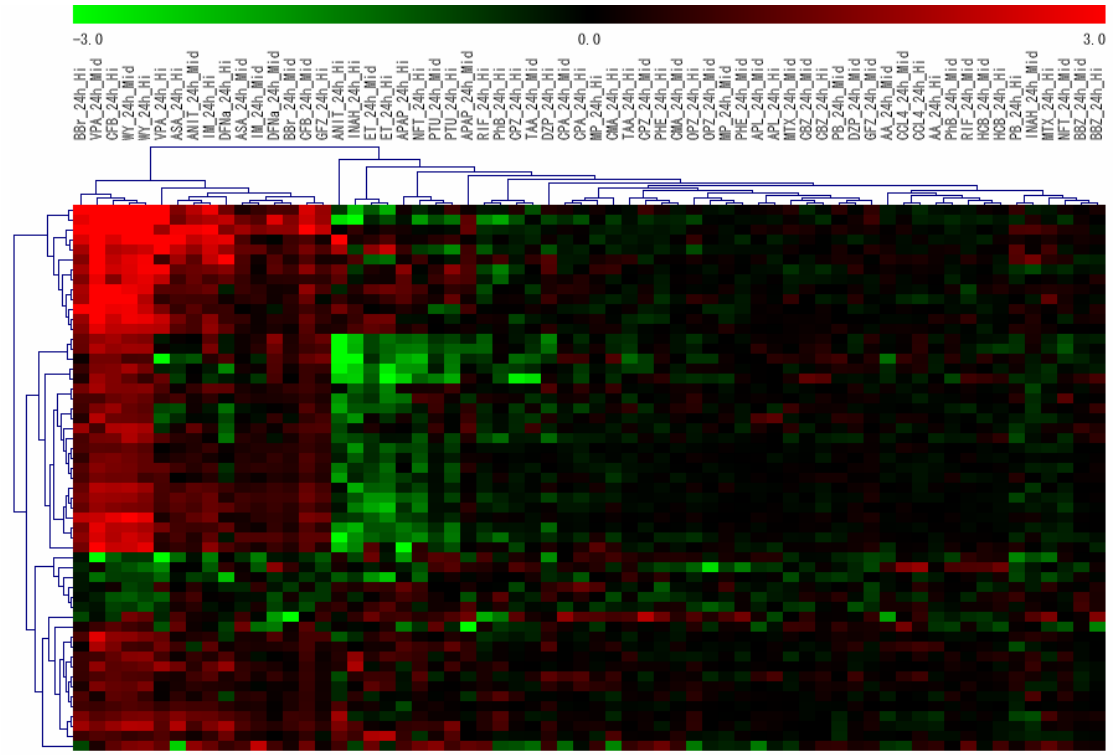

Fig. 1-4.

A heat map view of the gene expression profile for the 32 compounds *in vitro*. Hierarchical clustering analysis of the compounds (middle & high concentrations, 24 hours of exposure) was conducted using the genes that were increased (1398310_at, 1394194_x_at, 1390383_at, 1390370_at, 1389253_at, 1388924_at, 1388756_at, 1388644_at, 1388211_s_at, 1388108_at, 1387783_a_at, 1387740_at, 1386946_at, 1386927_at, 1386901_at, 1386885_at, 1386880_at, 1383205_at, 1379361_at, 1377037_at, 1376076_at, 1374556_at, 1374478_at, 1374265_at, 1370818_at, 1370436_at, 1370397_at, 1370355_at, 1370313_at, 1370310_at, 1370237_at, 1369150_at, 1369111_at, 1368934_at, 1368797_at, 1368669_at, 1368435_at, 1368283_at, 1368150_at, 1368034_at, 1368021_at, 1367950_at, 1367897_at, 1367836_at, 1367777_at, 1367742_at, 1367689_a_at, 1367672_at, 1367659_s_at) or decreased (1387246_at, 1375791_at, 1373261_at, 1369093_at, 1368798_at, 1368342_at) in 24 hours of exposure (complete linkage method, Euclidean distance). A cluster consisting of 3 fibrates (CFB, WY, GFZ), 3 NSAIDs (asprin [ASA], indomethacin [IM] and diclofenac sodium [DFNa]), valproic acid (VPA) and benzbromarone (BBr) was identified on the left side. Although the middle dose of ANIT belonged to the same cluster, its high dose did not.

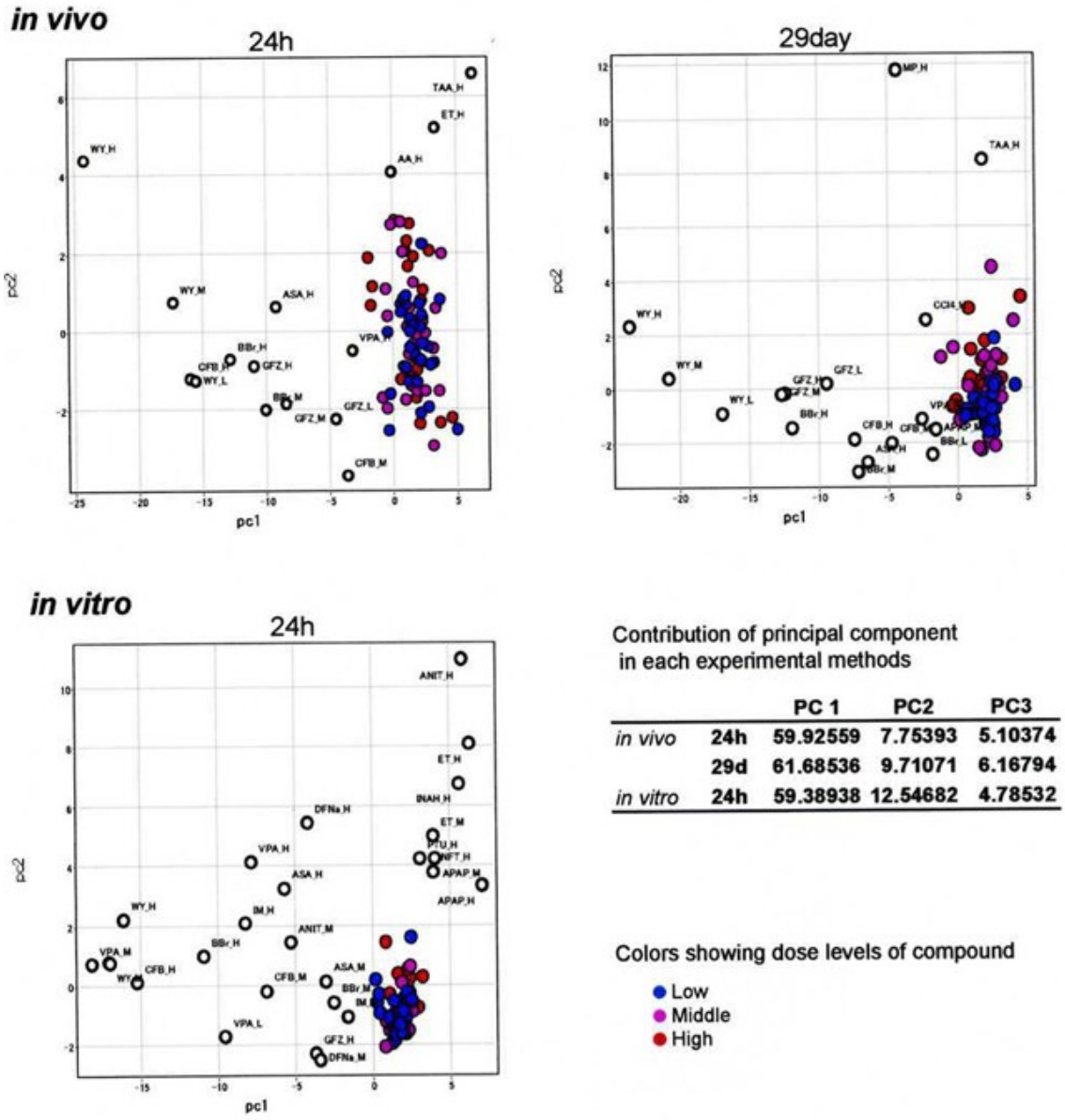

Fig. 1-5.

Two dimensional visualization of principal component analysis of the 32 compounds *in vivo* and *in vitro* using the commonly up-regulated 41 genes between *in vivo* and *in vitro*. The upper two panels show the *in vivo* studies and the lower left panel shows the *in vitro* study. Within each plot, the highest contributing factor to the overall variability is shown on the x-axis as the first component (PC1). The y-axis shows the second highest component (PC2). These plots show the principal separation of samples due to putative PPARα activity toward the negative direction on the x-axis, PC1. The contributions (%) of principal components for each experiment are summarized in the table on the lower right. .

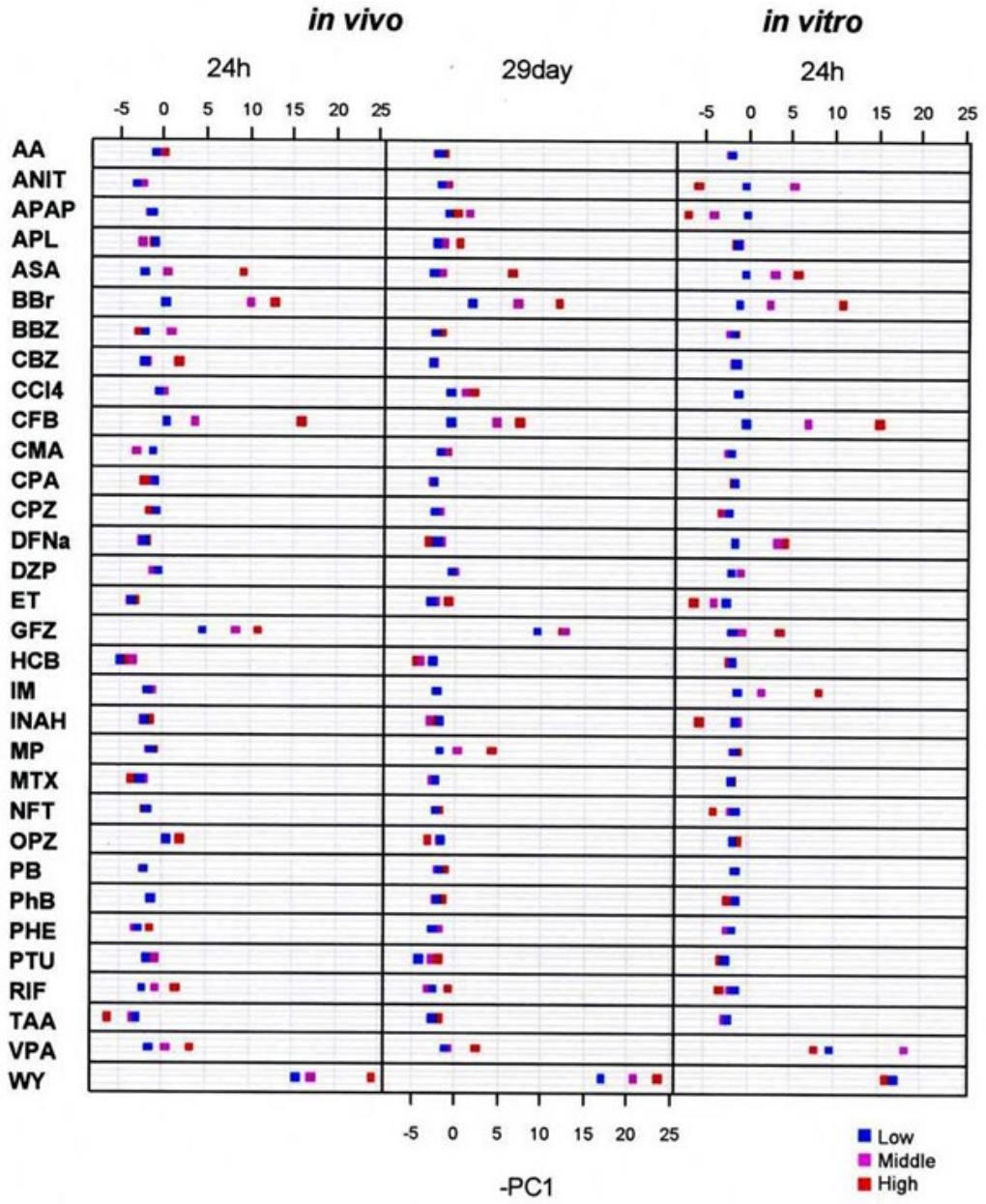

Fig. 1-6.

Plotting of the first principal component (PC1) from the 32 compounds examined *in vivo* and *in vitro*. The left two panels show the *in vivo* studies, i.e., 24 hr after single dose and 24 hr after the last dose of the 28-day repeated dose, and the right panel shows the *in vitro* study, 24 hr exposure. The x-axis for each shows the negative value of PC1, as in Fig. 1-5, and the y-axis shows the compounds aligned alphabetically. The abbreviations of the compounds are found in Table 1-1. Note that the three fibrates (CFB, GFZ, WY), aspirin (ASA), and benzbromarone (BBr) show high values in this parameter for *in vivo* experiments and that diclofenac sodium (DFNa) and indomethacin (IM) show high values in addition to the drugs above.

Chapter 2

Comparison of Gene Expression Profiles among Papilla, Medulla and Cortex in Rat Kidney

Abstract

The aim of this study was to compare gene expression profiles in the different regions of kidney as the basis for transcriptome analysis of kidney. Rat kidney was separated into papilla, medulla and cortex, and total RNA was isolated from these and from the whole slice. Gene expression profiling was performed using Affymetrix Rat Genome 230 2.0 Array. When global normalization was applied, the expression of β-actin or GAPDH varied among the regions. It was considered that such a comparison could not be made, especially between papilla and other portions, since the production of total mRNA in the former was relatively low. In fact, ANOVA was performed on the gene expression values with global normalization, in papilla, medulla, cortex, and whole slice, and the numbers of genes were appeared to be the highest in papilla. It was also observed that many genes showed their maximum or minimum in the whole slice, which was theoretically impossible. To overcome the problems associated with global normalization, the "percellome" normalization (a way to obtain the values directly related to the copies of mRNA per cell) was employed to compare the regions. In applying this procedure, probe sets with regional difference in expression were efficiently extracted by ANOVA. When they were sorted by the fold difference to other regions, the higher rank was occupied by genes characteristic to the functions of kidney, i.e., channels, transporters, and metabolic enzymes. Some of them were consistent with the literature and were related to pathophysiological phenomena. Comprehensive comparison of data of gene expression in the renal anatomical region will greatly enhance studies of the physiological function and mechanism of toxicity in kidney.

Furthermore, regarding toxicity through a drug target molecule, the toxicity is concerned to develop in various organs if the target molecule is distributed systemically. Accurate investigation of target molecule distribution using percellome normalization would enable us to choose drug target molecules with less toxicity

concern and to predict organs where the toxicity develops

Introduction

It is well known that kidney consists of a variety of cell types and the physiological functions, including gene expression, differ between the anatomical portions, i.e., papilla, medulla, and cortex. Therefore, I expected that different gene expression profiles would be obtained either when kidney is analyzed as a whole or separated into each portion. For an exploratory test, I checked potential region-related differences in gene expression before starting transcriptome analysis of ICR-derived glomerulonephritis (ICGN) mice kidney in chapter 4. Furthermore, regarding toxicity through a drug target molecule, the toxicity is concerned to develop in organs with expression of the drug target molecule. Accurate investigation on the region-related differences in gene expression will help us to know precise distribution of a drug target molecule and to predict organ where drug-induced toxicity develops.

In employing global normalization, based on the assumption that the total amount of mRNA is constant, it can cause a bias in the comparison of the different portions, since the rate of transcription varies with the cell types. In the present study, gene expression values were able to converted to a value proportional to the copies of mRNA per cell (the values normalized by externally adding standard mRNA in an amount proportional to the DNA content in the homogenate) by employing a system, "percellome" (Kanno *et al*., 2006). Quantification by this system was compared to that of global normalization.

Materials and methods

Animals and Sampling

Male Sprague-Dawley rats were purchased from Charles River Japan Inc., (Kanagawa, Japan) at 5-weeks of age. After a 7-day quarantine and acclimatization period, 6 of the animals were euthanized by exsanguination from the abdominal veins and arteries under ether anesthesia. Kidneys were collected from each animal, and sliced horizontally at its middle portion with ca. 1mm thickness by a pair of razor blades with a spacer in between. The slice was put into RNA later (Ambion, Austin, TX, USA) overnight for expression profiling. The fixed slices from three (No. 1 to 3) out of 6 animals were then separated into papilla, medulla, and cortex, as shown in Fig. 2-1. The remaining three (No. 4 to 6) were analyzed as a whole slice. The experimental protocols were reviewed and approved by the Ethics Review Committee for Animal Experimentation of the National Institute of Health Sciences.

Expression profiling

The kidney samples (whole slice, papilla, medulla and cortex) were homogenized using Mill Mixer (Qiagen) and zirconium beads. Total RNA was isolated from the kidney homogenate using RNeasy kit. Purity of the RNA was checked by gel electrophoresis, and the 260/280 nm ratio was between 2.0-2.2. Microarray analysis was conducted on 3 samples for each group by using GeneChip Rat Genome 230 2.0 Arrays (Affymetrix, Santa Clara, CA, USA) containing 31,099 probe sets. The procedure was basically conducted according to the manufacturer's instructions using Superscript Choice System (Invitrogen, Carlsbad, CA, USA) and T7-(dT)24-oligonucleotide primer (Affymetrix) for cDNA synthesis, cDNA Cleanup Module (Affymetrix) for purification, and IVT Labeling Kit (Affymetrix) for synthesis of biotin-labeled cRNA. Twenty μg of the fragmented cRNA was hybridized to a Rat

Genome 230 2.0 Array for 18 hr at 45°C at 60 rpm after which the array was washed and stained by streptavidin- phycoerythrin using Fluidics Station 450 (Affymetrix) and then scanned by Gene Array Scanner (Affymetrix). The data was analyzed by using GeneSpring version 6.1 (Silicon Genetics, Santa Clara, CA, USA), 2003 (Microsoft, Redmond, WA, USA) and MeV version 3.1 (The Institute for Genomic Research, Rockville, MD, USA). Expression data were customarily normalized using the mean value, multiplied by 500 (global mean normalization). Filtering of the data was performed either by flags (present, absent and marginal call) or ANOVA.

Percellome normalization

I customarily use global mean normalization for transcriptome analysis. However, to compare a sample from a different region of kidney, in which the activity of transcription might be different, global normalization based on the total mRNA appeared not to provide the correct result. In the present study, I employed "percellome normalization" to normalize data as well.

The Percellome method reported by Kanno *et al*. (2006) was shown to be effective to compare the data from different tissues or different platform. In this method, the grade-dosed spike cocktail (GSC), which consists of five different Bacillus subtilis mRNA with different concentrations, was added to the tissue homogenate in proportion to its DNA contents before RNA extraction, assuming that all the cells contain a fixed amount of genomic DNA (g/cell) across the samples. The copy number of the RNA in one cell was calculated from the function of signal values of GSC and their copy number. Therefore, the effect of the difference in the total gene expression between samples can be avoided and a direct comparison of the expression data of samples from different sources is enabled.

The GSC used in this study was generously provided by Dr. Kanno, and the experimental procedure and calculations of the percellome method was conducted

according to the original procedure. By separate experiments, I confirmed that GSC did not affect signals of other RNA and that the effect on global mean value was negligible.

Results

First, analyses were conducted by a common method for normalization, global normalization, in which each signal intensity was divided by the mean of each chip and multiplied by an arbitrary number to adjust the mean of each to the same value. In order to check the efficacy of the normalization procedure, the values of β-actin and GAPDH in each sample were divided by the mean value of the total 12 samples (Table 2-1). Expressed by this number, the values of β-actin varied between 0.91 – 0.99 in papilla, 0.98 – 1.12 in medulla, 0.97 - 1.14 in cortex, and 0.94 - 1.04 in the whole slice, resulting in an overall range of 0.91 – 1.14 (25 % variation). The expression of GAPDH varied 0.76 – 0.85 in papilla, 1.01 – 1.05 in medulla, 1.11 – 1.19 in cortex, and 1.02 – 1.04 in the whole slice, resulting in an overall range of 0.76 – 1.19 (50% variation). Although they are relatively close to 1 (the mean value was 0.94, 1.02, and 1.03 for β-actin and 0.81, 1.03 and 1.16 for GAPDH in papilla, medulla, and cortex, respectively), the differences seemed to be too large to be ignored.

Using the data analyzed with global normalization, Pearson's correlation was calculated for each pair of the samples and is shown in Table 2-2A. The correlation coefficients were quite high among 3 samples from the same region, i.e., all were larger than 0.985. The correlation between papilla and others were lower than that between medulla and cortex, i.e., 0.821 – 0.860 between papilla and medulla, 0.741 – 0.789 between papilla and cortex, whereas it was 0.936 – 0.955 between medulla and cortex. The correlation coefficients between each of the three regions and the whole slice were in this order: cortex (0.981 - 0.987) > medulla (0.954 – 0971) > papilla (0.770 - 0.814), suggesting that gene expression in the whole slice preferentially represents that in cortex but it does not well represent that in papilla.

To try to identify genes with differential expression in the three regions, I first used a parameter of GeneChip data, detection call (present, marginal, and absent).

Probe sets with present call in all samples in a region but all absent in other regions were selected as region-specific genes (Fig. 2-2). Genes with present call in all samples of papilla but absent in all of medulla and cortex were 448, and only 27 (6%) were all present in the whole slice. Genes with present call in all samples of medulla but absent in others were quite rare, i.e., 18 probe sets, of which 2 (11%) had present call in all of the whole slices. Cortex-specific probes were found to be 44 and 34 (77%) were present in all of the samples of the whole slice. The relatively small number in the latter two portions indicates that most of the genes are common between medulla and cortex, and the gene expression in papilla is unique. These results suggest again that the region specific genes (in other than cortex) are difficult to detect by analysis of the whole slice.

The above results clearly indicate that the population of genes expressed in each region is quite different. Theoretically, absolute values of expression should be used when an accurate comparison is made between regions with different total mRNA contents. In order to further elucidate this point, the "percellome procedure" was employed to compare with global normalization.

The mean of copy numbers (or the values directly related to copy numbers) of β-actin was calculated to be 234, 291, 341, and 309 in papilla, medulla, cortex and the whole slice, respectively, i.e., the ratio in papilla, medulla, and cortex (whole slice = 1) was 0.76, 0.94 and 1.10, respectively. The mean of copy numbers of GAPDH was calculated to be 208, 298, 369 and 343, in papilla, medulla, cortex and the whole slice, respectively, i.e., the ratio in papilla, medulla, cortex (whole slice = 1) was 0.61, 0.87 and 1.08, respectively. These values clearly differ from those by global normalization, namely, the expression values in papilla were apparently overestimated by global normalization. The correlation coefficients calculated from the values normalized by percellome (Table 2-2B) were almost identical to that in Table 2-2A except between papilla and others, which showed a relatively large decrease in value. These results

again indicated that global normalization was problematic, especially for papilla among the portions, most possibly because of the low amount of mRNA production in that region, compared with others.

After normalization either by global mean or percellome, the genes with absent call in all the samples were discarded and analyzed by ANOVA ($p<0.01$) in order to extract probe sets showing different expression in any region(s). The numbers of extracted probe sets were 12,322 for percellome and 8,161 for global normalization. Fig. 2-3 shows the results of K-means clustering (Euclidean, 10 clusters) of the expression values converted into z-scores in order to see the trend of expression in each region.

By percellome normalization (Fig. 2-3A), clusters of probe sets with characteristic region-dependent expression were efficiently extracted. It was also obvious from the figure that there was only one cluster containing only 293 probe sets that showed specifically high expression in papilla, and the other probe sets showed the lowest value in papilla compared to any other clusters. This indicates that most of the probe sets showed the lowest expression in papilla and the highest ones were exceptional. On the other hand, the clusters of global normalization (Fig. 2-3B) showed various, inconsistent patterns. Contrasting with the case of percellome normalization, there were many clusters in which gene expression was highest in papilla, or where papilla was equivalent to other region(s).

An obvious contradiction was noted between the two normalizations as described above, so further comparison was made. After the elimination of the probe sets that had absent call in all samples, the probe sets were classified into categories where the values showed maximum or minimum. Fig. 2-4 shows their counts in papilla, medulla, cortex, and whole slice for each normalization method. In the case of percellome normalization (A), the numbers of probe sets showing a maximal value were dominantly found in cortex, while the most of those showing a minimum were in

papilla. On the other hand, in the case of global normalization (B), many of the probe sets showing their maximum were in papilla, while the numbers of probe sets with minimal expression were distributed evenly among the samples. It is noteworthy that very many (>3,000) probe sets showed minimal expression in the whole slice. However, this is theoretically impossible because the whole slice contains all the other 3 portions. Therefore, it should be concluded that the extraction of the genes with region-specific expression based on global normalization gives an error, and thus percellome normalization should be used in this case.

Based on the above results, region-specific genes in kidney were extracted as follows. After selection by ANOVA ($p<0.01$) for the data of percellome normalization, genes were categorized by the position at which they showed the larger expression value and then aligned in the order of their ratio to the minimum, for papilla (Table 2-3), medulla (Table 2-4) and cortex (Table 2-5). As is obvious from Figs. 2-3 and 2-4, the production of mRNA per cell was considered to be in the order of cortex>medulla>papilla, and the numbers of region-specific probe sets were also in this order. For simplicity, probe sets without any annotation were eliminated, and the ones with the ratio of >3 for papilla, >10 for medulla, and >30 for cortex, are presented in the tables.

In all these three tables, the higher rank is generally occupied by the genes related to channels, transporters and metabolic enzymes, suggesting that the gene lists are meaningful for analysis of specific renal functions.

In most of the papilla-enriched genes (Table 2-3), the ratio of papilla/cortex is larger than that of papilla/medulla, since the composition of papilla is closer to medulla than to cortex. The exceptional genes (highest in papilla and lowest in medulla) are shaded in the table. The outstanding feature of this table is that heat shock proteins and cytoskeleton/extracellular matrix proteins are present, in addition to the channel/transporters and metabolic enzymes.

In most of the medulla-enriched genes (Table 2-4), the ratio of medulla/cortex is less than 2, suggesting that their expression is relatively similar between these two portions. The genes with ratio of >3 are shaded in the table, but they are only 3 sets, indicating that medulla-specific genes are rare. The higher rank of the list in Table 2-4 is also occupied by channel/transporters and metabolic enzymes, and cytoskeletal proteins are scarce. A unique feature of medulla is the existence of 4 probe sets for prolactin receptor. This might occur simply because the quality of these multiple probes for one prolactin receptor is uniformly high.

Table 2-5 shows genes that showed the highest value in the cortex. It is noteworthy that many genes show more than 3 fold (shaded in the table) for the cortex/medulla ratio, indicating that there are many cortex-specific genes. The higher rank of this table is also occupied by channel/transporters and metabolic enzymes, but the numbers of metabolic enzymes are more prominent than in medulla.

Table 2-6 summarizes the genes categorized as channel/transporters, metabolic enzymes, cytoskeletons, and others for each portion.

Discussion

The kidney is composed of various types of cells, and each portion (papilla, medulla, and cortex) has specific functions with wide variety, and the adverse effects of drugs vary with each portion. For example, aminoglycoside causes necrosis mainly in the proximal tubules, while puromycin does the same on glomerulus (Schnellmann, 2001). Regarding toxicity through drug target molecule, the toxicity is concerned to develop in various organs if a target molecule is distributed systemically. Accurate investigation of a target molecule distribution would enable us to choose drug target molecules with less toxicity concern and to predict organs where the toxicity develops

In the present study, I compared the gene expression profile among each portion, papilla, medulla, and cortex, as well as between the whole slice and each portion. Although various genes or proteins with region-specific expression have been reported, their localization was toward glomerulus, distal/proximal tubules, or collecting duct, i.e., tissues from specific cell types, not the anatomical location. This way is of course desirable for cell physiological study, but is inconvenient when a potential bias in the gene expression analysis based on the position of sampling is concerned, and reports focusing on this point are scarce. It can be generally said that papilla is enriched in collecting duct and relatively scarce in glomerulus, but their proportion varies with the sampling.

When comparison between each portion was made by correlation coefficient, the correlation was decreased between the portions compared to within the same portion. The correlation of gene expression profile between cortex and medulla was relatively high, whereas that between papilla and cortex or medulla was low. Based on the correlation of each portion to the whole slice, it was concluded that gene expression in the whole slice largely reflected that of cortex, followed by medulla. The main reason is that the volume of the portion comprising the whole slice is in this

order: cortex > medulla > papilla (Fig. 2-1). If the production of mRNA per cell is constant throughout the portions, the region-specific gene can be extracted by global normalization. However, this was found to be inappropriate.

To extract region-specific genes, detection call (absent, present, and marginal) included in the GeneChip data was utilized, i.e., genes with present call in a particular region but absent call in all others were extracted, and they were checked whether they had present call in the whole slice. The important point of this result is that the majority (94%) of genes specifically expressed in papilla are not detectable in the whole slice. This is consistent with the result of the correlation coefficient. It is thus concluded that the expression changes of such genes occurring in papilla cannot be detected when they are decreased, and it is difficult to measure when they are increased, but their extent is not so large, as in the analysis of the whole slice. Attention should be paid when these genes are used for the marker genes in the toxicogenomics of kidney.

As obvious from Figs. 2-3 and 2-4, global normalization of the data leads to an incorrect result in the comparison among different regions. This might be due to the fact that the transcriptional activity in papilla is much less than that in the others, and subsequently the expression of each gene in papilla was over-estimated by the normalization, using a low value. This does not mean that the global normalization is useless when drug effects are tested on the samples separated into different portions. As global normalization gives relative values to the total mRNA amount, it efficiently reveals the drug effect unless the drug brings about a large change in the total mRNA. In the present case, it became problematic simply because the comparison was made among tissues with largely different mRNA contents. An alternative way is to normalize each gene by a house-keeping gene, e.g., β-actin or GAPDH. However, as already shown above, there is no guarantee that expression of these genes is constant throughout the different tissues.

Based on the data normalized by the percellome procedure, genes with region-specific expression were extracted and aligned in the order of their relative specificity. It was then found that the majority of genes with high region-specificity were related to channel/transporter and metabolic enzyme, suggesting a good correlation between gene expression and physiological function.

There are many known members of the solute carrier family (slc), whose distribution showed an interesting and marked difference among the three portions. In papilla, slc4a family members (anion transporter) were specifically expressed. In medulla, the expression of slc21a family (organic anion transporting polypeptides; OATPs), was outstanding. There were also other members such as Slc23a3 (xanthine/uracil permease), Scl6a18 (monocarboxylic acid transporter), Scl38a3 (SNAT family) (Gu *et al*., 2005), Slc22a2 (organic cation transporter), Slc7a12 (cationic amino acid transporter), and Slc15a2 (H+/peptide transporter), which were specifically expressed. In cortex, Slc17a (Na-phosphate co-transporter), Slc22a12 and Slc12a3 (both anion transporters), Slc16a6 (monocarboxylic acid transporter), and Slc27a2 (fatty acid transporter) were found to be specific.

There have been some reports regarding region-specific transporters. As glucose transport is known to be operational in the proximal tubule, it is expected that glucose transporters are enriched in cortex and medulla compared with papilla. Among the genes judged as significant by ANOVA, slc2a4 and 2a13 were glucose transporters and their expression was about 3.5 fold higher in medulla and cortex compared with papilla (this number was not large enough to be shown in the tables). It is also known that slc14a2, involved in urea transport, is highly expressed in the collecting duct (Karakashian *et al*., 1999). Although the ratio was not large enough to be in Table 2-3, its expression in papilla was twofold compared with cortex, consistent with the literature.

Aquaporin (Aqp) 3 and 4 were specifically expressed in papilla while Aqp 7

and 11 were in cortex (Table 2-6). Although the ratio was not large enough to be in Table 2-3, Aqp 2 was also preferentially expressed in papilla (1.9 and 2.3 fold compared with medulla and cortex, respectively). There have been supportive reports that Aqp2 (Jo *et al*., 1997) and Aqp3 (Echevarria *et al*., 1994) are enriched in collecting duct and Aqp7 is highly expressed in cortex (Nejsum *et al*., 2000).

Kidney produces renin to control blood pressure. Renin is synthesized in juxtaglomerular cells and converts angiotensinogen to angiotensin I, which is further converted to angiotensin II by angiotensin converting enzyme (ACE). The renin gene (Ren1) was expressed highest in cortex while ACE (ace2) was highest in medulla (Table 2-6).

Probes for prolactin receptor are 4 sets on the chip and all of them showed quite low expression in papilla (expression ranged 60 – 90 fold in cortex and 70 - 130 fold in medulla, compared with papilla, for these 4 probe sets). Prolactin is known as a natriuretic hormone which interacts with the renal dopamine system, and its natriuretic response is associated with inhibition of proximal tubular Na, K-ATPase (Ibarra *et al*., 2005). The location of its receptor in kidney (enriched in medulla and cortex) elucidated in the present study was consistent with the region where the hormone works.

NSAID-induced nephrotoxicity is well known as a typical toxicity toward kidney (Schnellmann, 2001). Its mechanism is believed to be inhibition of cyclooxygenase (COX). COX-1 is a constitutive, house-keeping enzyme and reported to be much present in collecting duct. COX-2 is an inducible enzyme involved in the inflammatory process, while it is reported to be always present at a low level in kidney without inflammation (Harris *et al*., 1994). The genes for these enzymes (ptgs1 and ptgs2) were both highest in papilla. Moreover, phospholipase A2 IVA was also highest in papilla. These observations are consistent with previous reports and might be related to the fact that nephrotoxicity by NSAID is frequently associated with necrosis in

papilla (Schnellmann, 2001).

On the other hand, other prostaglandin-related genes were uniformly low in papilla. The expression of the gene of 15-hydroxyprostaglandin dehydrogenase (Hpgd), which is involved in prostaglandin metabolism, was 60 and 102 fold in medulla and cortex, respectively, compared with papilla. Other prostaglandin-related genes without large enough specificity for the table were prostaglandin D2 synthase (Ptgds), prostaglandin E receptor 1 (Ptger1), prostaglandin E receptor 3 (Ptger3), and prostaglandin E receptor 4 (Ptger4), which were 6 and 26 fold, 3 and 4 fold, 5 and 2 fold, 3 and 6 fold, in medulla and cortex, respectively, compared with papilla. The expression of prostaglandin E synthase (Ptges) was exceptionally the same in papilla and medulla, and 4.5 fold of these was found in cortex.

Kallikrein that produces bradykinin is biosynthesized in cortex of kidney (Xiong *et al*., 1989). Kallikrein 7 (Klk7) is found in Tables 2-5 showing 15 fold and 285 fold expression in medulla and cortex, respectively, compared with papilla. This is again consistent with the anatomical feature.

One unique point in the tables is that genes related to cytoskeletal proteins and heat shock proteins (both HSP70 and HSP27) selectively expressed high in papilla (Table 2-3 and 2-6). If the analysis was done by global normalization, it could be that the relative expression of these genes was apparently overestimated because of the low expression of other gene populations, such as transporters or enzymes. However, the present analysis was based on percellome normalization, and the values are directly related to the copy numbers per cell (or DNA). Therefore, enrichment of these genes means that the copy numbers of these genes are actually high. The potential involvement of HSP70 in nephrotoxicity has been investigated in relation to renal cell survival and apoptosis, and the relationship between hsp27 and cytoskeletal proteins has also been discussed in relation to renal injury after ischemia-reperfusion (van de Water *et al*., 2006).

In summary, use of global normalization has a problem when the regions containing different total amount of RNA are compared, and the problem is solved by percellome normalization. When percellome normalization was used, many of the genes related to kidney functions showed region-related differences in their expression and some of them were consistent with previous reports. There are also many genes with unique region-related differences in the table, which have not been described in the literature and it would be worthwhile to start new investigations based on these data. In conclusion, comprehensive comparison data of gene expression in the renal anatomical areas would greatly enhance studies of physiological function and mechanism of toxicity in kidney. Moreover, regarding toxicity through the drug target molecule, the toxicity is concerned to develop in various organs if the target molecule is distributed systemically. Accurate investigation of target molecule distribution using percellome normalization would enable us to choose drug target molecules with less toxicity concern and to predict organs where the toxicity develops.

Table 2-1. Signal Intensity of β–Actin and GAPDH

Value type	Gene Title	Papilla			Medulla			Cortex			Whole		
		No.1	No.2	No.3	No.1	No.2	No.3	No.1	No.2	No.3	No.1	No.2	No.3
Signal intensity	β-actin	19619	20290	18700	20158	22911	20379	19881	23365	20759	19277	19278	21390
	GAPDH	17008	16029	15284	20169	21086	20291	22338	23834	23006	20765	20430	20458
Signal intensity	β-actin	0.95	0.98	0.90	0.98	1.11	0.99	0.96	1.13	1.00	0.93	0.93	1.03
Mean of signal intensity	GAPDH	0.85	0.81	0.77	1.01	1.06	1.02	1.12	1.20	1.16	1.04	1.03	1.03

Expression of β-actin and GAPDH in the three portions of kidney slice, papilla, medulla, and cortex, from three different rats (No. 1 – 3) as well as in the whole slice of three different rats (No. 4 – 6). Signal intensity of each gene was divided by the mean of all probes in the chip multiplied by 500 (global mean normalization, upper columns), after which each value was divided by the mean of these 12 values (per gene normalization).

Table 2-2. Pearson's correlation coefficient between samples.

A		Papilla			Medulla			Cortex			Whole		
		No1	No2	No3	No1	No2	No3	No1	No2	No3	No4	No5	No6
Papilla	No1	1	0.989	0.986	0.847	0.843	0.837	0.765	0.758	0.761	0.814	0.811	0.812
	No2		1	0.985	0.853	0.853	0.846	0.778	0.773	0.775	0.827	0.825	0.825
	No3			1	0.815	0.812	0.811	0.738	0.73	0.735	0.789	0.785	0.786
Medulla	No1				1	0.994	0.991	0.947	0.933	0.937	0.958	0.967	0.956
	No2					1	0.991	0.943	0.935	0.938	0.957	0.968	0.955
	No3						1	0.953	0.943	0.953	0.964	0.972	0.962
Cortex	No1							1	0.991	0.992	0.986	0.983	0.986
	No2								1	0.991	0.983	0.979	0.984
	No3									1	0.984	0.98	0.985
Whole	No4										1	0.996	0.994
	No5											1	0.992
	No6												1

0.90 –
0.85 –
0.80 –
0.75 –
– 0.75

B		Papilla			Medulla			Cortex			Whole		
		No1	No2	No3	No1	No2	No3	No1	No2	No3	No4	No5	No6
Papilla	No1	1	0.989	0.985	0.837	0.833	0.826	0.755	0.755	0.752	0.801	0.797	0.801
	No2		1	0.982	0.843	0.844	0.834	0.768	0.769	0.764	0.813	0.81	0.814
	No3			1	0.801	0.798	0.795	0.725	0.723	0.724	0.771	0.766	0.77
Medulla	No1				1	0.994	0.991	0.946	0.934	0.937	0.957	0.967	0.955
	No2					1	0.991	0.942	0.936	0.937	0.956	0.967	0.954
	No3						1	0.953	0.945	0.953	0.963	0.971	0.961
Cortex	No1							1	0.992	0.992	0.987	0.984	0.986
	No2								1	0.992	0.986	0.982	0.986
	No3									1	0.985	0.981	0.985
Whole	No4										1	0.996	0.994
	No5											1	0.992
	No6												1

0.90 –
0.85 –
0.80 –
0.75 –
– 0.75

A: Calculated on the data of global normalization.

B: Calculated on the data of percellome.

Table 2-3. A list of probe sets specifically expressed in papilla of kidney

Probe sets	papilla/ cortex	papilla/ medulla	medulla/ cortex	Gene Symbol	Gene Name	channel transporter	Metabolic enzymes	cytoskeleton/ extracellular matrix
1368259_at	32.0	12.7	2.5	Ptgs1	prostaglandin-endoperoxide synthase 1			
1389067_at	29.5	10.7	2.8	Slco4a1	solute carrier organic anion transporter family, member 4a1			
1372190_at	23.8	8.1	2.9	Aqp4	Aquaporin 4			
1394200_at	22.9	4.9	4.7	Hspa2	heat shock protein 2			
1387092_at	17.5	5.4	3.2	Fxyd4	FXYD domain-containing ion transport regulator 4			
1367847_at	17.4	5.4	3.2	Nupr1	nuclear protein 1			
1388460_at	16.8	5.6	3.0	Capg_predicted	capping protein (actin filament), gelsolin-like (predicted)			
1383469_at	7.2	14.6	0.5	Aldh1a3	Aldehyde dehydrogenase family 1, subfamily A3			
1376711_at	13.3	7.1	1.9	Cldn11	claudin 11			
1383319_at	13.2	2.5	5.3	Slc4a11_predicted	solute carrier family 4, sodium bicarbonate transporter-like, member 11 (predicted)			
1367734_at	13.1	7.9	1.7	Akr1b4	aldo-keto reductase family 1, member B4 (aldose reductase)			
1368765_at	10.7	2.5	4.2	Clcnk1	chloride channel K1			
1370229_at	10.5	1.9	5.4	Ndr4	N-myc downstream regulated 4			
1369841_at	10.3	4.2	2.4	Hspa2	heat shock protein 2			
1382303_at	3.8	8.8	0.4	RGD:1303187	phosphatase and actin regulator 1			
1378690_at	7.6	3.9	2.0	Ly6a_predicted	lymphocyte antigen 6 complex, locus A (predicted)			
1367661_at	6.8	3.7	1.8	S100a6	S100 calcium binding protein A6 (calcyclin)			
1374207_at	6.6	2.5	2.6	Agpt2	angiopoietin 2			
1369113_at	6.1	3.9	1.6	Grem1	gremlin 1 homolog, cysteine knot superfamily (Xenopus laevis)			
1368858_at	5.9	2.1	2.8	Ugt8	UDP-glucuronosyltransferase 8			
1368247_at	5.4	3.7	1.5	Hspa1a /// Hspa1b	heat shock 70kD protein 1A /// heat shock 70kD protein 1B			
1370334_at	3.2	5.4	0.6	Plekhb1	evectin-1			
1367650_at	5.1	3.1	1.6	Lcn7	lipocalin 7			

Table 2-3. (continued)

Probe sets	papilla/ cortex	papilla/ medulla	medulla/ cortex	Gene Symbol	Gene Name	channel transporter	Metabolic enzymes	cytoskeleton/ extracellular matrix
1374861_at	5.1	2.1	2.4	Tle2_predicted	transducin-like enhancer of split 2, homolog of Drosophila E(spl) (predicted)			
1387100_at	4.1	5.1	0.8	Aqp3	aquaporin 3			
1369949_at	5.0	3.6	1.4	Lu	Lutheran blood group (Auberger b antigen included)			
1369263_at	5.0	2.4	2.0	Wnt5a	wingless-type MMTV integration site 5A			
1370312_at	4.9	1.5	3.4	Spon1	spondin 1			
1388459_at	4.7	2.9	1.6	Col18a1	collagen, type XVIII, alpha 1			
1388456_at	4.3	3.0	1.4	S100a1	S100 calcium binding protein A1			
1393209_at	3.6	4.3	0.8	bsnd	Bartter syndrome, infantile, with sensorineural deafness (Barttin)			
1373733_at	4.3	2.8	1.5	Bok	Bcl-2-related ovarian killer protein			
1388547_at	4.2	2.5	1.7	Cldn4_predicted	claudin 4 (predicted)			
1396152_s_at	4.1	2.4	1.7	Igfbp5	insulin-like growth factor binding protein 5			
1367812_at	4.0	3.3	1.2	Spnb3	beta-spectrin 3			
1367577_at	3.4	3.9	0.9	Hspb1	heat shock 27kDa protein 1			
1372755_at	3.9	2.5	1.6	Mal2	mal, T-cell differentiation protein 2			
1370834_at	3.8	1.8	2.2	Hs3st1	heparan sulfate (glucosamine) 3-O-sulfotransferase 1			
1388155_at	3.8	3.3	1.2	Krt1-18	keratin complex 1, acidic, gene 18			
1372299_at	3.7	2.3	1.6	Cdkn1c	cyclin-dependent kinase inhibitor 1C (P57)			
1387886_at	3.6	2.7	1.3	Prelp	proline arginine-rich end leucine-rich repeat protein			
1368527_at	1.7	3.6	0.5	Ptgs2	prostaglandin-endoperoxide synthase 2			
1388102_at	1.9	3.5	0.5	Ltb4dh	leukotriene B4 12-hydroxydehydrogenase			
1370048_at	3.4	2.8	1.2	Edg2	endothelial differentiation, lysophosphatidic acid G-protein-coupled receptor, 2			

Table 2-3. (continued)

Probe sets	papilla/ cortex	papilla/ medulla	medulla/ cortex	Gene Symbol	Gene Name	channel transporter	Metabolic enzymes	cytoskeleton/ extracellular matrix
1371004_at	3.4	1.7	2.0	Sort1	sortilin 1			
1397830_at	3.4	2.3	1.5	Igfbp5	Insulin-like growth factor binding protein 5			
1369953_a_at	3.3	1.5	2.2	Cd24	CD24 antigen			
1367912_at	3.2	2.3	1.4	Ltbp1	latent transforming growth factor beta binding protein 1			
1387566_at	3.2	1.6	2.0	Pla2g4a	phospholipase A2, group IVA (cytosolic, calcium-dependent)			
1370912_at	3.2	2.3	1.4	Hspa1b	heat shock 70kD protein 1B			
1398318_at	3.2	2.1	1.5	Muc1	mucin 1, transmembrane			
1371625_at	3.1	2.8	1.1	Pygb	brain glycogen phosphorylase			
1370026_at	3.1	1.1	2.8	Cryab	crystallin, alpha B			
1393048_at	3.1	1.1	2.8	Adra2a	Adrenergic receptor, alpha 2a			
1388143_at	3.1	2.4	1.3	Col18a1	collagen, type XVIII, alpha 1			
1393958_at	3.1	2.1	1.5	Arhgap4	Rho GTPase activating protein 4			
1369084_a_at	3.1	2.8	1.1	Bok	Bcl-2-related ovarian killer protein			
1371499_at	3.0	1.8	1.7	Cd9	CD9 antigen			
1391830_at	3.0	1.9	1.6	Cpne8_predicted	copine VIII (predicted)			
1368342_at	3.0	1.9	1.6	Ampd3	adenosine monophosphate deaminase 3			
1384192_at	3.0	2.1	1.4	Chst1_predicted	carbohydrate (keratan sulfate Gal-6) sulfotransferase 1 (predicted)			
1398431_at	1.2	3.0	0.4	Car8_predicted	carbonic anhydrase 8 (predicted)			
1375170_at	3.0	1.6	1.9	S100a11_predicted	S100 calcium binding protein A11 (calizzarin) (predicted)			
1367759_at	3.0	1.2	2.5	H1f0	H1 histone family, member 0			
1387040_at	3.0	1.6	1.8	Mal	myelin and lymphocyte protein			

After selection by ANOVA ($p<0.01$) for the data of percellome normalization, genes maximally expressed in papilla were selected. The genes were aligned in the order of the ratio to the lower expression value, either in medulla or in cortex. As the genes listed here are expressed higher in medulla than cortex, in general, exceptional cases (ratio < 0.6) are shaded in the medulla/cortex column. The genes categorized to "channel/transporters", "metabolic enzymes", or "cytoskeleton/extracellular matrix"

are also shaded. Proteases or enzymes involving signal transduction are not included in the category of “metabolic enzymes”. For simplicity, genes with less than 3 fold specificity are omitted.

Table 2-4. A list of probe sets specifically expressed in medulla of kidney

Probe sets	medulla/ papilla	cortex/ papilla	medulla/ cortex	Gene Symbol	Gene Name	channel transporter	Metabolic enzymes	cytoskeleton/ extracellular matrix
1370377_at	204.8	124.5	1.6	Cyp2d9 /// Cyp2d10	cytochrome P450, family 2, subfamily d, polypeptide 9 /// cytochrome P450, family 2, subfamily d, polypeptide 10			
1387567_at	184.9	119.7	1.5	Slc21a1 /// LOC497799	solute carrier family 21, member 1 /// hypothetical gene supported by NM_017111			
1369401_at	153.0	69.6	2.2	Slc21a13	solute carrier family 21, member 13			
1387328_at	149.6	100.5	1.5	Cyp2c	Cytochrome P450, subfamily IIC (mephenytoin 4-hydroxylase)			
1368288_at	147.9	90.7	1.6	Gc	group specific component			
1368498_a_at	147.3	102.7	1.4	RGD:621387	kidney specific organic anion transporter			
1386454_at	133.0	46.7	2.8	Slc23a3_predicted	solute carrier family 23 (nucleobase transporters), member 3 (predicted)			
1370789_a_at	132.6	91.8	1.4	Prlr	prolactin receptor			
1387987_at	120.1	43.9	2.7	Slc22a19	solute carrier family 22 (organic anion transporter), member 19			
1390569_at	117.4	74.7	1.6	RGD:1359493	similar to carnosinase 1			
1369450_at	114.9	92.3	1.2	UST5r	integral membrane transport protein UST5r			
1369493_at	89.1	62.1	1.4	Prlr	prolactin receptor			
1368575_at	88.9	70.0	1.3	Slc6a18	solute carrier family 6 (neurotransmitter transporter), member 18			
1370824_at	88.2	60.3	1.5	Slc38a3	solute carrier family 38, member 3			
1387382_at	88.0	42.0	2.1	Hnmt	histamine N-methyltransferase			
1387303_at	83.1	59.2	1.4	Slc22a2	solute carrier family 22 (organic cation transporter), member 2			
1378247_at	81.5	41.3	2.0	Eaf2	ELL associated factor 2			

Table 2-4. (continued)

Probe sets	medulla/ papilla	cortex/ papilla	medulla/ cortex	Gene Symbol	Gene Name	channel transporter	Metabolic enzymes	cytoskeleton/ extracellular matrix
1373990_at	78.5	24.0	3.3	Slc7a12_predicted /// LOC361914	solute carrier family 7 (cationic amino acid transporter, y+ system), member 12 (predicted) /// similar to solute carrier family 7 (cationic amino acid transporter, y+ system), member 12			
1389756_at	78.0	57.9	1.3	Melk_predicted	maternal embryonic leucine zipper kinase (predicted)			
1384775_s_at	74.6	51.7	1.4	Tmprss8	transmembrane protease, serine 8 (intestinal)			
1370384_a_at	73.9	60.3	1.2	Prlr	prolactin receptor			
1368208_at	72.9	60.3	1.2	Cml1	camello-like 1			
1376944_at	72.5	68.6	1.1	Prlr	Prolactin receptor			
1385132_at	69.0	32.5	2.1	Mybl1_predicted	myeloblastosis oncogene-like 1 (predicted)			
1368651_at	66.4	49.0	1.4	Pklr	pyruvate kinase, liver and RBC			
1368304_at	65.8	57.1	1.2	Fmo3	Flavin containing monooxygenase 3			
1397205_at	54.9	42.8	1.3	Dhrs7_predicted /// LOC500672	dehydrogenase/reductase (SDR family) member 7 (predicted) /// similar to Down-regulated in nephrectomized rat kidney #3			
1398612_at	51.8	37.6	1.4	Akr1c12_predicted	aldo-keto reductase family 1, member C12 (predicted)			
1384639_at	51.6	49.0	1.1	Dp1l1_predicted	deleted in polyposis 1-like 1 (predicted)			
1368627_at	49.7	35.7	1.4	Rgn	regucalcin			
1368366_at	47.1	42.1	1.1	Cml2	Camello-like 2			
1387234_at	44.2	42.4	1.0	Azgp1	alpha-2-glycoprotein 1, zinc			
1368163_at	43.3	43.2	1.0	Dpp4	dipeptidylpeptidase 4			
1372841_at	41.7	32.3	1.3	Dp1l1_predicted	deleted in polyposis 1-like 1 (predicted)			
1398255_at	38.7	20.9	1.8	Slc15a2	solute carrier family 15 (H+/peptide transporter), member 2			
1367905_at	38.2	29.7	1.3	Enpp3	ectonucleotide pyrophosphatase/phosphodiesterase 3			

Table 2-4. (continued)

Probe sets	medulla/ papilla	cortex/ papilla	medulla/ cortex	Gene Symbol	Gene Name	channel transporter	Metabolic enzymes	cytoskeleton/ extracellular matrix
1370688_at	33.0	27.8	1.2	Gclc	glutamate-cysteine ligase, catalytic subunit			
1368374_a_at	31.9	29.2	1.1	Ggt1	gamma-glutamyltransferase 1			
1387218_at	30.2	23.1	1.3	Tff3	trefoil factor 3			
1370714_a_at	30.0	17.1	1.8	Siat1	sialyltransferase 1			
1373773_at	29.4	25.3	1.2	Gpm6a	glycoprotein m6a			
1387357_at	28.1	24.8	1.1	Tmlhe	trimethyllysine hydroxylase, epsilon			
1380962_at	27.6	23.3	1.2	Ace2	Angiotensin I converting enzyme (peptidyl-dipeptidase A) 2			
1370144_at	26.9	18.1	1.5	Gtpbp4 /// LOC364763 /// LOC498786	G protein-binding protein CRFG /// similar to GTP-binding protein NGB /// similar to GTP-binding protein NGB			
1387209_at	24.6	22.3	1.1	Rgpr	regucalcin gene promotor region related protein			
1367838_at	24.5	17.9	1.4	Cth	CTL target antigen			
1390855_at	23.9	12.7	1.9	Prep	Prolyl endopeptidase			
1371913_at	23.4	11.8	2.0	Tgfbi	transforming growth factor, beta induced			
1368234_at	23.4	12.1	1.9	Prep	prolyl endopeptidase			
1388145_at	22.5	22.4	1.0	Tnxa	tenascin XA			
1370365_at	22.3	14.3	1.6	Gss	glutathione synthetase			
1381350_at	20.3	17.4	1.2	Idb4	Inhibitor of DNA binding 4			
1394022_at	18.0	11.8	1.5	Idb4	inhibitor of DNA binding 4			
1368164_at	17.9	14.7	1.2	Blvra	biliverdin reductase A			
1379300_at	17.5	17.0	1.0	Chst2_predicted	carbohydrate sulfotransferase 2 (predicted)			
1387296_at	17.1	15.7	1.1	Cyp2j4	cytochrome P450, family 2, subfamily J, polypeptide 4			
1377408_at	16.9	16.2	1.0	Pla2g6	phospholipase A2, group VI			
1369407_at	16.8	10.4	1.6	Tnfrsf11b	tumor necrosis factor receptor superfamily, member 11b (osteoprotegerin)			

Table 2-4. (continued)

Probe sets	medulla/ papilla	cortex/ papilla	medulla/ cortex	Gene Symbol	Gene Name	channel transporter	Metabolic enzymes	cytoskeleton/ extracellular matrix
1382868_at	16.5	9.9	1.7	Sema6a_predicted	sema domain, transmembrane domain (TM), and cytoplasmic domain, (semaphorin) 6A (predicted)			
1387819_at	16.3	16.3	1.0	Ela1	elastase 1, pancreatic			
1372523_at	16.3	14.9	1.1	Gclc	glutamate-cysteine ligase, catalytic subunit			
1387941_s_at	16.1	14.6	1.1	Pla2g6	phospholipase A2, group VI			
1372750_at	3.7	0.2	15.9	Fst	Follistatin			
1370072_at	15.6	12.1	1.3	Mme	membrane metallo endopeptidase			
1387966_at	15.5	11.4	1.4	Asrgl1	asparaginase-like sperm autoantigen			
1384831_at	15.1	11.7	1.3	Slc7a13_predicted	solute carrier family 7, (cationic amino acid transporter, y+ system) member 13 (predicted)			
1368189_at	14.8	11.3	1.3	Dhcr7	7-dehydrocholesterol reductase			
1367798_at	14.5	11.2	1.3	Ahcy	S-adenosylhomocysteine hydrolase			
1371059_at	14.5	14.4	1.0	Prkar2a	protein kinase, cAMP-dependent, regulatory, type 2, alpha			
1369158_at	14.4	14.3	1.0	Casr	calcium-sensing receptor			
1370030_at	14.1	11.5	1.2	Gclm	glutamate cysteine ligase, modifier subunit			
1398350_at	14.0	12.9	1.1	Basp1	brain abundant, membrane attached signal protein 1			
1369728_at	13.7	10.7	1.3	Hist1h4m_predicted	histone 1, H4m (predicted)			
1387223_at	13.6	12.2	1.1	Aadat	aminoadipate aminotransferase			
1370529_a_at	12.8	7.7	1.7	Pld1	phospholipase D1			
1384603_at	12.8	9.8	1.3	Abca4_predicted	ATP-binding cassette, sub-family A (ABC1), member 4 (predicted)			
1369494_a_at	12.0	6.6	1.8	Ghrhr	growth hormone releasing hormone receptor			
1367729_at	11.9	11.4	1.0	Oat	ornithine aminotransferase			

Table 2-4. (continued)

Probe sets	medulla/ papilla	cortex/ papilla	medulla/ cortex	Gene Symbol	Gene Name	channel transporter	Metabolic enzymes	cytoskeleton/ extracellular matrix
1374565_at	11.8	9.7	1.2	Nek6	NIMA (never in mitosis gene a)-related expressed kinase 6			
1368431_at	11.6	10.3	1.1	Hpn	hepsin			
1382274_at	11.5	5.5	2.1	Rarres1_predicted	retinoic acid receptor responder (tazarotene induced) 1 (predicted)			
1374871_at	11.2	7.3	1.5	Asrgl1	asparaginase-like sperm autoantigen			
1392965_a_at	11.0	2.3	4.8	Smoc2_predicted	SPARC related modular calcium binding 2 (predicted)			
1370163_at	11.0	6.5	1.7	Odc1	ornithine decarboxylase 1			
1390208_at	10.7	10.7	1.0	Htatip2_predicted	HIV-1 Tat interactive protein 2 (predicted)			
1370530_a_at	10.6	5.7	1.9	Pld1	phospholipase D1			
1376852_at	10.5	8.3	1.3	Mccc1_predicted	methylcrotonoyl-Coenzyme A carboxylase 1 (alpha) (predicted)			
1369184_at	10.5	6.8	1.5	Cldn16	claudin 16			
1385970_at	10.4	9.5	1.1	Sh2bp1_predicted	SH2 domain binding protein 1 (tetratricopeptide repeat containing) (predicted)			
1383742_at	10.1	9.4	1.1	Snx7_predicted	sorting nexin 7 (predicted)			

After selection by ANOVA ($p<0.01$) for the data of percellome normalization, genes maximally expressed in medulla were selected. The genes were aligned in the order of the ratio to the lower expression value, either in papilla or in cortex. As the genes listed here are expressed in medulla and cortex to a similar extent, exceptional cases (ratio >3) are shaded in the medulla/cortex column. The genes categorized to "channel/transporters", "metabolic enzymes", or "cytoskeleton/extracellular matrix" are also shaded. Proteases or enzymes involving signal transduction are not included in the category of "metabolic enzymes". For simplicity, genes with less than 10 fold specificity are omitted.

Table 2-5. A list of probe sets specifically expressed in cortex of kidney

Probe sets	cortex/ papilla	medulla/ papilla	cortex/ medulla	Gene Symbol	Gene Name	channel trasnporter	Metabolic enzymes	cytoskeleton/ extracellular matrix
1387314_at	312.0	259.8	1.2	Sult1b1	sulfotransferase family 1B, member 1			
1387820_at	284.9	14.7	19.4	Klk7	kallikrein 7			
1388172_at	245.4	110.3	2.2	Ust1r	integral membrane transport UST1r			
1368064_a_at	230.1	19.6	11.8	Ddc	dopa decarboxylase			
1390591_at	224.2	166.1	1.3	Slc17a3	Na/Pi cotransporter 4			
1368467_at	217.1	117.6	1.8	Cyp4f2	cytochrome P450, family 4, subfamily F, polypeptide 2			
1368600_at	210.7	75.0	2.8	Slc26a1	solute carrier family 26 (sulfate transporter), member 1			
1396039_at	202.5	188.6	1.1	Slc22a12_predicted	solute carrier family 22 (organic anion/cation transporter), member 12 (predicted)			
1387230_at	193.9	13.2	14.7	Slc12a3	solute carrier family 12, member 3			
1368245_at	192.4	134.7	1.4	Upb1	ureidopropionase, beta			
1367917_at	192.3	124.6	1.5	Cyp2d26	cytochrome P450, family 2, subfamily d, polypeptide 26			
1367871_at	187.8	32.3	5.8	Cyp2e1	cytochrome P450, family 2, subfamily e, polypeptide 1			
1376267_at	185.1	13.9	13.4	Slc16a6	Solute carrier family 16 (monocarboxylic acid transporters), member 6			
1384877_at	183.4	73.9	2.5	Aqp11	aquaporin 11			
1398282_at	174.5	75.2	2.3	Kynu	kynureninase (L-kynurenine hydrolase)			
1370547_at	169.5	56.4	3.0	Pzp	pregnancy-zone protein			
1368563_at	149.7	96.7	1.5	Aspa	aspartoacylase			
1383111_at	149.3	60.1	2.5	Acmsd	2-amino-3-carboxymuconate-6-semialdehyde decarboxylase			
1370991_at	146.7	32.6	4.5	Cml3	camello-like 3			
1387188_at	144.5	86.8	1.7	RGD:620099	solute carrier family 17 (sodium phosphate), member 1			
1370936_at	143.4	91.3	1.6	Dmgdh	dimethylglycine dehydrogenase precursor			
1367804_at	142.8	21.8	6.5	Sap	serum amyloid P-component			

Table 2-5. (continued)

Probe sets	cortex/ papilla	medulla/ papilla	cortex/ medulla	Gene Symbol	Gene Name	channel trasnporter	Metabolic enzymes	cytoskeleton/ extracellular matrix
1368915_at	141.5	87.2	1.6	Kmo	kynurenine 3-monooxygenase (kynurenine 3-hydroxylase)			
1398511_at	138.7	16.8	8.3	Susd2_predicted	sushi domain containing 2 (predicted)			
1387851_at	129.9	78.3	1.7	Pter	phosphotriesterase related			
1376051_at	127.0	63.2	2.0	Cryl1	crystallin, lamda 1			
1384112_at	125.1	80.6	1.6	Nt5	5 nucleotidase			
1393894_at	123.8	94.1	1.3	RGD:628846	cytochrome P450, 4a12			
1370725_a_at	116.9	15.4	7.6	G6pc	glucose-6-phosphatase, catalytic			
1386980_at	116.6	64.2	1.8	Apom	apolipoprotein M			
1377125_at	116.3	28.0	4.2	Dnajc6_predicted	DnaJ (Hsp40) homolog, subfamily C, member 6 (predicted)			
1368317_at	114.8	70.5	1.6	Aqp7	aquaporin 7			
1370615_at	114.4	28.0	4.1	RGD:708417	UDP-glucuronosyltransferase			
1368236_at	113.4	105.5	1.1	Mep1a	meprin 1 alpha			
1373386_at	113.2	110.8	1.0	Gjb2	gap junction membrane channel protein beta 2			
1369636_at	112.6	41.2	2.7	Sord	sorbitol dehydrogenase			
1368521_at	110.8	46.3	2.4	Napsa	napsin A aspartic peptidase			
1368150_at	110.4	78.2	1.4	Slc27a2 /// LOC497779	solute carrier family 27 (fatty acid transporter), member 2 /// hypothetical gene supported by NM_031736			
1369635_at	109.5	42.4	2.6	Sord	sorbitol dehydrogenase			
1368180_s_at	107.9	73.9	1.5	Gsta2	glutathione-S-transferase, alpha type2			
1368190_at	105.6	12.1	8.7	Ren1	renin 1			
1377051_at	104.7	17.9	5.8	Mpv17l_predicted	Mpv17 transgene, kidney disease mutant-like (predicted)			
1387336_at	102.7	89.7	1.1	Nat8	N-acetyltransferase 8 (camello like)			
1387631_at	102.4	59.8	1.7	Hpgd	15-hydroxyprostaglandin dehydrogenase			
1379885_at	100.7	91.4	1.1	Fmo4	flavin containing monooxygenase 4			
1368659_at	100.0	60.0	1.7	Agxt2	alanine-glyoxylate aminotransferase 2			
1370259_a_at	99.6	31.1	3.2	Pthr1	parathyroid hormone receptor 1			

Table 2-5. (continued)

Probe sets	cortex/ papilla	medulla/ papilla	cortex/ medulla	Gene Symbol	Gene Name	channel trasnporter	Metabolic enzymes	cytoskeleton/ extracellular matrix
1368188_at	94.6	25.6	3.7	Hpd	4-hydroxyphenylpyruvic acid dioxygenase			
1369200_at	93.4	56.3	1.7	Nt5	5 nucleotidase			
1387053_at	90.3	37.7	2.4	Fmo1	flavin containing monooxygenase 1			
1388569_at	88.3	50.7	1.7	Serpinf1	serine (or cysteine) proteinase inhibitor, clade F), member 1			
1390857_at	87.5	26.6	3.3	Xylb_predicted	xylulokinase homolog (H. influenzae) (predicted)			
1387375_at	86.9	64.4	1.4	Khk	ketohexokinase			
1387034_at	86.3	17.7	4.9	Pah	phenylalanine hydroxylase			
1397740_at	86.3	51.0	1.7	Sfxn1_predicted	sideroflexin 1 (predicted)			
1368736_at	84.2	18.9	4.4	Tsx	testis specific X-linked gene			
1398514_at	82.6	81.3	1.0	Hgd_predicted	homogentisate 1, 2-dioxygenase (predicted)			
1368515_at	81.1	7.2	11.3	Epb4.1l3	erythrocyte protein band 4.1-like 3			
1368794_at	81.0	78.4	1.0	Haao	3-hydroxyanthranilate 3,4-dioxygenase			
1370964_at	80.8	27.0	3.0	Ass	arginosuccinate synthetase			
1368077_at	79.6	43.0	1.9	Fbp1	fructose-1,6-biphosphatase 1			
1370397_at	77.6	68.8	1.1	Cyp4a14	cytochrome P450, family 4, subfamily a, polypeptide 14			
1368397_at	76.3	36.6	2.1	Ugt2b5 /// Ugt2b4	UDP-glucuronosyltransferase 2 family, member 5 /// UDP glycosyltransferase 2 family, polypeptide B4			
1368282_at	74.3	24.9	3.0	Dpep1	dipeptidase 1 (renal)			
1395026_at	73.7	59.0	1.2	Fmo4	flavin containing monooxygenase 4			
1380577_at	70.1	53.6	1.3	Abcg2	ATP-binding cassette, sub-family G (WHITE), member 2			
1387339_at	69.4	19.2	3.6	Sepp1	selenoprotein P, plasma, 1			
1382913_at	68.9	16.8	4.1	Cttnbp2	cortactin binding protein 2			

Table 2-5. (continued)

Probe sets	cortex/ papilla	medulla/ papilla	cortex/ medulla	Gene Symbol	Gene Name	channel trasnporter	Metabolic enzymes	cytoskeleton/ extracellular matrix
1376327_at	68.9	24.2	2.8	Tnfrsf14_predicted	tumor necrosis factor receptor superfamily, member 14 (herpesvirus entry mediator) (predicted)			
1368178_at	66.6	32.4	2.1	Pdzk1	PDZ domain containing 1			
1377672_at	66.3	37.3	1.8	Sult1c2	sulfotransferase family, cytosolic, 1C, member 2			
1387084_at	65.5	55.5	1.2	Dpp4	dipeptidylpeptidase 4			
1374512_at	63.7	35.5	1.8	Cdh7	Cadherin 7, type 2			
1371824_at	63.6	40.8	1.6	Ak3l1	adenylate kinase 3-like 1			
1369412_a_at	63.4	37.9	1.7	Slc19a1	solute carrier family 19, member 1			
1373803_a_at	63.1	39.2	1.6	Ghr	growth hormone receptor			
1387259_at	62.9	29.4	2.1	Cdh2 /// LOC497718	cadherin 2 /// hypothetical gene supported by NM_031333			
1389166_at	62.8	31.1	2.0	Cib2_predicted	calcium and integrin binding family member 2 (predicted)			
1371354_at	62.1	8.0	7.8	Tncc_predicted	troponin C, cardiac/slow skeletal (predicted)			
1372672_at	58.8	36.8	1.6	Qprt_predicted	quinolinate phosphoribosyltransferase (predicted)			
1369491_at	58.4	36.1	1.6	Dao1	D-amino acid oxidase			
1387111_at	57.3	33.4	1.7	Ddah1	dimethylarginine dimethylaminohydrolase 1			
1367988_at	57.1	22.1	2.6	Cyp2c23	cytochrome P450, family 2, subfamily c, polypeptide 23			
1368607_at	56.5	51.1	1.1	RGD:628846	cytochrome P450, 4a12			
1370881_at	55.8	22.9	2.4	Tst	thiosulfate sulfurtransferase			
1369259_at	55.6	28.4	2.0	Dio1	deiodinase, iodothyronine, type I			
1376709_at	55.2	42.5	1.3	Slc39a8_predicted	solute carrier family 39 (metal ion transporter), member 8 (predicted)			
1387013_at	55.2	27.3	2.0	Tmem27	kidney-specific membrane protein			
1387808_at	54.9	5.1	10.8	Slc7a7	solute carrier family 7 (cationic amino acid transporter, y+ system), member 7			

Table 2-5. (continued)

Probe sets	cortex/ papilla	medulla/ papilla	cortex/ medulla	Gene Symbol	Gene Name	channel trasnporter	Metabolic enzymes	cytoskeleton/ extracellular matrix
1368283_at	54.7	29.8	1.8	Ehhadh	enoyl-Coenzyme A, hydratase/3-hydroxyacyl Coenzyme A dehydrogenase			
1373337_at	53.4	22.5	2.4	Grhpr_predicted	glyoxylate reductase/hydroxypyruvate reductase (predicted)			
1383654_a_at	53.2	14.7	3.6	Fnsk	similar to fructosamine-3-kinase			
1368924_at	51.8	42.4	1.2	Ghr	growth hormone receptor			
1368092_at	50.7	35.9	1.4	Fah	fumarylacetoacetate hydrolase			
1380171_at	49.4	39.5	1.3	Adra2b	Adrenergic receptor, alpha 2b			
1367952_at	45.8	26.5	1.7	Lrp2	low density lipoprotein receptor-related protein 2			
1369705_at	44.1	42.6	1.0	RGD:621651	X transporter protein 3			
1368680_a_at	43.6	25.3	1.7	Slc34a1	solute carrier family 34 (sodium phosphate), member 1			
1367627_at	43.5	14.8	2.9	Gatm	glycine amidinotransferase (L-arginine:glycine amidinotransferase)			
1379950_at	42.9	37.7	1.1	Cml2	Camello-like 2			
1367775_at	42.6	32.3	1.3	Amacr	alpha-methylacyl-CoA racemase			
1388176_at	42.4	24.0	1.8	Cml5	camello-like 5			
1368322_at	42.1	8.2	5.1	Sod3	superoxide dismutase 3, extracellular			
1372264_at	42.1	15.9	2.7	Pck1	phosphoenolpyruvate carboxykinase 1			
1397647_at	41.9	17.1	2.5	Slc25a15_predicted	solute carrier family 25 (mitochondrial carrier; ornithine transporter) member 15 (predicted)			
1369073_at	41.9	12.2	3.4	Nr1h4	nuclear receptor subfamily 1, group H, member 4			
1368877_at	41.6	13.7	3.0	Znf354a	zinc finger protein 354A			
1390119_at	41.4	4.9	8.4	Sfrp2	secreted frizzled-related protein 2			
1367774_at	41.1	31.8	1.3	Gsta5	glutathione S-transferase A5			
1376191_at	40.1	27.6	1.5	Hpgd	15-hydroxyprostaglandin dehydrogenase			

Table 2-5. (continued)

Probe sets	cortex/ papilla	medulla/ papilla	cortex/ medulla	Gene Symbol	Gene Name	channel trasnporter	Metabolic enzymes	cytoskeleton/ extracellular matrix
1397526_at	39.3	23.5	1.7	Gcdh_predicted	glutaryl-Coenzyme A dehydrogenase (predicted)			
1374384_at	38.8	16.3	2.4	Crygc	Crystallin, gamma C			
1387491_at	38.5	10.9	3.5	Gyk	glycerol kinase			
1386944_a_at	38.3	7.7	5.0	G6pc	glucose-6-phosphatase, catalytic			
1367999_at	37.7	22.6	1.7	Aldh2	aldehyde dehydrogenase 2			
1369182_at	37.6	9.6	3.9	F3	coagulation factor 3			
1382975_at	37.4	20.8	1.8	Ceacam1	CEA-related cell adhesion molecule 1			
1374200_at	36.1	16.7	2.2	Slc29a3	solute carrier family 29 (nucleoside transporters), member 3			
1369973_at	35.6	9.6	3.7	Xdh /// LOC497811	xanthine dehydrogenase /// hypothetical gene supported by NM_017154			
1372306_at	35.4	22.9	1.5	Ethe1_predicted	ethylmalonic encephalopathy 1 (predicted)			
1370818_at	34.6	12.5	2.8	Decr2	2-4-dienoyl-Coenzyme A reductase 2, peroxisomal			
1397797_at	33.3	29.3	1.1	Tigd3	Tigger transposable element derived 3 (predicted)			
1372323_at	32.9	23.4	1.4	Sardh	sarcosine dehydrogenase			
1368412_a_at	32.5	5.3	6.1	Ptpro	protein tyrosine phosphatase, receptor type, O			
1390036_at	32.5	6.0	5.4	Slc16a6	solute carrier family 16 (monocarboxylic acid transporters), member 6			
1397744_at	32.5	22.2	1.5	Sardh	Sarcosine dehydrogenase			
1368642_at	32.4	19.5	1.7	Cdh2 /// LOC497718	cadherin 2 /// hypothetical gene supported by NM_031333			
1373188_at	32.0	12.2	2.6	Scn4b	sodium channel, voltage-gated, type IV, beta			
1373667_at	31.8	14.0	2.3	Ccbl1_predicted	cysteine conjugate-beta lyase (predicted)			
1372031_at	31.7	7.5	4.2	Dab2	Disabled homolog 2 (Drosophila)			
1390585_at	31.7	10.9	2.9	Masp1	mannan-binding lectin serine peptidase 1			

Table 2-5. (continued)

Probe sets	cortex/ papilla	medulla/ papilla	cortex/ medulla	Gene Symbol	Gene Name	channel trasnporter	Metabolic enzymes	cytoskeleton/ extracellular matrix
1386981_at	31.6	3.7	8.4	Slc16a1	solute carrier family 16 (monocarboxylic acid transporters), member 1			
1368253_at	31.5	28.7	1.1	Gamt	guanidinoacetate methyltransferase			
1388537_at	31.4	15.2	2.1	Nipsnap1 _predicte d	4-nitrophenylphosphatas e domain and non-neuronal SNAP25-like protein homolog 1 (C. elegans) (predicted)			
1387165_at	31.1	4.4	7.1	Maf	v-maf musculoaponeurotic fibrosarcoma (avian) oncogene homolog (c-maf)			
1384273_at	30.9	10.2	3.0	Carkl_pr edicted	carbohydrate kinase-like (predicted)			
1380393_at	30.9	30.7	1.0	Cryz_pre dicted	crystallin, zeta (predicted)			
1393947_at	30.7	12.7	2.4	Slc25a15 _predicte d	solute carrier family 25 (mitochondrial carrier; ornithine transporter) member 15 (predicted)			
1378197_at	30.4	9.5	3.2	KIFC2	kinesin family member C2			
1379582_a_a t	30.1	14.5	2.1	Ccna2	cyclin A2			
1382434_at	30.0	23.5	1.3	Entpd5	ectonucleoside triphosphate diphosphohydrolase 5			

After selection by ANOVA ($p<0.01$) for the data of percellome normalization, genes maximally expressed in cortex were selected. The genes were aligned in the order of the ratio to the lower expression value, either in papilla or in medulla. Among the genes listed here, relatively specific ones for cortex (ratio >3) are shaded in the cortex/medulla column. The genes categorized to “channel/transporters”, “metabolic enzymes”, or “cytoskeleton/extracellular matrix” are also shaded. Proteases or enzymes involving signal transduction are not included in the category of “metabolic enzymes”. For simplicity, genes with less than 30 fold specificity are omitted.

Table 2-6. Regionally specific genes in rat kidney.

	Channel/transporter	Metabolizing enzymes	Cytoskeleton/ extracellular matrix	Others of interest
Papilla	Slco4a1, Aqp3, Aqp4, Fxyd4, Slc4a11, Clcnk1, bsnd	Ptgs1, Ptgs2, Aldh1a3, Akr1b4, Ugt8, Ltb4dh	Capg, Plekhb1, Coll8a1, Spnb3, Hs3st1, Krt1-18	Hspa2, Hspa1a, Hspb1
Medulla	Scl21a1, Scl21a13, Slc23a3, Slc21a9, UST5r, Scl6a18, Scl38a3, Slc22a2, Slc7a12, Slc15a2	CYP2d9, CYP2c, Hnmt, Pklr, Fmo3, Dhrs7, Akr1c12, Gclc, Ggt1, Tmlhe		Prlr, Ace2
Cortex	Ust1r, Slc17a3, Slc26a1, Slc22a12, Slc12a3, Slc16a6, Aqp11, Aqp7, Gjb2, Slc27a2	Sult1b1, Klk7, Ddc, CYP2d26, CYP2e1, CYP4f2, Upb1, Aspa, Acmsd, Dmgdh, Kmo		Ren1

Genes categorized in channel/transporter, metabolizing enzyme, and cytoskeleton/extracellular matrix from high rank in Tables 2-3, 2-4, 2-5 are summarized by using gene symbols which can be referred to in the preceding tables. Interesting genes discussed in the text are included as “others”.

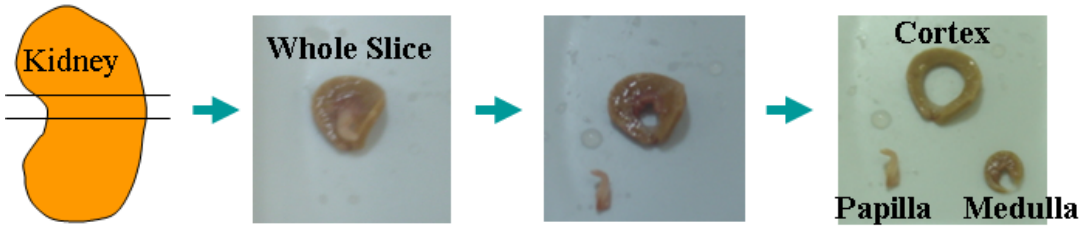

Animal No. 1 ⇒ Whole slice No. 1
Animal No. 2 ⇒ Whole slice No. 2
Animal No. 3 ⇒ Whole slice No. 3
Animal No. 4 ⇒ Papilla No. 4, Medulla No. 4, Cortex No. 4
Animal No. 5 ⇒ Papilla No. 5, Medulla No. 5, Cortex No. 5
Animal No. 6 ⇒ Papilla No. 6, Medulla No. 6, Cortex No. 6

Fig. 2-1.
Sampling and preparation of kidney for GeneChip analysis.

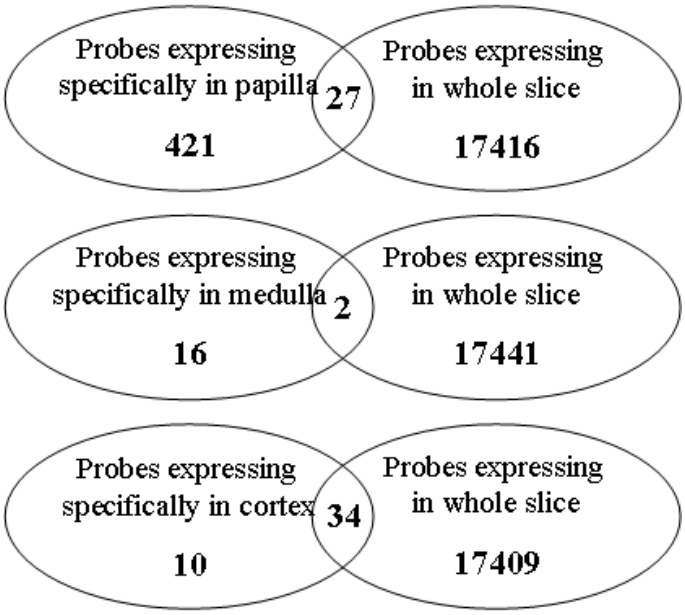

Fig. 2-2.

Venn diagram of region-specific genes extracted by flags (present, absent and marginal call). The probes having "present call" in all samples of papilla and "absent call" in all samples of medulla and cortex were considered to be papilla-specific. The medulla- and cortex-specific probes were also extracted in the same manner and examined whether they were absent in the whole slice.

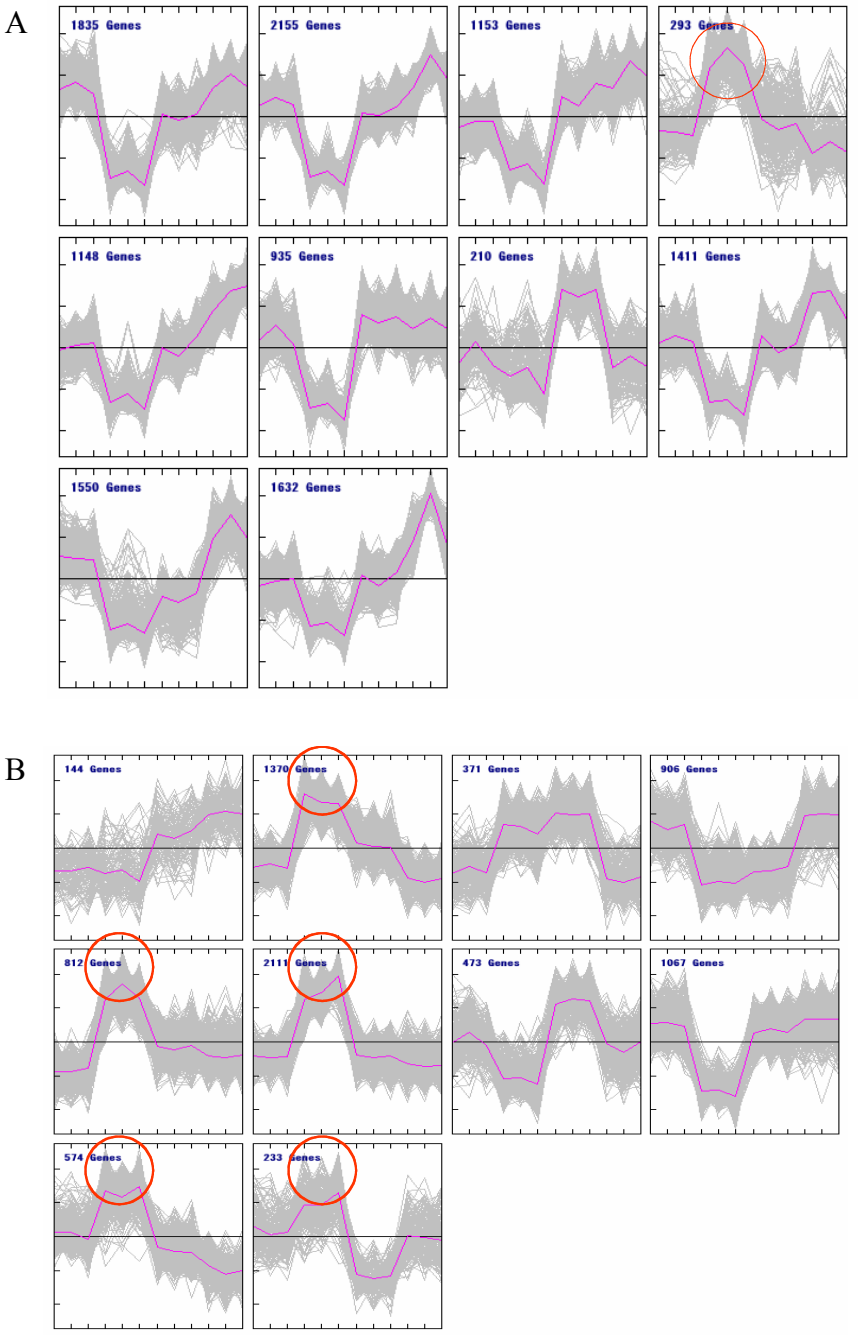

Fig. 2-3.

K-means clustering of genes expressed in papilla, medulla, cortex, and whole slice of kidney. Data were processed by percellome normalization (A) or global mean normalization (B), and then converted into z-scores. K-means clustering (Euclidean, 10 clusters) was performed with MeV version 3.1 (The Institute for Genomic Research, Rockville, MD, USA). In each cluster, individual samples are aligned from left to right: whole slice (3), papilla (3), medulla (3), and cortex (3). Red circles indicate where papilla showed specifically high expression values.

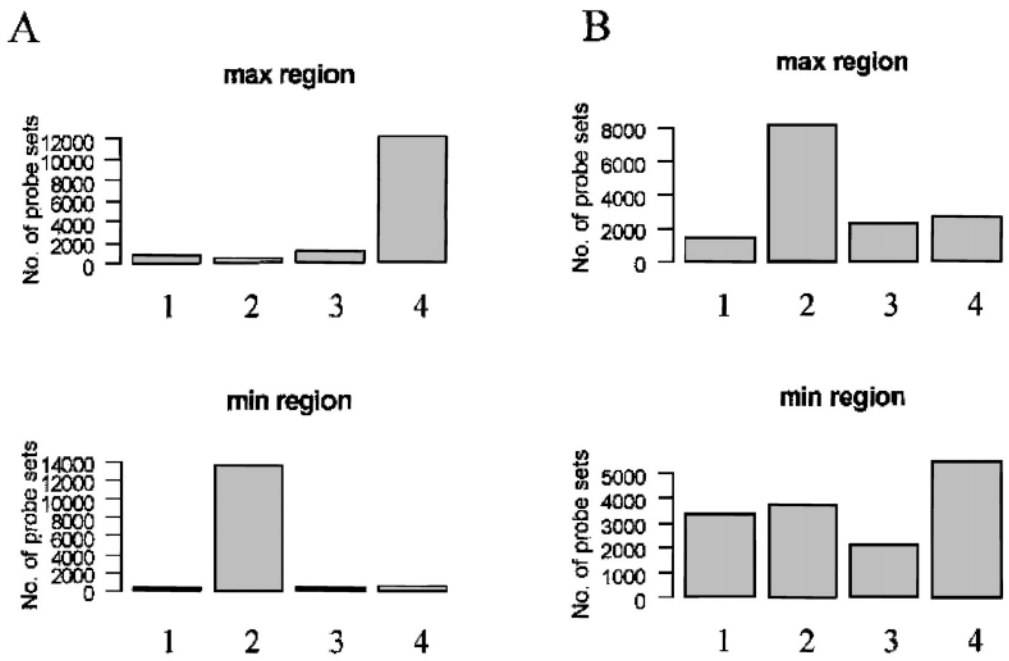

Fig. 2-4.

The numbers of probe sets where their expression was maximal or minimal in whole slice, papilla, medulla, or cortex of kidney. After normalization by percellome (A) or global mean (B), probes with absent call in all samples were eliminated, and the numbers of probe sets with maximal (upper panels) or minimal (lower panels) were counted for each region, i.e., whole slice (1), papilla (2), medulla (3), and cortex (4).

Chapter 3

Carbohydrate Profile in the Kidneys of Hereditary Nephrotic Mice (ICGN Strain)

Abstract.

The ICR-derived glomerulonephritis (ICGN) mice consist of heterozygous and homozygous groups and are considered to be a good model for human idiopathic nephrotic syndrome. To fully understand pathological process of nephrotic syndrome in ICGN mice before transcriptome analysis of these mice (chapter 4), I evaluated progress of nephrotic syndrome in male heterozygous and homozygous ICGN mice throughout their lifetime (at 10, 30 and 50 week of age) with clinical chemistry, urinary and histopathological examination and histochemical quantification of total and type I collagens. Additionally, I histologically evaluated changes in the cell-surface carbohydrate structures in the kidneys using 24 types of lectins. ICR mice were also evaluated as healthy controls.

In heterozygous ICGN mice, there were no significant differences in serum albumin, creatinine, total cholesterol, blood urea nitrogen (BUN) and renal total and type I collagen levels as compared with ICR mice at any time point examined. Histopathological examination detected moderate expansion of mesangial matrix. In homozygous ICGN mice, aged animal (50 weeks) manifested clinical abnormalities such as the exercise intolerance, pale ears, weight loss as well as edema. The nephrotic state progressed in an age-dependent manner. Severe albuminuria and hypoalbuminemia, marked increases in serum creatinine and BUN, and significant increases in renal total and type I collagen levels were observed at 30 and 50 week of age. Histopathological examination detected expansion of the mesangial areas with an apparent increase in the mesangial matrix, appearance of cysts, extension of renal tubules and infiltration of inflammatory cells in the kidney of 50-week-old animals. Such histopathological abnormalities progressed in an age-dependent manner. With these results, I fully understood pathological process of nephrotic syndrome in ICGN mice before transcriptome analysis of ICGN mice.

In evaluation of changes in the cell-surface carbohydrate structures in ICGN mice kidneys, bandeiraea simplicifolia lectin-I (BSL-I), which specifically binds to α-D-galactopyranosyl groups, showed positive staining in the glomeruli of ICGN mice, but not in those of ICR mice. Positive BSL-I staining was observed only in distal tubules of homozygous ICGN mice. Lectin blotting for BSL-I demonstrated characteristic glycoproteins (45, 58 and 64 kD) in ICGN but not in ICR mice, and the levels of these molecules augmented in homozygous ICGN mice with the progression of renal failure. In conclusion, lectin histochemistry provided useful information for the diagnosis and prognosis of nephrotic lesions. Characteristic BSL-I binding glycoproteins may be pathogenic factors which cause renal disease in ICGN mice and are good tools to investigate the molecular mechanism of renal disorders in ICGN mice.

Introduction

Hereditary spontaneous nephrotic mice (ICGN mice), a novel mutant mouse strain derived from the ICR strain, were established in the National Institute of Infectious Diseases (Ogura *et al*., 1989a; Ogura *et al*., 1989b). The ICGN mice consist of homozygous (100% of mice with severe symptoms) and heterozygous groups (approximately 40% of mice with symptoms; health female ICGN mice x homozygous male ICGN). All homozygous ICGN mice show proteinuria at a young age and develop severe hypoproteinemia and hyperlipidemia, while some of the mice also develop systemic edema (Ogura *et al*., 1994). Histopathological analyses of the ICGN mice kidney showed glomerular lesions consisting of thickened glomerular basement membrane (GBM) with irregular spike-like protrusions and enlargement of the mesangial area without cellular proliferation (Ogura *et al*., 1989b). Ultrastructurally, multilaminar splitting of the lamina densa of the thickened GBM and fusion of the epithelial foot processes were noted (Ogura *et al*., 1991; Ogura *et al*., 1990; Ogura *et al*., 1995). Such ultrastructural glomerular alterations were already observed in the kidneys of neonatal ICGN mice (4–6 days after birth) (Ogura *et al*., 1995). Deletion mutation of tensin 2 (*Tns2*), a focal adhesion molecule, has been suggested to be responsible for nephrotic syndrome in ICGN mice (Cho *et al.*, 2006), however, existence of other associative factors has been suggested (Nishino *et al*., 2010; Nishino *et al.*, 2012).

Lectins have been widely used as histopathological probes, and it has been revealed that changes in cell-surface carbohydrates detected by lectin staining are good markers for histopathological diagnosis (Muramatsu, 1988). Cell-surface carbohydrates play important roles in cell recognition and interactions during cellular differentiation, and changes in cell-surface carbohydrates have been observed in various pathological conditions in both humans and experimental animals. For instance,

tumor cells with malignant phenotypes show neoplastic transformation-related changes in oligosaccharide biosynthesis (Tucker-Burden *et al*., 2012; Li *et al*., 2013). Cell-surface carbohydrates are reliable markers for histopathological diagnosis, and lectins recognizing these macromolecules or cell-surface carbohydrates have been extensively used as biochemical and histopathological probes in cell biology and pathology (Arab *et al.*, 2010; de Melo-Junior *et al.*, 2011; Rego *et al*., 2013).

In the present study, to fully understand pathological process of nephrotic syndrome in ICGN mice before transcriptome analysis of these mice (chapter 4), I evaluated progress of nephrotic syndrome in male heterozygous and homozygous ICGN mice throughout their lifetime (at 10, 30 and 50 week of age) with clinical chemistry, urinary and histopathological examination. Additionally, to identify the key factors in the pathogenesis and the markers for renal failure, I examined differences in cell-surface carbohydrate structures in the kidneys using 24 kinds of biotinylated lectins as histopathological probes.

Materials and Methods

Animals and tissue preparation

Nephrotic mice (ICGN strain) were prepared by mating between homozygous males (nep/nep) and heterozygous females (nep/-) at the laboratory of National Institute of Infectious Diseases. Ten-, 30- and 50-week-old male homozygous and heterozygous ICGN mice and age-matched male ICR mice purchased from Clea Japan (Tokyo, Japan) were used. All animals were given a standard diet (CM, Oriental Yeast Co., Tokyo, Japan) and tap water ad libitum in an air conditioned room (23 ± 1°C), under controlled lighting conditions (12L/12D). They received humane care as outlined in the "Guide for the Care and Use of Laboratory Animals" (Kyoto University Animal Care Committee according to NIH #86–23; revised 1985). For clinical biochemical analyses, urine samples during the 24 hr before sacrifice (24 hr urine samples) were collected, and blood samples were obtained from the cervical vein under ether anesthesia. Serum was prepared by centrifugation at 1,000 rpm for 10 min. The animals were killed under deep ether anesthesia, and then the kidneys were rapidly removed. The left kidney was immediately fixed in 10% neutral-buffered formalin (pH 7.4) for conventional histopathological evaluation and lectin histochemistry, while the right kidney was frozen in liquid nitrogen for histochemical measurement of total and type I collagens and for lectin blot analysis.

Clinical biochemical analysis

To evaluate nephrotic state, 24 hr urine and serum samples were examined on the basis of the following biochemical parameters. Urinary and serum albumin (uAlb and sAlb, respectively) levels were measured by a bromo-cresol green method using an A/GB test kit (Wako Pure Chemical Co., Osaka, Japan) to assess the severity of albuminuria and hypoalbuminemia. To assess the loss of renal function, serum

creatinine (sCr) and blood urea nitrogen (BUN) levels were measured by Jaffé's method with a creatinine test kit (Wako) and by the urease indophenol method with a nitrogen-B test kit (Wako), respectively. To evaluate the degree of hypercholesteremia, the serum total cholesterol (sTC) level was determined by an enzymatic method with a Cholesterol-E test kit (Wako). All procedures were performed according to the manufacturers' protocols.

Renal histopathology

After fixation, the kidney samples were dehydrated through a graded ethanol series and embedded in Histosec (Merck Co., Darmstadt, Germany). Sections 3 μm thick were prepared on a microtome, mounted on glass slides precoated with 3-aminopropyltriethoxysilane (Aldrich Chemical, Milwaukee, WI, USA), deparaffinized with xylene and rehydrated through a graded ethanol series. For conventional histopathological evaluation, some of the sections were stained with hematoxylin and eosin according to the standard method. As previously reported (Manabe *et al*., 1994; Uchio *et al*., 1999; Uchio *et al*., 2000), the extent of glomerulosclerosis was expressed as the degree of collagen deposition, which was assessed on sections stained with Sirius red solution (saturated picric acid in distilled water containing 0.1% Sirius red F3B; BDH Chemicals Ltd., Poole, UK) (Manabe *et al*., 1993; Manabe *et al*., 1994; Manabe *et al*., 1995). All slides were mounted with Entellan (Merck), and examined by light microscopy at least three sections/mouse. In each kidney specimen, approximately 100 glomeruli were selected at random and evaluated by light microscopy as described previously (Manabe *et al*., 1994; Uchio *et al*., 1999; Uchio *et al*., 2000). Briefly, the mesangial expansion in the glomeruli was scored according to the extent of the sclerotic lesion in the glomerulus and graded from 0 to 4 (0 = normal; 1 = change affecting < 25%; 2 = change affecting < 25–50%; 3 = change affecting < 50–75%; 4 = change affecting > 75%). In addition, the

morphological changes in the glomeruli (capillary aneurysm and hypercellularity) (Raij *et al*., 1984), and tubular (cystic tubular dilation, epithelial cellular atrophy and intraluminal cast formation) (Shih *et al*., 1988) and tubulointerstitial (tubulointerstitial expansion and mononuclear cell filtration around arterioles) (Nakamura *et al*., 1995) lesions were also recorded. Each glomerulus was classified into three categories: normal (glomerulus without mesangial expansion), expansion of mesangial areas (glomerulus graded from 1 to 4), and capillary aneurysm (glomerulus with severe degeneration, i.e. not only with expansion of mesangial but also with capillary aneurysm and hypercellularity). Morphological changes of glomeruli were expressed as percentage of glomeruli in each category.

Histochemical quantification of total and type I collagens

The degree of ECM deposition in kidney sections is a good indicator of glomerular sclerosis. Total and type I collagen levels in each frozen section of mouse kidney cortex were measured by microquantitation method as previously described (Manabe *et al*., 1993; Manabe *et al*., 1994; Manabe *et al*., 1995).

Lectin histochemistry and blot analysis

To identify the localization of specific carbohydrate chains, paraffin embedded serial sections were incubated with 24 biotinylated lectins. Carbohydrate binding specificities of the 24 lectins are summarized in Table 3-1. The localization of specific carbohydrate chains in the kidney sections was visualized using the avidin-biotin peroxidase complex (ABC) method as previously described (Kimura *et al*., 1999; Miyamoto *et al*., 1997; Miyamoto *et al*., 1998). Briefly, after deparaffinization and rehydration, the sections were incubated with avidin and biotin blocking solution (Vector Laboratories, Burlingame, CA, U.S.A.) at room temperature (RT; 23–25°C) for 15 min to block endogenous binding sites, and then washed with

PBS. The sections were incubated with biotinylated lectins diluted appropriately with PBS (see Table 3-1) for 24 hr at 4°C, washed with PBS, and then incubated with ABC reagent (Vector) for 60 min at RT. After washing, they were colorized with 0.002% H2O2, 0.1% 3,3'-diaminobenzidine-4HCl (DAB; Wako) in 0.1 M phosphate buffer (pH 7.4), and then counterstained with Mayer's hematoxylin. After dehydration, they were mounted in Entellan and examined under a light microscope. Negative control sections were incubated without biotinylated lectins or ABC reagent. As specific controls, lectins were incubated with 0.002–0.2 M solutions of corresponding sugar haptens (see Table 3-1) before and during application of the lectin solution to the tissue sections (Hsu and Raine, 1982; Kimura *et al*., 1999; Kuroki *et al*., 1991; Miyamoto *et al*., 1997; Miyamoto *et al*., 1998; Murphy and Goldstein, 1977; Yamamoto *et al*., 1992).

As characteristic staining of Bandeiraea simplicifolia lectin-I (BSL-I) was demonstrated histochemically, lectin blot analysis was performed as previously described (Kimura *et al*., 1999; Miyamoto *et al*., 1997). Briefly, frozen kidney sections (at least 10 mg) were mixed with 0.0625 M Tris-HCl (pH 6.8) containing 2% Nonidet-P40, 2% sodium dodecyl sulfate (SDS) and 5% 2-mercaptoethanol (Sigma Chemical, St. Louis, MO, U.S.A.), heated for 3 min at 100°C, and then urea was added at a final concentration of 8 M. The protein concentration of each sample was determined by a modification of the method of Bradford (Bradford, 1976). The sample proteins (30 μg/lane) and molecular weight standard (Sigma) were fractionated by 7.5% SDS-polyacrylamide gel electrophoresis (SDSPAGE). The fractionated proteins were visualized by staining with Coomassie brilliant blue (CBB), and then subsequently transferred electrophoretically onto polyvinylidene difluoride (PVDF) membranes (Millipore, Bedford, MA, U.S.A.). The PVDF membranes were preincubated with 10 mM Tris-HCl buffer (pH 7.4) containing 500 mM NaCl, 0.05% Tween 20 (TST), and then incubated with biotinylated BSL-I. After washing with TST,

they were reacted with HRP-conjugated avidin (Honen Corporation, Tokyo, Japan), washed, and then colorized with 100 mM phosphate buffer (pH 7.4) containing 0.003% H2O2 and 0.03% DAB.

Statistical analysis

ANOVA analysis with Fisher's least significant differences test comparison for biochemical data, and Wilcoxon's signed rank test for morphologic estimation were carried out with the Statview IV program using a Macintosh computer. Differences at a probability of $p<0.05$ were considered significant. All data are expressed as mean values ± SD (n=10).

Results

Clinical parameters

Aged homozygous ICGN mice (50 weeks) manifested clinical abnormalities such as the exercise intolerance, pale ears, weight loss as well as edema. Urinary and serum biochemical data are summarized in Table 3-2. There were no significant differences in serum albumin, creatinine, total cholesterol or BUN between ICR and heterozygous ICGN mice at any time point examined, but low levels of urine albumin (weak albuminuria) and mild disorders in other nephrotic parameters were seen in heterozygous ICGN mice. The nephrotic state progressed in an age-dependent manner in homozygous ICGN mice. Thirty- and 50-week-old homozygous ICGN mice showed severe albuminuria (6.29-fold and 9.30-fold increases as compared with age-matched heterozygous ICGN mice) and hypoalbuminemia (1.53-fold and 1.51-fold decreases as compared with age-matched heterozygous ICGN mice). Marked increases in sCr (2.41-fold and 3.02-fold increases as compared with age-matched heterozygous ICGN mice) and BUN (1.83-fold and 2.23-fold increase as compared with age-matched heterozygous ICGN mice) indicated the loss of renal function in 30- and 50-week-old homozygous ICGN mice. Increased serum total cholesterol (1.50-fold and 1.82-fold increases as compared with age-matched heterozygous ICGN mice) suggested severe hypercholesterolemia in 30- and 50-week-old homozygous ICGN mice.

Renal collagen levels and histopathology

Renal total and type I collagen levels assessed by a microquantification method are shown in Table 3-3. There were no significant differences in total or type I collagen levels in kidney cortex sections between ICR and heterozygous ICGN mice at any time point examined. When compared with 30- and 50-week-old heterozygous ICGN mice, age-matched homozygous ICGN mice showed 1.35-fold and 1.65-fold

increases in total collagen levels, and 1.49-fold and 1.66-fold increases in type I collagen levels.

Histopathological examination revealed that most ICR and heterozygous ICGN mice had kidneys with normal glomeruli (more than 98% and 89%, respectively), but all 50-week-old homozygous ICGN mice had kidneys with abnormal glomeruli (77 ± 9% and 23 ± 9% of glomeruli with expanded mesangial area and with capillary aneurysm, respectively; see Table 3-4). There were no marked differences in renal histopathological findings between ICR (used as normal healthy controls) and heterozygous ICGN mice (Fig. 3-1A and C). However, expansion of the mesangial areas with an apparent increase in the mesangial matrix, appearance of cysts, extension of renal tubules and infiltration of inflammatory cells were observed in the kidney sections of 50-week-old homozygous ICGN mice (Fig. 3-1B and D). Such histopathological abnormalities progressed in an age-dependent manner in homozygous ICGN mice. In aged heterozygous ICGN mice, kidneys exhibited moderate expansion of mesangial matrix (9 ± 2% and 2 ± 1% of glomeruli with expansion of mesangial areas and with capillary aneurysm, respectively; see Table 3-4), but no proliferation of mesangial cells was observed. Moreover, when compared with 50-week-old ICR and heterozygous ICGN mice (Fig. 3-1C), progressed fibrotic degeneration in the glomeruli was observed in the kidney sections of 50-week-old homozygous ICGN mice (Fig. 3-1D). Thus, glomerulonephritic and glomerular-fibrotic degeneration became severe only in homozygous ICGN mice.

Lectin histochemistry

All controls in which staining was performed following treatment with specific inhibitory sugars were negative, indicating that the lectin staining patterns observed in this study were specific. Histochemical staining intensity of each lectin in the glomerulus, proximal tubule, distal tubule and vessel walls located among the renal

tubules was estimated semiquantitatively, and representative histological findings of lectin histochemistry in the kidney sections of 50-week-old ICR, heterozygous and homozygous ICGN mice are summarized in Table 3-5. No positive staining with Sophora japonica agglutinin (SJA) was seen in any kidney sections. No differences in staining patterns of the eleven lectins, i.e. Jacalin, Lycopersicon esculentum lectin (LEL), wheat germ agglutinin (WGA), Solanum tuberosum lectin (STL), Maackia amurensis lectin (MAM), Pisum sativum agglutinin (PSA), peanut agglutinin (PNA), soybean agglutinin (SBA), BSL-II, concanavalin A (ConA) and Vicia villosa agglutinin (VVA), were observed in any parts of the kidney sections among ICR, heterozygous and homozygous ICGN mice. The intensity of Ricinus communis agglutinin-I (RCA-I), Phaseolus vulgaris agglutinin-E and -L (PHA-E and -L, respectively), Lens culinaris agglutinin (LCA) and Erythrina cristagalli agglutinin (ECL) staining in glomerular mesangium of homozygous ICGN mice increased with nephritis aggravation, but no such changes in lectin staining was seen in ICR or heterozygous ICGN mice. It was remarkable that no positive staining with BSL-I was seen in the kidney sections of ICR mice (Fig. 3-2A and B), but strong staining with BSL-I was demonstrated in glomerular capillary walls, i.e. endothelial cells of glomerular capillaries, and some their walls located among the renal tubules in the kidney sections of both heterozygous (Fig. 3-2C and D) and homozygous (Fig. 3-2E and F) ICGN mice. Luminal apical cell membranes of distal tubules were consistently stained with succinylated wheat germ agglutinin (s-WGA) in all ICR (Fig. 3-3A), heterozygous (Fig. 3-3B) and homozygous ICGN mouse kidney sections. A granular staining pattern with s-WGA was seen in epithelia of proximal tubules of a proportion of heterozygous ICGN mice and all homozygous ICGN mice, but those in ICR mice were never stained with s-WGA. No positive staining was observed with s-WGA, Dolichos biflorus agglutinin (DBA), Aleuria aurantia lectin (AAL) or Ulex europaeus agglutinin-I (UEA-I) in glomerular mesangium in the kidney sections of ICR (Fig. 3-3A; s-WGA) or heterozygous ICGN

mice (Fig. 3-3B and C; s-WGA and DBA, respectively), but positive staining with these lectins was seen in the glomerular mesangium in the sections of homozygous ICGN mice (Fig. 3-3D; DBA staining). In the kidneys of homozygous ICGN mice, the vessel walls located between the renal tubules as well as their interstitium were stained with DBA (Fig. 3-3D), but no such staining pattern with DBA was seen in the kidneys of ICR (Fig. 3-3C) or heterozygous-ICGN mice. No positive staining with Sambucus sieboldiana agglutinin (SSA) was seen in brush borders of extended proximal tubules of ICR or heterozygous ICGN (Fig. 3-3E) mice, but those of homozygous ICGN mice (Fig. 3-3F) were strongly stained with SSA. In brush borders of proximal tubules, staining intensity of Aleuria aurantia lectin (AAL), PHA-E and PHA-L increased with nephritis aggravation in homozygous ICGN mice. The interstitial of both proximal and distal tubules were stained with Lycopersicon esculentum lectin (LEL), SSA and Pisum sativum agglutinin (PSA), but no staining with these lectins was seen in the kidneys of ICR or heterozygous ICGN mice.

Lectin blot analysis

As described above, positive staining with BSL-I was histochemically demonstrated in heterozygous and homozygous ICGN mice, but not in ICR mice. So, I performed lectin blot analysis with BSL-I to determine the specific glycoproteins expressed in heterozygous and homozygous ICGN mice. No distinct differences were observed in the protein bands prepared from kidney lysates of ICR, heterozygous and homozygous ICGN mice (Fig. 3-4; lanes 1, 2 and 3, respectively). When the separated proteins were stained with BSL-I, three distinct bands (45, 58 and 64 kD) of ICGN mouse kidney were observed (Fig. 3-4; lanes 5 and 6, arrows). A strong band with a molecular mass of 64 kD was seen in the homozygous ICGN mouse kidney. These changes in the staining intensity of kidney glycoproteins were consistent with the histochemical results described above.

Discussion

In heterozygous ICGN mice, there were no significant differences in serum albumin, creatinine, total cholesterol, blood urea nitrogen (BUN) and renal total and type I collagen levels as compared with ICR mice at any time point examined. Histopathological examination detected moderate expansion of mesangial matrix. In homozygous ICGN mice, aged animal (50 weeks) manifested clinical abnormalities such as the exercise intolerance, pale ears, weight loss as well as edema. The nephrotic state progressed in an age-dependent manner. Severe albuminuria and hypoalbuminemia, marked increases in serum creatinine and BUN, and significant increases in renal total and type I collagen levels were observed at 30 and 50 week of age. Histopathological examination detected expansion of the mesangial areas with an apparent increase in the mesangial matrix, appearance of cysts, extension of renal tubules and infiltration of inflammatory cells in the kidney of 50-week-old animals. Such histopathological abnormalities progressed in an age-dependent manner. With these results, I understood pathological process of nephrotic syndrome in ICGN mice throughout their lifetime before transcriptome analysis of the mice.

Some lectins, especially BSL-I, showed characteristic staining patterns in ICGN mouse kidneys with renal failure. BSL-I showed positive staining in the glomeruli of both homozygous and heterozygous ICGN mice, but those of ICR mice were negative, and the staining intensity of BSL-I in the glomeruli of homozygous ICGN mice was stronger than that of heterozygous ICGN mice. Positive staining of BSL-I in distal tubules was only observed in homozygous ICGN mice. Moreover, lectin blot analysis for BSL-I revealed characteristic glycoproteins bands with molecular weights of 45, 58 and 64 kD in heterozygous and homozygous ICGN mice but not in ICR mice, and increased staining was observed in homozygous ICGN mice. These three specific glycoproteins may be key factors in the pathogenesis of renal

failure and are considered to be good markers for it. BSL-I consists of five isolectins, which are tetrameric structures composed of various combinations of two different subunits designated as A and B (BSL-A4, BSLA3B1, BSL-A2B2, BSL-A1B3 and BSL-B4) (Murphy and Goldstein, 1977). The A-subunit exhibits a primary specificity for α-D-Nacethylgalactopyranosyl (α-D-GalNAcp) groups and also reacts weakly with α-D-galactopyranosyl (α-D-Galp) group. Binding patterns of BSL-A4, homo-tetramer of A-subunits, in kidney sections were different among normal and diabetic mice, and different staining patterns have been seen among mouse strains (C57BL/6J, ICR, BALB/c and NSY) (Yonezawa *et al*., 1983a; Yonezawa *et al*., 1983b; Yonezawa *et al*., 1986). The B-subunit shows a high degree of specificity toward α-D-Galp but not α-D-GalNAcp groups. BSL-B4, homo-tetramer of B-subunits, exhibited binding to the glomerular and peritubular basement membrane in frozen sections of mouse and rabbit kidneys, but not in those of humans (Peters and Goldstein, 1979). Biotinylated BSL-I used in the present study is a mixture of five isolectins, binds mainly with α-D-Galp groups (Murphy and Goldstein, 1977). Miyamoto *et al*. (1997 and 1998) showed that histochemical staining of BSL-I demonstrated species-specific and strain-specific patterns, and its staining patterns specifically correspond to pathological condition. As described above, BSL-I specifically bound to endothelial cells of glomerular capillaries and of capillary vessel located among the proximal and distal tubules in the kidneys of ICGN mice, but not those in the kidneys of ICR mice. These histological results corresponded to the specific binding with 45, 58 and 64 kD glycoproteins detected only in ICGN mice. Moreover, the intensity of BSL-I staining increased corresponding to the degree of renal disorder in ICGN mice, mainly reflecting the increase in 64 kD-glycoprotein in ICGN mice with severe nephrotic disorder. Interestingly, the ICGN strain was established from the ICR strain, but BSL-I exhibited a different binding pattern between ICGN and ICR mice. This phenotypic difference was considered to be based on hereditary differences related to genetic nephrotic syndrome. BSL-I binding

64 kD-glycoprotein may be one of the causes of renal disease in ICGN mice with unknown etiology and is a good clinical marker of hereditary nephrotic syndrome in ICGN mice.

Further interesting findings of lectin histochemistry were as follows: AAL, DBA, UEA-I and s-WGA showed positive staining only in the glomeruli of homozygous ICGN mice, but no staining was observed in those of heterozygous ICGN or ICR mice. The staining intensities of RCA-I, PHA-E, PHA-L, LCA and ECL in the glomeruli of homozygous ICGN mice were stronger than those of heterozygous ICGN and ICR mice. The present findings indicated that these lectins with which strong staining was demonstrated in homozygous ICGN mice with severe glomerular disorder may be good indicators for the diagnosis and prognosis of glomerular lesions. Moreover, positive staining with SSA was only observed in the proximal tubules of homozygous ICGN mice, and positive staining with BSL-I was only demonstrated in distal tubules of homozygous ICGN mice. In proximal tubules, positive staining with s-WGA was observed in both homozygous and heterozygous ICGN mice but not in ICR mice. Stronger levels of staining with DSL, AAL, PHA-E and PHA-L were demonstrated in homozygous ICGN mice compared with heterozygous ICGN and ICR mice. These lectins, whose stronger staining was seen in homozygous ICGN mice with severe renal tubular lesion, are considered to be good probes for histopathological diagnosis and prognosis of tubular disorders.

It is also interesting that the glomerular basement membrane is the obvious site with ultrastructural alterations observed as early as 5 weeks old as described in our previous report (Ogura *et al*., 1991). In the mesangium of ICGN mice, the histochemical intensities of RCA-I, PHA-E, PHA-L and LCA staining increased corresponding to nephritis aggravation. Moreover, no histochemical staining with AAL, DBA, UEA-I or s-WGA was observed in the mesangium of heterozygous ICGN or ICR mice, but positive staining with these lectins was demonstrated in homozygous

ICGN mice. In various human renal diseases, loss of UEAI binding glycoconjugate was observed in the sclerotic areas of the glomeruli (Yonezawa *et al*., 1983a; Yonezawa *et al*., 1983b), and this lectin is considered to be a good marker for diagnosis and prognosis of human renal diseases. Such species-specific discrepancy between ICGN mice and human in UEA-I staining may be caused by a difference in pathogenic molecules or by species-specific difference in cell-surface carbohydrates (Lis and Sharon, 1986). As described above, loss of BSL-A4 binding glycoprotein accompanying sclerosis of the glomeruli was observed in diabetic mice with renal disorder (Yonezawa *et al*., 1986). Moreover, brush borders of extended proximal tubules were strongly stained with SSA only in the kidneys of homozygous ICGN mice with severe renal disorders, but no such staining with SSA was ever seen in heterozygous ICGN or ICR mice. The intensities of AAL, PHA-E and PHA-L staining in brush borders of proximal tubules increased corresponding with nephritis aggravation in homozygous ICGN mice. There was a relation between alterations in the glycoconjugates stained with these lectins and extension of proximal tubules in homozygous ICGN mice. s-WGA exhibited a granular staining pattern in proximal tubular epithelia of a portion of heterozygous and of all homozygous ICGN mice, but not in ICR mice. In situ hybridization for erythropoietin mRNA demonstrated that the cortical peritubular cells are renal erythropoietin-producing cells (Maxwell *et al*., 1997). Erythropoietin is a circulating hormone that governs the rate of red blood cell production. I observed that all homozygous ICGN mice developed severe anemia, and that histopathological regression of cortical peritubular cells and abnormal histochemical staining with some lectins in the peritubular area. Thus, regressive changes in cortical peritubular cells, erythropoietin-producing cells, may cause severe anemia in homozygous ICGN mice. The present results suggested that some specific lectins can be used for histopathological diagnosis and prognosis of the development of renal glomerular and tubular diseases including hereditary nephrotic syndrome.

In conclusion, histopathological lectin staining can provide important information for diagnosis and prognosis of the development of hereditary nephrotic lesions. The lectins with which stronger staining was seen in homozygous ICGN mice with severe renal tubular lesions are good probes to investigate the molecular mechanism of renal disorders in ICGN mice. Particularly, three BSL-I binding glycoproteins (45, 58 and 64 kD; especially 64 kD glycoprotein), which may be the pathogenic factors causing renal disease in ICGN mice, are good tools to elucidate the etiology of the renal syndrome in ICGN mice.

Table 3-1 Carbohydrate binding specificities of the lectins used

Lectin	Source	Dilution[c] (μg/ml)	Binding specificity[d]
Jacalina[a]	*Artocarpus integrifolia*	4	α-Gal
LEL[a]	*Lycopersicon esculentum*	2	β-GlcNAc, Poly LacNAc, GlcNAc oligomer
RCA-I[a]	*Ricinus communis*	4	β-GalNAc, β-Gal, Galβ1→GlcNAc on complex glycan
SSA[b]	*Sambucus sieboldiana*	3	Siaα2→6Gal/GalNAc
WGA[a]	*Triticum vulgaris*	3	β-GlcNAc, Poly LacNAc, GlcNAc oligomer, Sia
DSL[a]	*Datura Stramonium*	2	β-GlcNAc, Poly LacNAc, Tri/tetra-antenna complex glycan
STL[a]	*Solanum tuberosum*	4	β-GlcNAc, Poly LacNAc, GlcNAc oligomer
AAL[b]	*Aleuria aurantia*	2	Fucα1→6GlcNAc
MAM[b]	*Maackia amurensis*	3	Siaα2→3Gal
PHA-E[a]	*Phaseolus vulgaris*	2	Bisected complex glycan
PHA-L[a]	*Phaseolus vulgaris*	2	Tri/tetra-antenna complex glycan
LCA[a]	*Lens culinaris*	3	α-Man, complex glycan with fucosylated core
PSA[a]	*Pisum sativum*	3	α-Man, complex glycan with fucosylated core
SJA[a]	*Sophora japonica*	8	β-GalNAc
DBA[a]	*Dolichos biflorus*	8	α-GalNAc, GalNAcα1→3GalNAc (Gal)
ECL[a]	*Erythrina cristagalli*	4	β-Gal, β-GalNAc
PNA[a]	*Arachis hypogaea*	8	β-Gal, O-linked glycan, Galβ1→3GalNAc
SBA[a]	*Glycine max*	8	α-GalNAc, O-linked glycan, GalNAcα1→3Gal
UEA-I[a]	*Ulex europaeus*	8	α-Fuc, Fucα1→2Gal
BSL-II[a]	*Bandeiraea simplicifolia*	6	α-, β-GlcNAc
Con A[a]	*Canavalia ensiformis*	4	α-Man, oligomannoside glycan, Bi-antenna complex glycan
BSL-I[a]	*Bandeiraea simplicifolia*	6	α-GalNAc, α-Gal, Galα1→3Gal
VVA[a]	*Vicia villosa*	6	β-GalNAc, O-linked glycan, GalNAcα1→3Gal
s-WGA[a]	*Triticum vulgaris*	8	β-GlcNAc, poly LacNAc, GlcNAc oligomer

a) Biotinylated lectins were purchased from Vector Laboratories (Burlingame, CA, U.S.A.).

b) Biotinylated lectins were purchased from Seikagaku Kogyo Co. (Tokyo, Japan).

c) Biotinylated lectins were diluted with PBS.

d) Abbreviation: Fuc: fucose, Gal: D-galactose, GalNAc: N-acetylgalactosamine, GlcNAc: N-acetylglucosamine, Lac-
NAc: N-acetyllactosamine, Man: mannose, Sia: sialic acid.

Table 3-2 Urine and serum biochemical features in control (ICR), heterozygous and homozygous ICGN mice

Strains	ICR			Heterozygous ICGN			Homozygous ICGN		
Age (weeks old)	10	30	50	10	30	50	10	30	50
Urine albumin (mg/m*l*)	ND	ND	ND	ND	1.4±0.8	2.3±1.9	8.8±1.5**	8.8±1.5**	21.4±3.8**
Serum albumin (g/d*l*)	3.10±0.08	3.14±0.11	3.11±0.13	2.99±0.07	3.08±0.15	2.98±0.11	2.55±0.25	2.01±0.33*	1.97±0.31*
Serum creatinine (mg/d*l*)	0.31±0.06	0.31±0.09	0.28±0.07	0.33±0.07	0.37±0.11	0.41±0.10	0.39±0.13	0.89±0.15**	1.24±0.24**
Blood urea nitrogen (mg/d*l*)	29.8±4.1	32.2±3.1	29.5±3.3	33.1±3.1	36.8±7.1	39.2±8.4	43.1±7.4	67.5±11.4*	87.3±20.7**
Serum total cholesterol (mg/d*l*)	95.1±8.5	119.6±9.7	145.4±15.8	104.1±8.2	136.9±18.2	156.9±20.5	140.4±8.8	205.1±30.5*	285.6±30.5**

For details, see Materials and Methods.

ND: Not detected.

* and **: $p<0.05$ and 0.01 vs each heterozygous ICGN group.

Table 3-3. Total and type I collagen levels in the renal cortex of control (ICR), heterozygous and homozygous ICGN mice

Strains	ICR			Heterozygous ICGN			Homozygous ICGN		
Age (weeks old)	10	30	50	10	30	50	10	30	50
Total collagen (mg/g protein)	4.49 ± 0.59	4.88 ± 0.73	4.63 ± 0.80	4.86 ± 0.91	5.22 ± 1.21	5.75 ± 1.39	5.02 ± 1.84	7.03 ± 2.42*	9.47 ± 2.87**
Type I collagen (mg/g protein)	1.78 ± 0.28	1.93 ± 0.33	1.84 ± 0.38	1.94 ± 0.31	2.02 ± 0.42	2.45 ± 0.56	2.02 ± 0.31	3.02 ± 0.55*	4.06 ± 0.62**

For details, see Materials and Methods.

* and **: $p<0.05$ and 0.01 vs each heterozygous ICGN group.

Table 3-4. Morphological changes of glomeruli in control (ICR), heterozygous and homozygous ICGN mice

Strains	ICR			Heterozygous ICGN			Homozygous ICGN		
Age (weeks old)	10	30	50	10	30	50	10	30	50
Normal (%)	100 ± 1	98 ± 1	98 ± 1	99 ± 1	94 ± 2	89 ± 4	92 ± 4	31 ± 11**	NO
Expansion of mesangial areas (%)	NO	2 ± 1	2 ± 1	1 ± 1	5 ± 1	9 ± 2	7 ± 2	54 ± 15**	77 ± 9**
Capillary aneurysm (%)	NO	NO	NO	NO	1 ± 1	2 ± 1	1 ± 1	15 ± 4**	23 ± 9**

These morphological changes are described in detail in Materials and Methods.
Not observed.
**: $p<0.05$ and 0.01 vs each heterozygous ICGN group.

Table 3-5. Histochemical staining patterns of biotinylated lectins in the kidney sections of 50-week-old ICR, heterozygous ICGN and homozygous ICGN mice

	Glomerulus			Proximal T.			Distal T.			Vessel wall		
	ICR	ICGN[1]	ICGN[2]	ICR	ICGN[1]	ICGN[2]	ICR	ICGN[1]	ICGN[2]	ICR	ICGN[1]	ICGN[2]
Jacalin	++	++	++	+	+	+	+	+	+	+	+	+
LEL	++	++	++	+	+	+	+++	+++	+++	+	+	+
RCA-I	+	+	++	++	++	++	++	++	++	–	–	–
SSA	++	++	++	–	–	++	+++	+++	+++	+	+	+
WGA	+++	+++	+++	++	++	++	+++	+++	+++	+	+	+
DSL	+	+	+	++	++	+++	+++	+++	+++	–	–	–
STL	++	++	++	++	++	++	+++	+++	+++	+	+	+
AAL	–	–	+	++	++	+++	+	+	+	–	–	–
MAM	++	++	++	–	–	–	+++	+++	+++	+	+	+
PHA-E	++	++	+++	++	++	+++	++	++	++	+	+	+
PHA-L	+	+	++	++	++	+++	+	+	+	–	–	–
LCA	+	+	++	++	++	++	–	–	–	–	–	–
PSA	+	+	+	+	+	+	+	+	+	–	–	–
SJA	–	–	–	–	–	–	–	–	–	–	–	–
DBA	–	–	++	–	–	–	+++	+++	+++	–	–	+++
ECL	+	+	++	+	+	+	++	++	++	-	–	–
PNA	+	+	+	+	+	+	+++	+++	+++	–	–	–
SBA	+	+	+	+	+	+	++	++	++	–	–	–
UEA-I	–	–	++	–	–	–	–	–	–	–	–	–
BSL-II	–	–	–	+	+	+	+	+	+	–	–	–
ConA	+	+	+	++	++	++	+	+	+	–	–	–
BSL-I	–	++	+++	–	–	–	–	–	++	–	++	+++
VVA	+	+	+	+	+	+	+++	+++	+++	–	–	–
s-WGA	–	–	++	–	++	++	+++	+++	+++	–	–	–

Abbreviations used: ICGN1, heterozygous ICGN mice; ICGN2, homozygous ICGN mice; Proximal T., proximal tubule; Distal T., distal tubule; Vessel wall, vessel walls located between the renal tubules.

Intensity: –, +, ++, +++ denote negative, weak, moderate and intense staining, respectively.

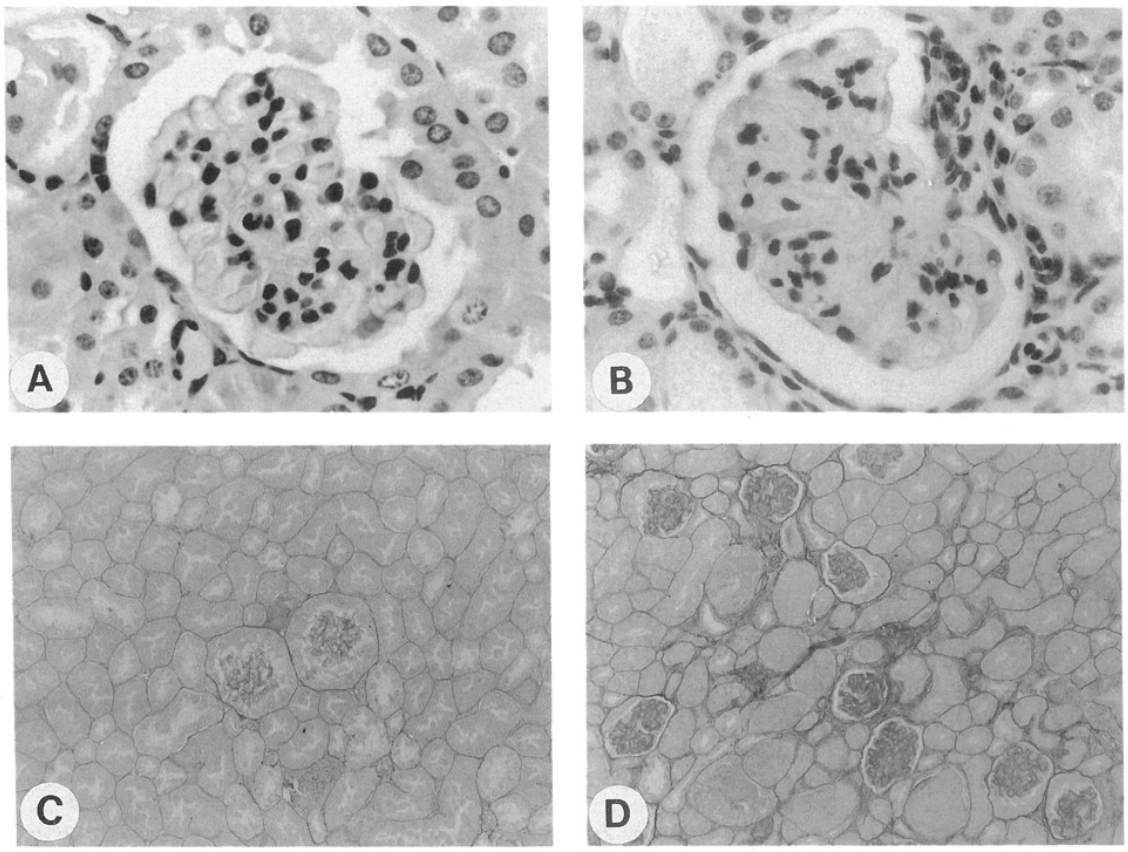

Fig. 3-1.

Kidney sections of 50-week-old male heterozygous (A and C) and homozygous ICGN mice (B and D) were stained with hematoxylin and eosin (A and B; × 600) and with Sirius red (C and D; × 150). As compared with heterozygous ICGN mice (A), expansion of mesangial matrix, but no proliferation of mesangial cells was seen in the kidneys of homozygous ICGN mice (B). Severe fibrotic degeneration in glomeruli and basement membrane of renal tubules, appearance of cysts, and extension of renal tubules were observed only in the kidneys of homozygous ICGN mice (D) but not in those of heterozygous ICGN mice (C).

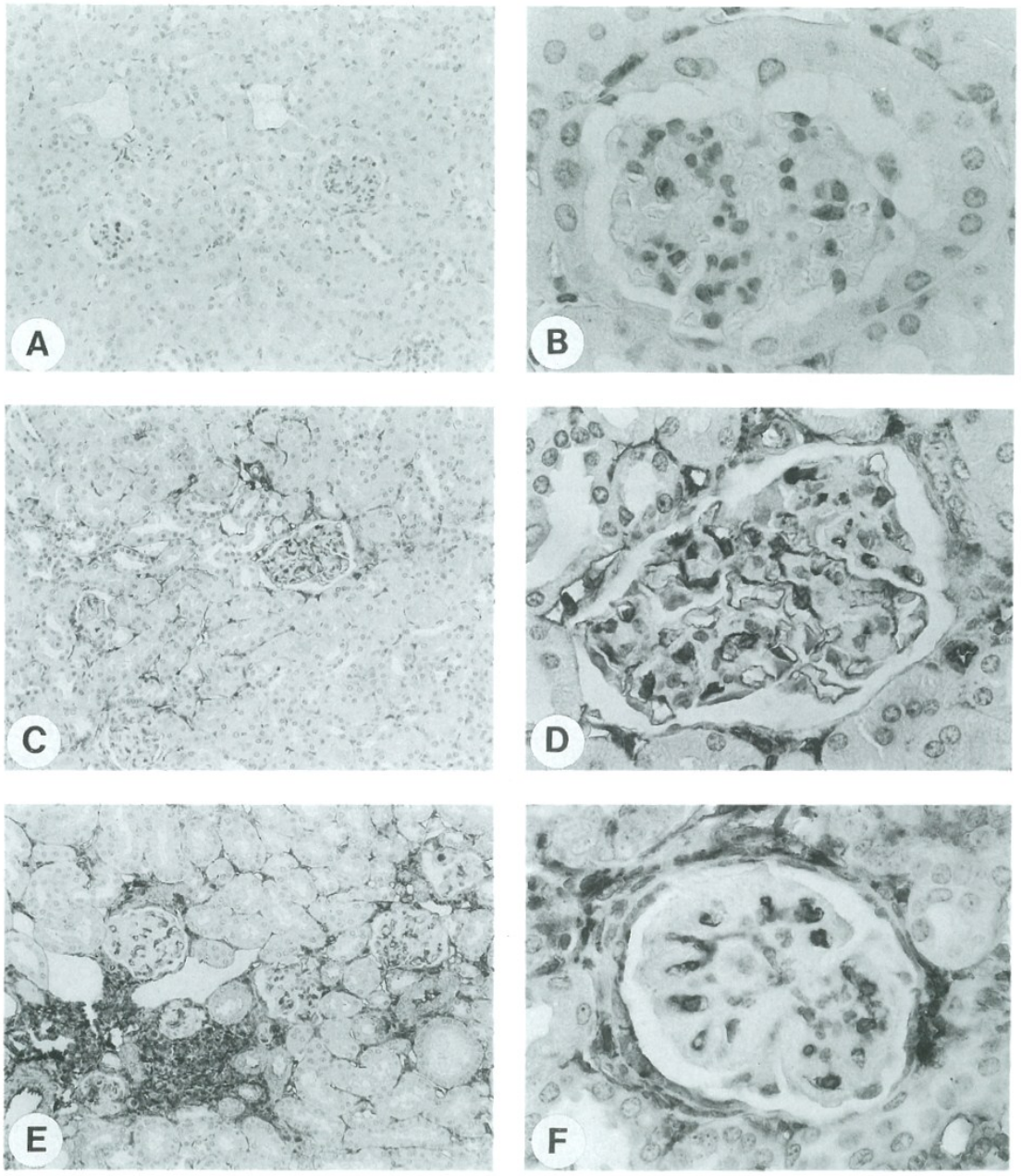

Fig. 3-2.

Staining intensity in kidney sections of 50-week-old male ICR (A and B; × 150 and 600, respectively), heterozygous (C and D; × 150 and 600, respectively) and homozygous (E and F; × 150 and 600, respectively) ICGN mice stained with Bandeiraea simplicifolia lectin-I (BSL-I). No positive staining was seen with BSL-I in the kidneys of ICR mice (A and B). In the kidneys of heterozygous (C and D) and homozygous (E and D) ICGN mice, endothelial cells of glomerular capillary vessels and some vessel walls located among the renal tubules were strongly stained with BSL-I.

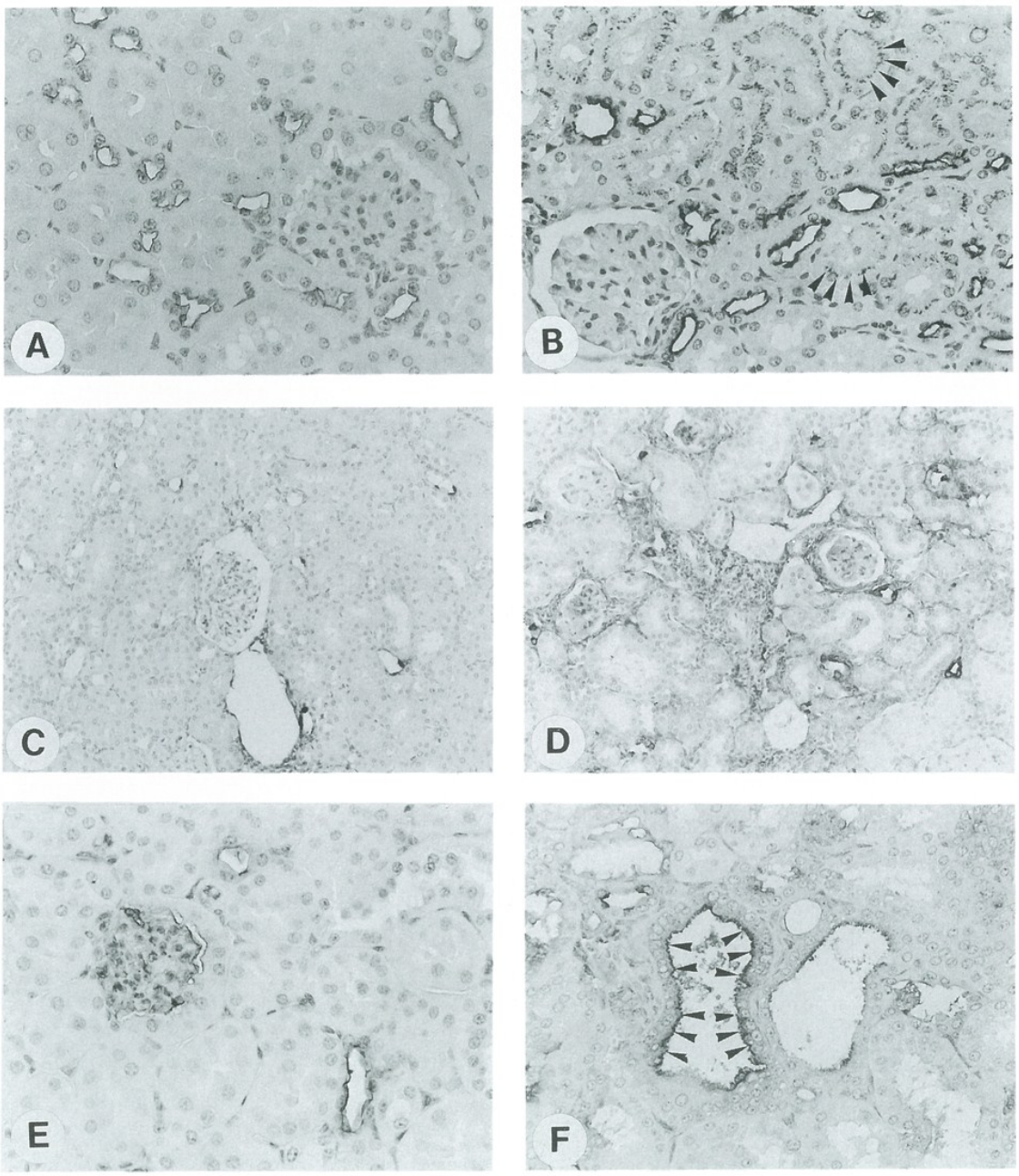

Fig. 3-3.

Kidney sections of 50-week-old male ICR (A; × 300), heterozygous (B, C and E; × 300, 150 and 300, respectively) and homozygous (D and F; × 150 and 300, respectively) ICGN mice were stained with succinylated wheat germ agglutinin (s-WGA) (A and B), Dolichos biflorus agglutinin (DBA) (C and D) and Sambucus sieboldiana agglutinin (SSA) (E and F). Luminal apical cell membranes of distal tubules in the kidney sections of ICR and heterozygous ICGN mice were consistently stained with s-WGA (A and B, respectively). Granular substances stained with s-WGA (arrowheads) were seen in the epithelia of proximal tubules of heterozygous ICGN mice (B), but no such positive staining was seen in those of ICR mice (A). Positive staining with DBA in glomerular mesangium and the vessel walls located among the renal tubules as well as their interstitium was observed in the kidneys of homozygous

ICGN mice (D), but no such positive staining was observed in the kidney of heterozygous ICGN mouse (C). Brush borders of extended proximal tubules were strongly stained with SSA in the kidneys of homozygous ICGN mice (F; arrowheads), but no such positive staining with SSA was seen in the kidneys of ICR or heterozygous ICGN mice (E).

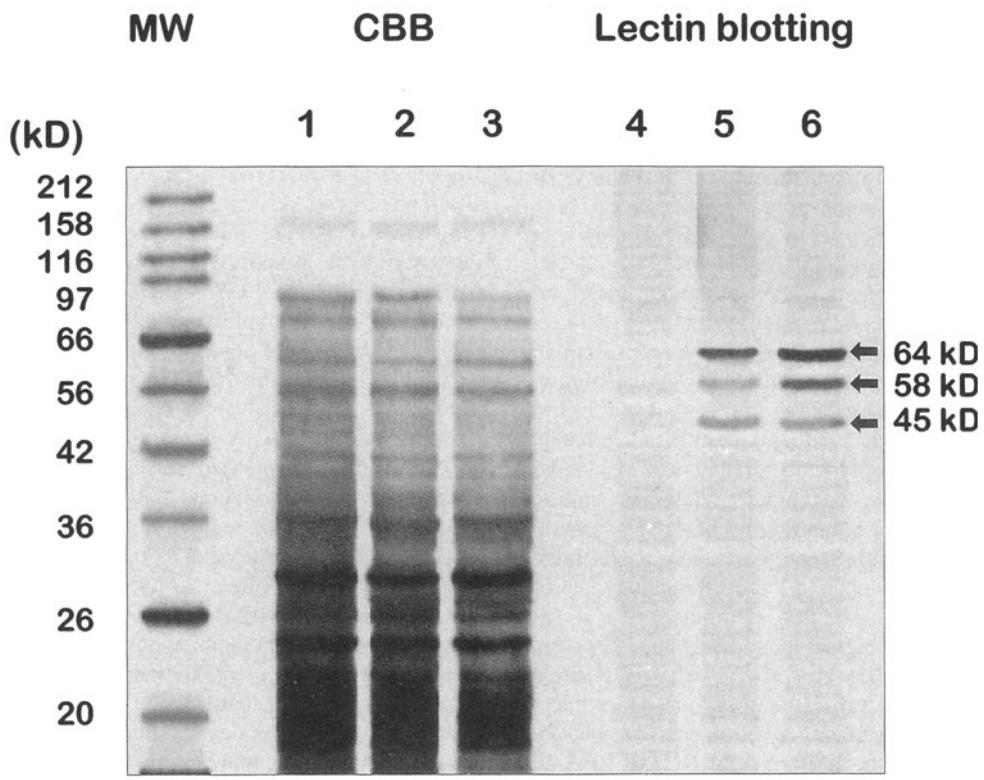

Fig. 3-4.

Lectin blots stained with Coomassie brilliant blue (M and lanes 1, 2 and 3) and Bandeiraea

simplicifolia lectin-I (BSL-I) (lanes 4, 5 and 6). Lane M: molecular markers; lane 1 and 4: kidney lysate from ICR mouse; lane 2 and 5: kidney lysate from heterozygous ICGN mouse; and lane 3 and 6: kidney lysate from homozygous ICGN mouse. Characteristic glycoprotein bands with molecular weights of 45, 58 and 64 kD (arrows) were detected in heterozygous and homozygous ICGN mice (lanes 5 and 6), but not in ICR mouse (lane 4). Increased staining of these bands was seen in homozygous ICGN mouse kidney (lane 6).

Chapter 4

Gene Expression Analysis Detected Low Expression Level of C1s Gene in ICR-derived Glomerulonephritis (ICGN) Mice

Abstract

ICR-derived glomerulonephritis (ICGN) strain is a novel inbred strain of mice with a hereditary nephrotic syndrome. Deletion mutation of tensin 2 (*Tns2*), a focal adhesion molecule, has been suggested to be responsible for nephrotic syndrome in ICGN mice, however, existence of other associative factors has been suggested. To identify additional associative factors and to better understand onset mechanism of nephrotic syndrome in ICGN mice, I conducted comprehensive gene expression analysis of renal cortex of homozygous ICGN mice using DNA microarray. Immune-related pathways were markedly altered in ICGN mice kidney as compared with ICR mice. Furthermore, gene expression level of complement component 1, s subcomponent (*C1s*), whose human homologue has been reported to associate with lupus nephritis, was markedly low in ICGN mice kidney. Real-time quantitative reverse transcription-polymerase chain reaction confirmed low expression level of *C1s* in ICGN mice liver where C1s protein is mainly synthesized. High serum level of anti-dsDNA antibody and deposits of immune complexes were also detected in ICGN mice by enzyme-linked immunosorbent assay and immunohistochemical analyses, respectively. These results suggest that immune system, especially complement system, is associated with nephrotic syndrome in ICGN mice. I identified low expression level of *C1s* gene as additional associative factor for nephrotic syndrome in ICGN mice. Further studies are needed to elucidate the role of complement system in the onset of nephrotic syndrome in ICGN mice.

The results obtained in this chapter demonstrated that transcriptome analysis is useful for accurate understanding of pathology of diseases in model animals. Right choice of disease model animals for drug efficacy evaluation is expected to improve extrapolation of drug efficacy to human. I showed that ICGN mice are good animal model for evaluation of drugs for lupus nephritis.

Introduction

The ICGN mice strain is a good model for human idiopathic nephrotic syndrome. Early stage of nephrotic syndrome in ICGN mice were explained in the introduction in chapter 3. Furthermore, progress of nephrotic syndrome in ICGN mice throughout their lifetime (at 10, 30 and 50 week of age) was examined in chapter 3.

The proteinuria seen in ICGN mice was reported to be controlled by at least one autosomal recessive gene (*nep*), which was mapped on the distal part of chromosome 15 by linkage analysis (Okamoto *et al*., 2001). In addition, quantitative trait locus analysis and DNA sequencing raised the possibility that a deletion mutation of tensin 2 (*Tns2*), also located on chromosome 15, was responsible for nephrotic syndrome in ICGN mice (Cho *et al*., 2006). Tensin is a focal adhesion molecule that binds to actin filaments and participates in signaling pathway through integrin (Weigt *et al*., 1992). The *Tns2* gene was reported as *Tenc1*, tensin-like C1 domain containing phosphatase, in Mouse Genome Informatics (http://www.informatics.jax.org/). While *Tns2* is expressed in podocytes and tubular epithelial cells in normal mice, the deletion mutation in *Tns2* creates a premature terminal codon in ICGN mice (Cho *et al*., 2006). Although the deletion mutation of *Tns2* was suggested to be responsible for nephrotic syndrome in ICGN mice, some reports have suggested existence of other causative factors. Backcross progenies of (ICGN x MSM)F_1 x ICGN showed various degrees of proteinuria but did not segregate into the ICGN and MSM types (Cho *et al*., 2006). This result indicates that proteinuria is controlled by multiple genetic loci. Congenic strains carrying the mutation of *Tns2* on the C57BL/6J genetic background showed milder phenotypes than ICGN mice (Nishino *et al*., 2010). Additionally, congenic strains carrying the mutation of *Tns2* on the 129/SV genetic background did not show proteinuria, anemia, increase in blood urea nitrogen (BUN) or any severe histological changes until at least 16 weeks of age (Nishino *et al*., 2012). These results suggest the

absence of nephrotic syndrome in congenic strains carrying the mutation of *Tns2* on the C57BL/6J and the 129/SV genetic background was because they retained wild type expression for the multiple associative factors involved in the nephrotic syndrome seen in ICGN mice.

To identify additional associative factors for nephrotic syndrome in ICGN mice and to better understand onset mechanism of nephrotic syndrome in ICGN mice, microarray analysis was conducted on renal cortex from 4- and 8-week-old ICGN mice and the results were compared to that obtained from renal cortex harvested from ICR mice. In the present study, renal cortex was separated from kidney slice including papilla, medulla and cortex, and was used in transcriptome analysis. In chapter 2, high correlation within transcriptome data from the same renal region was confirmed when both global and percellome normalization method were used. Therefore, a common normalization method, global normalization, was applied in this transcriptome analysis.

Materials and Methods

Animals and tissue preparation

All animal experiments were performed in accordance with protocols approved by the Institutional Animal Care and Use Committees of National Institute of Biomedical Innovation (NIBIO, Osaka, Japan). Homozygous male ICGN mice (4- and 8-week-old) from a specific-pathogen-free colony at NIBIO and age-matched ICR mice (Clea Japan, Osaka, Japan) were used in this study. All animals were housed under environmentally controlled conditions (room temperature: 23 ± 1°C; light-dark conditions: 14 hr light/10 hr dark) in autoclaved cages and given a standard diet (CMF, Oriental Yeast, Tokyo, Japan) and tap water ad libitum. At 4 or 8 weeks of age, the animals were anesthetized, urine samples obtained from the bladder, blood samples from the cervical vein, and the kidneys and liver were rapidly removed. One kidney was immediately fixed in 10% (v/v) neutral-buffered formalin (pH 7.4) for conventional histopathological evaluation and immunohistochemical study while the other kidney was sectioned horizontally at its middle portion into approximately a 1 mm thick slice. The slices were fixed in RNA*later*® (Invitrogen, CA., USA) for microarray analysis. The median hepatic lobe was sectioned into approximately a 5 mm thick slice and then fixed in RNA*later*® for real-time quantitative reverse transcription-polymerase chain reaction (quantitative PCR).

Clinical biochemistry and Urinalysis

Clinical biochemical parameters associated with renal injury including serum total protein, serum creatinine, and BUN were assessed (7170 automated analyzer, Hitachi, Tokyo, Japan). Urinalysis parameters measured included urinary total protein and urinary creatinine levels (Fuji Dri-Chem FDC7000, Fuji Film, Tokyo, Japan). All procedures were performed according to the manufacturers' protocols.

Renal histopathology and immunohistochemistry

The fixed kidneys were dehydrated, embedded in paraffin, cut into approximately 3 μm thick sections. To evaluate glomerular region, sections were stained with hematoxylin and eosin (H&E) and Periodic acid-Schiff (PAS). The degree of histopathological change was determined and scored on a scale of 0 to 4 as follows: 0 – no findings, 1 – slight changes, 2 – mild changes, 3 – moderate changes, and 4 – severe changes. To analyze deposition of antibodies, immunohistochemical staining for immunoglobulin (Ig) A, IgG and IgM were also conducted. Sections were treated with protease K (Dako, Glostrup, Denmark) for 10 min for antigen retrieval, and then incubated with primary antibody for 1 hr at room temperature. After washing with Tris-buffered saline with Tween 20 (pH 7.6), the sections were incubated with secondary antibody for 1 hr at room temperature. The primary antibodies were polyclonal goat anti-mouse IgA (Bethyl Laboratories, TX., USA, code No. A90-103P), goat anti-mouse IgG, (Rockland Immunochemicals, PA., USA, code No. 710-1332) and goat anti-mouse IgM (Bethyl Laboratories, code No. A90-101P) and used at dilution of 1:100. The second antibody was Alexa Fluor 488-labeled chicken anti-goat IgG antibody (Molecular Probes, OR., USA, code No. A-21467) and used at dilution of 1:200. The sections were visualized with fluorescence microscopy (DMRBE, Leica Microsystems, GmbH, Germany). Images were exported from the Pixcera digital camera system (Penguin 600CL/In Studio v.1.0, Pixcera corporation, CA., USA).

Microarray analysis

Microarray analysis was conducted with RNA harvested from the renal cortex of 4- and 8-week-old ICGN and ICR mice. The samples of renal cortex were separated from the slices fixed in RNA*later*® as reported in chapter 2 and homogenized using the Mill Mixer (Qiagen, Hilden, Germany) with zirconium beads. Total RNA was

isolated from the kidney homogenate using the RNeasy kit (Qiagen). Microarray analysis was conducted by using the GeneChip® Mouse Genome 430 2.0 Array (Affymetrix, CA., USA). The procedure was conducted according to the manufacturer's instructions. The cDNA synthesis and purification were performed with the Superscript Choice System (Invitrogen), the T7-(dT)24-oligonucleotide primer (Affymetrix), and the cDNA Cleanup Module (Affymetrix). The biotinylated cRNA synthesis and purification were performed using the GeneChip Expression 3-Amplification Reagents for IVT Labeling (Affymetrix) and the cRNA Cleanup Module (Affymetrix). Fragmented cRNA (20 μg) was hybridized to a Mouse Genome 430 2.0 Array for 18 hr at 45˚C at 60 rpm, after which the array was washed and stained by streptavidin-phycoerythrin (Fluidics Station 400, Affymetrix) then scanned by the Gene Array Scanner (Affymetrix). Non-normalized MAS5 signals were imported into the Microsoft Office Excel 2007 (Microsoft Corporation, WA., USA) and normalized for each microarray by setting the mean signal intensity to be equal across microarrays. The normalized ICGN values were compared to age-matched ICR values and expressed as fold change (ICGN/ICR). The Student's t-test p-values were calculated using the Microsoft Office Excel 2007. The data discussed in this publication have been deposited in NCBI's Gene Expression Omnibus and are accessible through GEO Series accession number GSE 45005 (http://www.ncbi.nlm.nih.gov/geo/query/acc.cgi?acc=GSE45005).

Pathway analysis

Genes for the canonical pathway analysis were selected using the fold change cutoff of >2 or <-2 and the p-value cutoff of <0.01. Pathway analysis was conducted using the Ingenuity Pathway Analysis software (IPA, Ingenuity Systems, CA., USA, www.ingenuity.com). This software identified the canonical pathways from the IPA library of canonical pathways that were most significant to the selected genes. Fisher's

exact test was used to calculate a p-value determining the probability that the association between the genes in the dataset and the canonical pathway was due to chance.

Quantitative PCR

Single-stranded cDNA was synthesized from 1 μg of total liver RNA using the High Capacity RNA-to-cDNA Master Mix (Applied Biosystems, CA., USA). Quantitative PCR was performed on the ABI Prism 7900 (Applied Biosystems), using the TaqMan Universal Master Mix II (Applied Biosystems) with sets of primers and Universal ProbeLibrary probes (Roche, Basel, Switzerland) designed online with the ProbeFinder version 2.45 for mouse (Roche). Probes specific for mouse *C1s* (forward primer: 5'-TGGATACTTCTGCTCCTGTCC, reverse primer: 5'-CAGGGCAGTGAACACATCTC, and Universal ProbeLibrary probe #69, which gives a 94-nt amplicon); and beta-Actin (Actb) (forward primer: 5'-CTAAGGCCAACCGTGAAAAG, reverse primer: 5'-ACCAGAGGCATACAGGGACA, and Universal ProbeLibrary probe #64, which gives a 104-nt amplicon) were used. Each sample was amplified with 1 cycle at 95°C for 10 min (to activate the polymerase) and followed by 40 cycles at (95°C for 15 sec and 60°C for 1 min).

Enzyme-linked immunosorbent assay (ELISA) of anti-double stranded (ds) DNA antibody

Serum anti-dsDNA antibody was measured using a mouse anti-dsDNA ELISA Kit (Shibayagi, Gunma, Japan) according to the manufacturer's instructions.

Statistical analysis

Aspin-Welch's t-test was performed for ELISA of anti-dsDNA antibody.

Student's t-test was performed for all other measured values. For the microarray data, p-values <0.01 were considered significant while for all other data, p-values <0.05 were considered significant.

Results

Clinical biochemistry and Urinalysis

Blood and urinary biochemical parameters are summarized in Table 4-1. At 4 weeks of age, ICGN mice showed significant increase in BUN (1.74-fold higher than the ICR control values) and significant decrease in urinary creatinine levels (43% of the ICR control values). At 8 weeks of age, ICGN mice showed markedly lower urinary creatinine levels (15.6% of ICR control levels), hypoproteinemia (58.4% of the ICR control values) and proteinuria (2.03-fold higher than the ICR control values).

Renal histopathology and immunohistochemistry

Histopathological examination is summarized in Table 4-2. All the four-week-old ICGN mice exhibited slight to mild mesangial expansion and thickening of the GBM and by 8 weeks of age, all the mice showed mild to moderate GBM findings (Table 4-2, Fig 4-1D). In addition, four of eight ICGN mice examined at 4 weeks of age showed slight tubulointerstitial injury consisting of inflammatory cell infiltration, basophilic tubules and protein cast (Table 4-2, Fig 4-1B). By 8 weeks old, all of the ICGN mice showed slight to severe tubulointerstitial findings (Table 4-2, Fig 4-1C). Immunohistochemical analysis revealed depositions of IgA, IgG and IgM on the thickened GBM of 4- and 8-week-old ICGN mice (Fig 4-2).

Microarray analysis

A total of 252 and 807 transcripts met the filtering criteria (fold change value of >2 or <-2 and p-value of <0.01) in the renal cortical tissue of 4- and 8-week-old ICGN mice, respectively. Of these, a total of 37 transcripts overlapped at the 4- and 8-week time period. A list of the 37 overlapping transcripts are presented in Table 4-3, and are arranged in order of absolute value of fold change at 4 weeks of age (early

stage of nephrotic syndrome). Of these 37 genes, *C1s* gene showed the largest change (2.2% of ICR control levels at 4 weeks of age).

Pathway analysis

Canonical pathway analysis using IPA was conducted to identify biological pathways which were significantly altered in the kidneys of 4- and 8-week-old ICGN mice. Forty-one pathways were significantly altered in ICGN mice (Table 4-4). Approximately 76 percent of the altered pathways (31 of 41 pathways) were categorized into "Humoral Immune Response", "Cellular Immune Response" and/or "Cytokine Signaling".

Quantitative PCR

Of the 37 overlapping transcripts in renal cortical tissue, the *C1s* gene expression appeared to be markedly altered (reduced) compared to the other transcripts (Table 4-3). Therefore, quantitative PCR was conducted to measure *C1s* mRNA in the livers where C1s protein is primarily produced. Quantitative PCR showed that *C1s* mRNA level was also markedly low in ICGN mice liver as compared with age-matched ICR mice (Fig. 4-3).

ELISA of anti-dsDNA antibody

Serum anti-dsDNA antibody was measured in 4- and 8-week-old ICGN mice and age-matched ICR mice. ELISA detected a markedly high level of serum anti-dsDNA antibody in 8-week-old ICGN mice as compared with age-matched ICR mice (ICR vs ICGN: 1.0 ± 3.0 vs 50.0 ± 38.8 U/mL) (Fig. 4-4).

Discussion

To identify additional associative factors for nephrotic syndrome in ICGN mice, and to better understand onset mechanism of nephrotic syndrome in ICGN mice, microarray analysis was conducted with the renal cortex from 4- and 8-week-old ICGN and ICR mice. As compared with age-matched ICR mice kidney, 252 and 807 transcripts met the filtering criteria in the kidneys of 4- and 8-week-old ICGN mice. Number of differentially expressed transcripts increased with progression of nephrotic syndrome. Canonical pathway analysis identified 41 significantly affected biological pathways in the kidneys of 4- and/or 8-week-old ICGN mice (Table 4-4). The fact that approximately 76 percent of the affected pathways (31 of 41 pathways) were categorized into “Humoral Immune Response”, “Cellular Immune Response” and/or “Cytokine Signaling” raises the possibility that immune-related pathways may play a key role in nephrotic syndrome in ICGN mice. The 37 differentially expressed transcripts (Table 4-3) are considered to be candidates for associative factors for nephrotic syndrome in ICGN mice. The most drastically altered gene was *C1s*, which is involved in complement system. In human, C1s deficiency has been reported to associate with lupus nephritis (Amano *et al*., 2008; Bienaime *et al*., 2010; Dragon-Durey *et al*., 2001; Inoue *et al*., 1998; Suzuki *et al*., 1992). Although it has not been fully understood what activity of the early proteins in the classical pathway of complement protects normal human from development of lupus nephritis, clearance of immune complexes is thought to be a candidate activity (Walport and Davies, 1996). The C1 complex of complement is composed of C1q, C1r, and C1s subcomponents, and is essential to initiate the classical pathway of complement activation. The classical pathway plays a key role in the clearance of circulating immune complexes (Walport, 2001a, b). In deficiency of the classical pathway, circulating immune complexes might escape normal elimination from plasma and deposit in tissues instead.

Then the immune complexes might cause inflammation and release of autoantigens, which in turn could stimulate an autoimmune response. Quantitative PCR revealed that *C1s* gene expression level in ICGN mice liver, where C1s is mainly produced, was markedly reduced as compared to ICR mice (Fig. 4-3). Pathway analysis also detected "Complement System" pathway as significantly altered pathway in the kidneys of ICGN mice at both 4 and 8 weeks of age (Table 4-4). Some of the genes on the "Complement System" pathway were altered in ICGN mice renal cortical tissue, however, *C1s* gene was the most drastically altered (Table 4-5). Decreased expression level of *C1s* gene was already present at 4 weeks of age, when only slight or mild histopathological changes were observed, and persisted to 8 weeks of age. Deposition of immune complexes in glomeruli is a common finding in the inflammatory glomerulonephritis, including lupus nephritis. Anti-dsDNA antibody is diagnostic for systemic lupus erythematosus (SLE) and its specificity is 97.4% (Kavanaugh and Solomon, 2002). Deposition of IgA, IgG and IgM in glomeruli, and marked high level of serum anti-dsDNA antibody observed in ICGN mice indicate that the low expression level of *C1s* gene associates with nephrotic syndrome in ICGN mice.

It has been suggested that deletion mutation of *Tns2* is responsible for nephrotic syndrome in ICGN mice and *Tns2* is expressed in podocytes and tubular epithelial cells in normal mice but not in ICGN mice (Cho *et al*., 2006). I also detected decreased expression level of *Tns2* gene in ICGN mice kidney. OSMR is one of the receptor proteins for Oncostatin M (OSM), which has both pro-inflammatory properties (Modur *et al*., 1997) and anti-inflammatory properties (Wallace *et al*., 1999). In the kidneys, gene expression of *Osmr* was detected in endothelial cells of peritubular capillaries (Tamura *et al*., 2002). OSM has been demonstrated to regulate expressions of tissue inhibitors of metalloproteinases (TIMPs) and matrix metalloproteinases (MMPs) in various types of cells (Gatsios *et al*., 1996; Korzus *et al*., 1997; Li and Zafarullah, 1998). We previously reported the excessive accumulation of

extracellular matrix components (type I, III and IV collagen, fibronectin, laminin and tenascin) and decreased expressions and/or activities of matrix metalloproteinase (MMP)-1, MMP-2, MMP-9 and MMP-12 (Uchio-Yamada *et al*., 2005; Uchio-Yamada *et al*., 2001; Uchio *et al*., 1999; Uchio *et al*., 2000; Uchio *et al*., 2009). The up-regulation of *Osmr* gene may relate to the decreased expressions and/or activities of MMPs in ICGN mice kidneys. Chemokine (C-C motif) receptor 5 (*Ccr5*) gene encodes a member of beta chemokine receptor family, and is preferentially expressed in T cells and macrophages. In human, CCR5-positive mononuclear cells were identified in areas of interstitial infiltration in biopsies of chronic glomerulonephritis, interstitial nephritis, and transplant rejection (Segerer *et al*., 1999). In murine lupus nephritis (MRL/lpr mice), microarray analysis revealed increased expression levels in many genes including *Ccr5* preferentially or exclusively expressed in hematopoietic lineages (Teramoto *et al*., 2008). Therefore, increased expression level of *Ccr5* gene in ICGN mice kidney was considered to be related to leukocytes accumulation. Histocompatibility 2, D region locus 1 (*H2-D1*) is a member of major histocompatibility complex (MHC) class I, which play a central role in the immune system by presenting endogenous antigen. MHC class I is expressed in all nucleated cell and induced by inflammatory cytokines including interferon (IFN) gamma and tumor necrosis factor (TNF) alpha (Hawkins *et al*., 1994; Ikeda *et al*., 1997). Therefore, the highly expressed MHC class I gene in ICGN mice kidney was possibly derived from cytokine-stimulated renal resident cells. Similarly, some of the 37 genes (histocompatibility 2, class II antigen A, alpha (*H2-Aa*) (Rohn *et al*., 1996); class II transactivator (*Ciita*) (Londhe and Davie, 2011); ceruloplasmin (*Cp*) (Mazumder *et al*., 1997); cathepsin S (*Ctss*) (Beers *et al*., 2003); guanylate binding protein 2 (*Gbp2*) (Degrandi *et al*., 2007); myelocytomatosis oncogene (*Myc*) (Rubio and Torres, 1999); tumor necrosis factor, alpha-induced protein 3 (*Tnfaip3*) (Lee *et al*., 2000); and pleckstrin (*Plek*) (Brumell *et al*., 1999)) were reported to be induced by IFN gamma,

TNF alpha and/or interleukin 6. To understand association between the remaining of the differentially expressed 37 transcripts and nephrotic syndrome in ICGN mice, further investigations are needed.

In several types of CD (cluster of differentiation) markers and MHC class II preferentially or exclusively expressed in immune cells, their expression levels were increased in ICGN mice kidney, especially at 8 weeks of age when immune cell infiltration was aggravated (Table 4-6). A part of increased gene expressions in 8-week-old ICGN mice kidney was considered to reflect aggravation of inflammatory cell infiltration. Gene expression levels of some collagen subtypes were also increased especially at 8 weeks of age (Table 4-6). Increased levels of total and type I collagens were detected histochemically in chapter 3. The increase in gene expression levels of collagens are considered to be related to fibrosis associated with progression of nephrotic syndrome.

In chapter 3, bandeiraea simplicifolia lectin-I (BSL-I) showed positive staining in the glomeruli of ICGN mice but not in those of ICR mice, however expression levels of glycosyltransferase genes were not significantly altered in ICGN mice kidney. We reported strong immunohistochemical staining of extracellular matrix (ECM) components (collagen III and IV, laminin and fibronectin) in glomeruli of ICGN mice as compared with ICR mice (Uchio *et al.*, 1999). Therefore, BSL-I may bind to carbohydrate chains of ECM components or that of protein which interact with ECM components.

In summary, our results suggest that immune system, especially complement system, is associated with nephrotic syndrome in ICGN mice. I identified low expression level of *C1s* gene as additional associative factor for nephrotic syndrome in ICGN mice. Further studies are needed to elucidate the mechanism of the marked decrease in *C1s* gene expression, and the role of complement system in the onset of nephrotic syndrome in ICGN mice. The results obtained in this chapter demonstrated

that transcriptome analysis is useful for accurate understanding of pathology of diseases in model animals. Right choice of disease model animals for drug efficacy evaluation is expected to improve extrapolation of drug efficacy to human. Furthermore, in this chapter, genes that increased their expression levels along with disease progression were identified (collagen, MHC class I, and CD markers). These genes are likely to be biomarkers for the diagnosis of disease progression. It is also demonstrated that transcriptome analysis is useful for searching biomarkers of disease progression.

Table 4-1. Blood chemistry and urinalysis

	4 weeks		8 weeks	
	ICR (4)	ICGN (8)	ICR (4)	ICGN (10)
BUN (mg/dL)	19.5 ± 1.9	34.0 ± 6.7**	24.5 ± 3.1	31.9 ± 10.6
serum creatinine (mg/dL)	0.10 ± 0.00	0.10 ± 0.00	0.05 ± 0.06	0.16 ± 0.16
serum total protein (g/dL)	4.05 ± 0.19	3.90 ± 0.30	4.95 ± 0.31	2.89 ± 0.49**
urinary total protein (g/dL)	0.25 ± 0.10	0.41 ± 0.32	1.50 ± 0.36	3.05 ± 0.98*
urinary creatinine (mg/dL)	152.5 ± 17.1	65.6 ± 17.3**	312.5 ± 110.9	48.6 ± 20.4**

Data represent mean ± standard deviation. * and **: $P<0.05$ and 0.01 compared with age-matched ICR mice, respectively. The numbers of mice examined are given in parentheses.

Table 4-2. Histopathological examination of ICR and ICGN mice kidney.

		4 weeks		8 weeks	
Findings	Grade[a)]	ICR (4)	ICGN (8)	ICR (4)	ICGN (10)
Expansion of mesangial areas	0	4	0	4	0
/Thickening of the GBM	1	0	7	0	0
	2	0	1	0	4
	3	0	0	0	6
	4	0	0	0	0
Tubulointerstitial injury	0	4	4	4	0
	1	0	4	0	1
	2	0	0	0	4
	3	0	0	0	3
	4	0	0	0	2

a) Grade of change: 0 = negative; 1 = slight; 2 = mild; 3 = moderate; 4 = severe.
The numbers of mice examined are given in parentheses.

Table 4-3. List of differentially regulated genes in ICGN mice kidney at both of 4 and 8 weeks of age

			Fold change	
Probe Set ID	Gene Symbol	Entrez Gene Name	4W	8W
1424041_s_at	*C1s*	complement component 1, s subcomponent	-45.1	-26.8
1423487_at	*Cript*	cysteine-rich PDZ-binding protein	-16.0	-5.4
1418837_at	*Qprt*	quinolinate phosphoribosyltransferase	6.1	6.1
1438858_x_at	*H2-Aa*	histocompatibility 2, class II antigen A, alpha	5.1	5.5
1449526_a_at	*Gdpd3*	glycerophosphodiester phosphodiesterase domain containing 3	4.8	31.7
1422141_s_at	*Csprs*	component of Sp100-rs	4.7	7.2
1460416_s_at	*Csprs /// Gm7592 /// Gm7609 /// LOC100503923*	component of Sp100-rs /// predicted gene 7592 /// predicted pseudogene 7609 /// hypothetical protein LOC100503923	4.2	4.4
1434833_at	*Map4k2*	mitogen-activated protein kinase kinase kinase kinase 2	-4.0	-3.8
1452264_at	*Tenc1, Tns2*	tensin like C1 domain-containing phosphatase (tensin 2)	-4.0	-3.4
1424727_at	*Ccr5*	chemokine (C-C motif) receptor 5	3.9	3.4
1445293_at	---	---	-3.4	-4.3
1426324_at	*H2-D1*	histocompatibility 2, D region locus 1	3.2	3.2
1421211_a_at	*Ciita*	class II transactivator	3.1	8.1
1425951_a_at	*Clec4n*	C-type lectin domain family 4, member n	3.1	3.7
1448734_at	*Cp*	ceruloplasmin	2.9	15.3
1417495_x_at	*Cp*	ceruloplasmin	2.9	14.4
1452661_at	*Tfrc*	transferrin receptor	-2.8	-2.5
1436905_x_at	*Laptm5*	lysosomal-associated protein transmembrane 5	2.7	4.6
1441975_at	*Acpp*	acid phosphatase, prostate	2.6	2.9
1437217_at	*Ankrd6*	ankyrin repeat domain 6	2.6	3.9
1442436_at	*Fn3k*	fructosamine 3 kinase	-2.6	-2.1
1457753_at	*Tlr13*	toll-like receptor 13	2.5	2.9
1448591_at	*Ctss*	cathepsin S	2.5	5.7
1416318_at	*Serpinb1a*	serine (or cysteine) peptidase inhibitor, clade B, member 1a	2.4	2.6
1426601_at	*Slc37a1*	solute carrier family 37 (glycerol-3-phosphate transporter), member 1	2.4	3.8
1436778_at	*Cybb*	cytochrome b-245, beta polypeptide	2.3	3.6
1435906_x_at	*Gbp2*	guanylate binding protein 2	2.3	3.5
1424942_a_at	*Myc*	myelocytomatosis oncogene	2.3	3.2
1418674_at	*Osmr*	oncostatin M receptor	2.2	2.9
1455700_at	*Mterfd3*	MTERF domain containing 3	2.2	2.2
1433699_at	*Tnfaip3*	tumor necrosis factor, alpha-induced protein 3	2.1	4.4
1448748_at	*Plek*	pleckstrin	2.1	3.2
1415698_at	*Golm1*	golgi membrane protein 1	2.1	3.6
1419004_s_at	*Bcl2a1a /// Bcl2a1b /// Bcl2a1d*	B-cell leukemia/lymphoma 2 related protein A1a /// B-cell leukemia/lymphoma 2 related protein A1b /// B-cell leukemia/lymphoma 2 related protein A1d	2.1	4.5
1460259_s_at	*Clca1 /// Clca2*	chloride channel calcium activated 1 /// chloride channel calcium activated 2	2.1	3.4
1417852_x_at	*Clca1*	chloride channel calcium activated 1	2.0	2.7
1450869_at	*Fgf1*	fibroblast growth factor 1	-2.0	-2.4

Data represent fold change value (ICGN/ICR, N=3)

Table 4-4. Canonical pathways affected significantly in ICGN mice kidney as compared with ICR mice kidney

Canonical pathway	Signaling Pathway Categories	-Log (p-value) 4W	8W
Type I Diabetes Mellitus Signaling	Apoptosis; Disease-Specific Pathways	5.26	
Role of NFAT in Regulation of the Immune Response	**Cellular Immune Response**; **Humoral Immune Response**; Intracellular and Second Messenger Signaling	4.33	
Acute Phase Response Signaling	**Cytokine Signaling**; Ingenuity Toxicity List Pathways	4.2	
NF-κB Activation by Viruses	**Cellular Immune Response**; Pathogen-Influenced Signaling	3.79	
PKCθ Signaling in T Lymphocytes	**Cellular Immune Response**	3.49	
Virus Entry via Endocytic Pathways	Pathogen-Influenced Signaling	3.34	
Nur77 Signaling in T Lymphocytes	Apoptosis; **Cellular Immune Response**; Nuclear Receptor Signaling	3.07	
Systemic Lupus Erythematosus Signaling	Disease-Specific Pathways	3.02	
Calcium-induced T Lymphocyte Apoptosis	Apoptosis; **Cellular Immune Response**	2.75	
CD28 Signaling in T Helper Cells	**Cellular Immune Response**	2.75	
CTLA4 Signaling in Cytotoxic T Lymphocytes	**Cellular Immune Response**	2.64	
IL-6 Signaling	**Cellular Immune Response**; **Cytokine Signaling**	2.61	
Docosahexaenoic Acid (DHA) Signaling	Intracellular and Second Messenger Signaling; Neurotransmitters and Other Nervous System Signaling	2.53	
IL-4 Signaling	**Cellular Immune Response**; **Cytokine Signaling**; **Humoral Immune Response**	2.45	
iCOS-iCOSL Signaling in T Helper Cells	**Cellular Immune Response**	2.3	
Rac Signaling	Intracellular and Second Messenger Signaling	2.26	
TNFR1 Signaling	Apoptosis; **Cytokine Signaling**	2.22	
fMLP Signaling in Neutrophils	**Cellular Immune Response**; **Cytokine Signaling**	2.22	
Graft-versus-Host Disease Signaling	**Cellular Immune Response**; Disease-Specific Pathways	5.74	5.38
Antigen Presentation Pathway	**Cellular Immune Response**; **Humoral Immune Response**	5.42	4.95
Autoimmune Thyroid Disease Signaling	**Cellular Immune Response**; Disease-Specific Pathways; **Humoral Immune Response**	4.8	4.06
Complement System	**Humoral Immune Response**	4.36	3.43
Allograft Rejection Signaling	**Cellular Immune Response**; Disease-Specific Pathways	4.32	3.39
Dendritic Cell Maturation	**Cellular Immune Response**; **Cytokine Signaling**; Pathogen-Influenced Signaling	4.27	5.92
IL-10 Signaling	**Cellular Immune Response**; **Cytokine Signaling**	4.03	2.94
Role of Pattern Recognition Receptors in Recognition of Bacteria and Viruses	**Cellular Immune Response**; Pathogen-Influenced Signaling	3.98	3.27
OX40 Signaling Pathway	**Cellular Immune Response**	3.82	2.73
Altered T Cell and B Cell Signaling in Rheumatoid Arthritis	**Cellular Immune Response**; Disease-Specific Pathways	3.64	7.49
B Cell Development	Cellular Growth, Proliferation and Development; **Humoral Immune Response**	3.25	5.44
Communication between Innate and Adaptive Immune Cells	**Cellular Immune Response**	3.16	7.77

Table 4-4. (continued)

Canonical pathway	Signaling Pathway Categories	-Log (p-value) 4W	8W
Cytotoxic T Lymphocyte-mediated Apoptosis of Target Cells	Apoptosis; **Cellular Immune Response**	3.15	3.15
Crosstalk between Dendritic Cells and Natural Killer Cells	**Cellular Immune Response**	3.02	2.22
Hepatic Fibrosis / Hepatic Stellate Cell Activation	Disease-Specific Pathways; Ingenuity Toxicity List Pathways	2.83	6.97
Pathogenesis of Multiple Sclerosis	Disease-Specific Pathways	2.16	4.54
TREM1 Signaling	**Cellular Immune Response**; **Cytokine Signaling**	2.12	2.27
Role of Hypercytokinemia/hyperchemokinemia in the Pathogenesis of Influenza	**Cellular Immune Response**; **Cytokine Signaling**	2.03	4.04
LXR/RXR Activation	Ingenuity Toxicity List Pathways; Nuclear Receptor Signaling	2.02	3.27
Atherosclerosis Signaling	Cardiovascular Signaling; Disease-Specific Pathways		4.39
Intrinsic Prothrombin Activation Pathway	Cardiovascular Signaling; Cellular Stress and Injury		3.32
T Helper Cell Differentiation	**Cellular Immune Response**; **Cytokine Signaling**		2.66
Primary Immunodeficiency Signaling	**Cellular Immune Response**; Disease-Specific Pathways; **Humoral Immune Response**		2.29

Bold: Significantly affected pathways which were categorized into “Humoral Immune Response”, “Cellular Immune Response” and/or “Cytokine Signaling”.

Table 4-5. Affected genes on Complement System pathway

Probe Set ID	Gene Symbol	Entrez Gene Name	Fold change 4W	Fold change 8W
1417381_at	*C1qa*	complement component 1, q subcomponent, alpha polypeptide	2.5	4.8
1417063_at	*C1qb*	complement component 1, q subcomponent, beta polypeptide	2.6	4.7
1437726_x_at	*C1qb*	complement component 1, q subcomponent, beta polypeptide	2.4	6.1
1449401_at	*C1qc*	complement component 1, q subcomponent, C chain	2.6	5.5
1424041_s_at	*C1s*	complement component 1, s subcomponent	-45.1	-26.8
1441912_x_at	*C2*	complement component 2 (within H-2S)	1.1	2.2
1423954_at	*C3*	complement component 3	4.3	20.7
1419483_at	*C3ar1*	complement component 3a receptor 1	2.5	2.1
1442082_at	*C3ar1*	complement component 3a receptor 1	2.5	4.8
1450876_at	*Cfh*	complement component factor h	1.2	3.0
1416625_at	*Serping1*	serine (or cysteine) peptidase inhibitor, clade G, member 1	1.2	2.4

The shaded columns: $p<0.01$ compared with age-matched ICR mice.

Table 4-6. Representative genes up-regulated significantly in ICGN mice kidney at 8 weeks of age

Probe Set ID	Gene Symbol	Entrez Gene Name	Fold change 4W	Fold change 8W
MHC class II				
1435290_x_at	*H2-Aa*	histocompatibility 2, class II antigen A, alpha	3.4	3.2
1438858_x_at	*H2-Aa*	histocompatibility 2, class II antigen A, alpha	5.1	5.5
1443687_x_at	*H2-DMb2*	histocompatibility 2, class II, locus Mb2	3.3	16.6
1422891_at	*H2-Ea-ps /// LOC100504404*	histocompatibility 2, class II antigen E alpha, pseudogene /// h-2 class II histocompatibility antigen, E-K alpha chain-like	9.5	15.9
1422892_s_at	*H2-Ea-ps /// LOC100504404*	histocompatibility 2, class II antigen E alpha, pseudogene /// h-2 class II histocompatibility antigen, E-K alpha chain-like	8.9	29.9
1417025_at	*H2-Eb1*	histocompatibility 2, class II antigen E beta	3.6	3.4
1425519_a_at	*Cd74*	CD74 antigen (invariant polypeptide of major histocompatibility complex, class II antigen-associated)	3.3	5.2
CD markers reported to be preferentially expressed in hematopoietic lineages				
1417268_at	*Cd14*	CD14 antigen	2.0	3.7
1437502_x_at	*Cd24a*	CD24a antigen	-1.2	2.1
1449473_s_at	*Cd40*	CD40 antigen	1.3	2.9
1449164_at	*Cd68*	CD68 antigen	1.8	3.3
1426112_a_at	*Cd72*	CD72 antigen	2.0	2.3
1425519_a_at	*Cd74*	CD74 antigen (invariant polypeptide of major histocompatibility complex, class II antigen-associated)	3.3	5.2
1420404_at	*Cd86*	CD86 antigen	3.0	2.9
1449858_at	*Cd86*	CD86 antigen	2.8	3.1
Collagen				
1455494_at	*Col1a1*	collagen, type I, alpha 1	-1.4	2.7
1423110_at	*Col1a2*	collagen, type I, alpha 2	-1.3	4.0
1450857_a_at	*Col1a2*	collagen, type I, alpha 2	-1.3	2.5
1427883_a_at	*Col3a1*	collagen, type III, alpha 1	-1.4	2.5
1427884_at	*Col3a1*	collagen, type III, alpha 1	-1.5	4.1
1416740_at	*Col5a1*	collagen, type V, alpha 1	-1.1	2.4
1416741_at	*Col5a1*	collagen, type V, alpha 1	1.2	3.2
1422437_at	*Col5a2*	collagen, type V, alpha 2	-1.0	3.5
1418441_at	*Col8a1*	collagen, type VIII, alpha 1	1.7	2.9
1455627_at	*Col8a1*	collagen, type VIII, alpha 1	1.2	3.6
1427391_a_at	*Col12a1*	collagen, type XII, alpha 1	1.3	3.0
1434411_at	*Col12a1*	collagen, type XII, alpha 1	1.6	3.8
1418237_s_at	*Col18a1*	collagen, type XVIII, alpha 1	1.6	4.0
1426955_at	*Col18a1*	collagen, type XVIII, alpha 1	1.5	3.0

The shaded columns: $p<0.01$ compared with age-matched ICR mice.

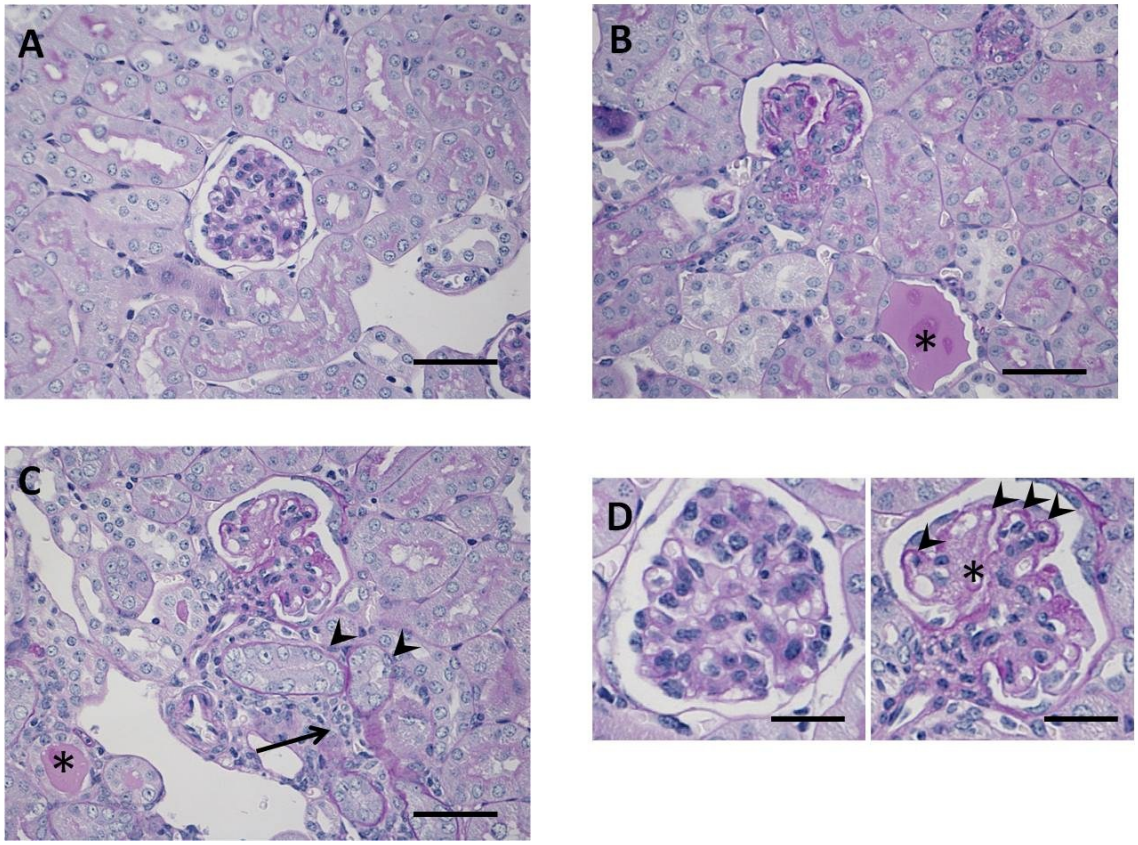

Fig. 4-1.

Kidney sections from 4-week-old ICR (A), 4-week-old ICGN (B) and 8-week-old ICGN (C) mice were stained with PAS. High magnifications of glomerulus in 4-week-old ICR (left) and 8-week-old ICGN (right) mice are shown in (D). Glomeruli with expanded mesangial area/thickening of the GBM and protein cast (asterisk) were observed in 4-week-old ICGN mice (B). In 8-week-old ICGN mice (C), not only lesions found in 4-week ICGN mice were progressed but inflammatory cell infiltration (arrows) and basophilic tubules (arrowheads) become marked. Glomeruli in 8-week-old ICGN mice showed prominent mesangial area expansion (asterisk) and thickening of the GBM (arrowheads) (D). Bars in (A), (B) and (C): 50 μm. Bars in (D): 25 μm

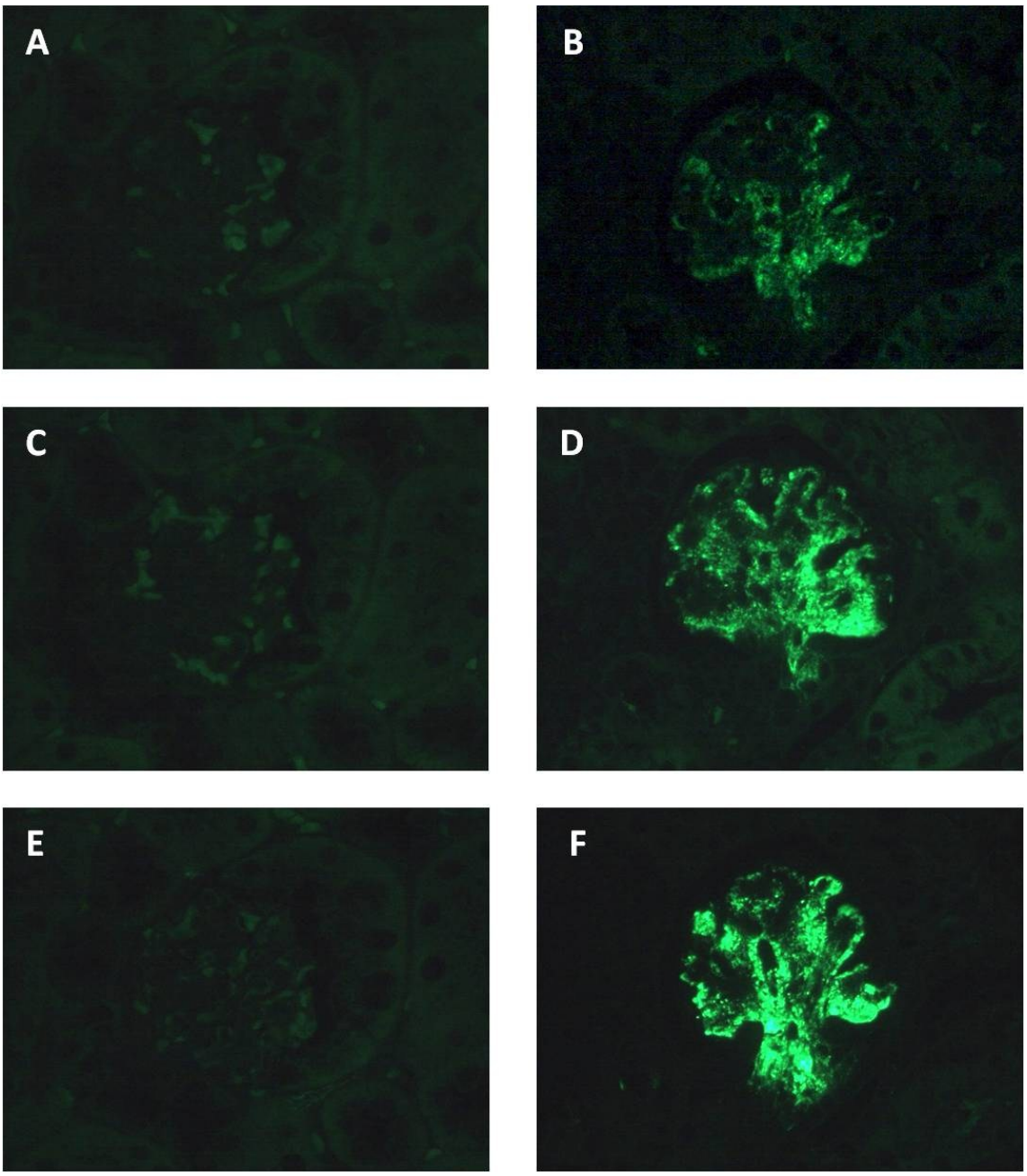

Fig. 4-2.
Representative photographs of IgA, IgG and IgM immunostaining. Kidney sections of 8-week-old ICR (A, C and E) and ICGN (B, D and F) mice were stained with antibodies to IgA (A and B), IgG (C and D) and IgM (E and F). Positive reactions were observed in GBM of ICGN mice (B, D and F).

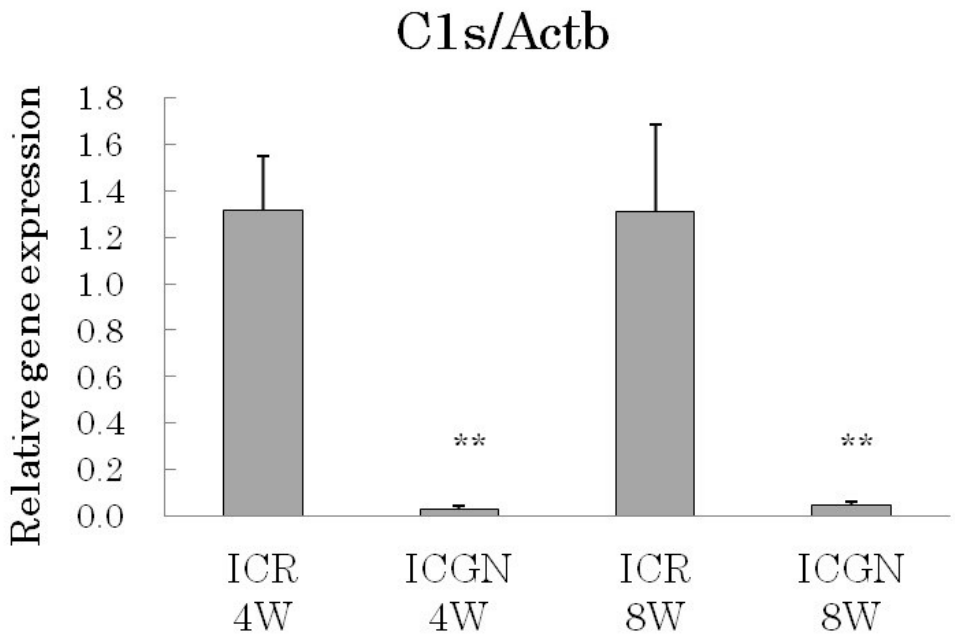

Fig. 4-3.

Expression level of *C1s* mRNA in the livers was assessed by quantitative PCR. *C1s* mRNA level was markedly low in ICGN mice as compared with age-matched ICR mice at both 4 and 8 weeks of age. Each value is averaged among 3 mice with error bar displaying the standard deviation. **: $P<0.01$ compared with age matched ICR mice.

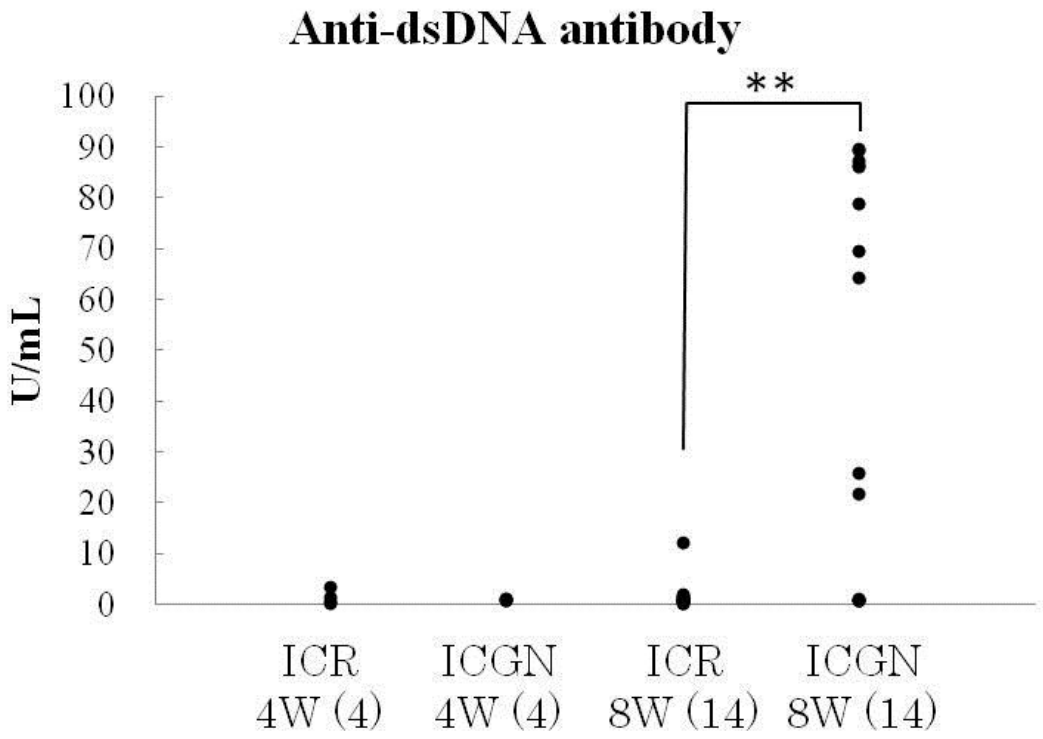

Fig. 4-4.

Serum anti-dsDNA antibody was measured by ELISA in 4- and 8-week-old ICGN mice and age-matched ICR mice. Markedly high level of serum anti-dsDNA antibody was observed in ICGN mice as compared with ICR mice. **: $P<0.01$ compared with age matched ICR mice. The numbers of mice examined are given in parentheses.

General Discussion

The draft of the human genome was completely sequenced in 2001 (Baltimore, 2001; Venter *et al*., 2001), offering a prospect of arrival of a new age in disease prevention and treatment. However, to date, not much development has been made. On the contrary, productivity of medical product R&D has continued to decline, causing an issue that confronts nations and pharmaceutical industries. Transcriptome analytic technologies that dramatically advanced along with the human genome sequencing study are applied to various stages of medical product R&D, having offered a prospect of improvement in productivity of R&D of medicines. However, the achievement has not emerged yet. Transcriptome analysis is superior to other omics studies including proteome and metabolome analyses in terms of throughput capacity of data acquisition and adaptability to database compilation. For example, while using GeneChip® by Affymetrix, we can obtain expression data of tens of thousands genes per sample for 50 samples for one week. There are currently over 70 public databases that store transcriptomic data (Fernandez-Suarez and Galperin, 2013). Successful and sufficient utilization of the potential of transcriptome analysis is expected to significantly improve productivity in medical product R&D. Moreover, It is consider that there is much room for technical improvement to transcriptome analysis of kidney since in this organ the physiological functions, including gene expression, differ between the anatomical regions (papilla, medulla, and cortex). Under such circumbstances, I investigated techniques and usages of transcriptome analysis for improving productivity of R&D of medicines aiming at the development of therapeutic drugs for kidney disease.

In chapter 1, I analyzed transcriptomic data of rat liver (*in vivo*) and rat primary hepatocytes (*in vitro*) treated with PPARα agonist using the toxicogenomics database (TG-GATEs) constructed by the Japanese national project. I was a member of this project, and engaged mainly in transcriptome data synthesis and its quality control.

PPARα agonists, antihyperlipidemic drugs, have been reported recently to possess kidney-protecting activity, and to potentially become drugs for chronic kidney disease (Kamijo *et al*., 2007a; Kamijo *et al*., 2007b; Kamijo *et al*., 2002; Kono *et al*., 2009). Analysis of transcriptomic data of the three PPARα agonists, Clofibrate, WY-14643, and gemfibrozil led to the finding that a number of genes related to β-oxidation of fatty acids were induced both *in vivo* and *in vitro*. However, expression changes of genes related to cellular proliferation, apoptosis, immune response, coaggulation, and stress reaction were observed only *in vivo*. Using the genes mobilized in two or three PPARα agonists, hierarchical cluster analysis of 32 compounds in the database were performed. In the profiling of an *in vivo* single dose, benzbromarone and aspirin were located in the same cluster of the three PPARα agonists. The clustering of *in vitro* data revealed that benzbromarone, three NSAIDs (Non-Steroidal Anti-Inflammatory Drug; aspirin, indomethacin and diclofenac sodium) and valproic acid belonged to the same cluster of PPARα agonists. Because benzbromarone and several NSAIDs have been reported to possess agonistic activity to PPARα (Bichet *et al*., 1990; Lehmann *et al*., 1997), this result seemed valid reflecting the presence or absence of agonistic activity to PPARα. In addition, analysis of the principal components using the genes induced both *in vivo* and *in vitro* demonstrated that the first principal component is useful for the extraction of PPARα agonist-like compounds from the database. These results indicate that transcriptomic data and their database of exposure experiments to compounds are useful for searching compounds with desired pharmacological activity. As mentioned above, PPARα agonist has been reported to possess kidney-protecting activity. Therefore, the compounds which were indicated to be PPARα agonist in the present transcriptome analysis potentially become a drug for chronic kidney disease as well as known PPARα agonists become.

In chapter 2, the transcriptomic data of papilla, medulla, cortex, and whole slice of kidney were compared and analyzed as a basis of transcriptome analysis of

kidney where physiological functions including gene expression differ among these three anatomical regions. The transcriptomic data were acquired using GeneChip® (Rat Genome 230 2.0, Affymetrix). Global normalization is a general normalization method for microarray data, in which mean or median values of expression levels of all genes are adjusted among samples. This normalization is based on an assumption that the total expression level of RNA is consistent among samples. Therefore, use of this correction method has a problem when the regions containing different total amount of RNA are compared, particularly when the papilla which has relatively lower total RNA amount is compared with other regions (medulla, cortex, and whole slice). Indeed, ANOVA was performed on the gene expression values with global normalization in papilla, medulla, cortex, and whole slice, and considerable number of genes appeared to be the highest in papilla. It can be considered that global normalization raised excessively the gene expression levels in papilla that were originally relatively lower. Furthermore, many genes in the whole slice showed either the highest or lowest expression level, which is theoretically unlikely. In order to solve the problems with global normalization, I applied "percellome" normalization (a way to obtain copy number of mRNAs per cell) to comparison of the transcriptomic data among the regions (Kanno *et al*., 2006). The principle of percellome normalization is simple. Instead of counting the number of cells in a sample, DNA amount is measured. Based on DNA amount, external standard mRNA (spike RNA) is added to the sample at designated number of molecules per cell, followed by RNA extraction and microarray experiment (measurement). Using the measurement value of the spike RNA as a reference, the value of each RNA in the sample is converted to the copy number per cell. The spike RNA used was a cocktail, which consists of 5 different *Bacillus subtilis* mRNA with different concentration. Use of percellome normalization allowed efficient extraction of differentially regulated genes among the regions by ANOVA. When they were sorted by the fold difference to other regions, the higher rank was occupied by

genes characteristic to the functions of kidney, i.e., channels, transporters, and metabolic enzymes. Some of the results obtained here were consistent with other reports and valid as well in terms of kidney physiology. The knowledge obtained in this chapter enables accurate comparison of gene expression levels among regions of an organ, or among multiple organs, and would be useful in investigation of target molecule distribution during the target search stage of the drug R&D.

In chapter 3, to fully understand pathological process of nephrotic syndrome in ICGN mice before transcriptome analysis of these mice (chapter 4), I evaluated progress of nephrotic syndrome in male heterozygous and homozygous ICGN mice throughout their lifetime (at 10, 30 and 50 week of age) with clinical chemistry, urinary and histopathological examination and histochemical quantification of total and type I collagens. Additionally, I histologically evaluated changes in the cell-surface carbohydrate structures in the kidneys using 24 types of lectins. ICR mice were also evaluated as healthy controls. In homozygous ICGN mice, aged animal (50 weeks) manifested clinical abnormalities such as the exercise intolerance, pale ears, weight loss as well as edema. The nephrotic state progressed in an age-dependent manner. Severe albuminuria and hypoalbuminemia, marked increases in serum creatinine and BUN, and significant increases in renal total and type I collagen levels were observed at 30 and 50 week of age. Histopathological examination detected expansion of the mesangial areas with an apparent increase in the mesangial matrix, appearance of cysts, extension of renal tubules and infiltration of inflammatory cells in the kidney of 50-week-old animals. Such histopathological abnormalities progressed in an age-dependent manner. In heterozygous ICGN mice, there were no significant differences in clinical chemistry and urinalysis parameters and collagen levels as compared with ICR mice at any time point examined, while histopathological examination detected moderate expansion of mesangial matrix. The reaction of Bandeiraea simplicifolia lectin-I (BSL-I) that specifically binds to

α-D-galactopyranosyl group was detected only in the kidneys of ICGN mice, and was more intense in homozygous mice in which the disease progressed more than that in heterozygous mice. Lectin blotting with BSL-I clarified that glycoproteins with a molecular weight of 45, 58, and 64 kD were specifically detected in kidney of ICGN mice, and that the 64-kD glycoprotein in particular increased in homozygous mice. Transcriptome analysis detected no significant change in expression levels of glycosyltransferase genes in ICGN mice kidney (chapter 4), while immunohistochemistry detected depositions of extracellular matrix (ECM) components (collagen III and IV, laminin and fibronectin) in glomeruli of ICGN mice as compared with ICR mice (Uchio *et al.*, 1999). Therefore, BSL-I may bind to carbohydrate chains of ECM components or that of proteins which interact with ECM components. This specific glycoprotein was likely to be a factor related with the onset of nephrotic syndrome in ICGN mice.

In chapter 4, I challenged to search causative genes and diagnostic biomarkers for nephrotic syndrome in ICGN mice, a model animal of hereditary nephrotic syndrome, through transcriptome analysis. ICGN mice are derived from ICR mice, and develop nephrotic syndrome as they age. In 2006, mutation of tensin2 gene (change to termination codon by frame shift mutation) was reported to be the cause of nephrotic syndrome in ICGN mice. However, existence of other causative genes has been indicated. Transcriptome analysis of ICGN and ICR renal cortex identified that in the kidneys of ICGN mice, genes involved in immune-related pathways were remarkably influenced compared with those in ICR mice. Moreover, complement component 1s subcomponent (*C1s*), which has been reported to be related with lupus nephritis in humans (Suzuki *et al*., 1992), showed remarkably low expression level in ICGN mice. The low expression of *C1s* gene was also observed by quantitative PCR in liver, a major complements-producing organ. High titer of blood anti-dsDNA antibody is a diagnostic indicator of systemic lupus erythematosus (specificity: 97.4%) (Kavanaugh

and Solomon, 2002). Among ICGN mice, some individuals showed remarkably higher titers than those of ICR mice. Complement component 1 (C1) plays an important role in the removal of immune complexes (Walport, 2001a, b). In the glomeruli of ICGN mice, deposition of IgA, IgG, and IgM was observed by immunostaining. Deposition of immune complexes in glomeruli is also a characteristic of lupus nephritis. These results indicated that low expression of *C1s* gene is involved in the onset of nephrotic syndrome in ICGN mice, and that ICGN mice are appropriate for an experimental model of lupus nephritis. The results obtained in this chapter demonstrated that transcriptome analysis is useful for accurate understanding of pathology of diseases in model animals. Right choice of disease model animals for drug efficacy evaluation is expected to improve extrapolation of drug efficacy to human. Furthermore, in this chapter, genes that increased their expression levels along with disease progression were identified (MHC class I, CD markers and collagens). They were considered to reflect aggravation of inflammatory cell infiltration or fibrosis. Regarding fibrosis, increased level of total collagen was detected histochemically in ICGN mice kidney in chapter 3. These genes are likely to be biomarkers for the diagnosis of disease progression. It is also demonstrated that transcriptome analysis is useful for searching biomarkers of disease progression.

Based on the results shown above, several solutions using transcriptome analysis for the reduced productivity in R&D of medicines was indicated (Fig. GD-1). First, in the target search stage of R&D of medicines, I considered that transcriptome analysis using percellome normalization is effective for accurately obtaining distribution data of the target molecules (chapter 2). In the stage of non-clinical evaluation of medicines, 44% of failure of drug development was reported to be due to toxicity (Suter *et al*., 2004). In the case of toxicity through the target molecule, the toxicity is concerned to develop in organs where the target molecule is expressed. For

example, in renal papillary necrosis by NSAIDs known as a typical case of drug-caused nephrotoxicity (Schnellmann, 2001), inhibition of cyclooxygenase (COX), a pharmacological activity of NSAIDs, is considered to be the mechanism of the toxicity. In chapter 2, genes of cyclooxygenase, *ptgs1* and *ptgs2*, were revealed to be expressed most in papilla in the kidney. The site of the toxicity development is consistent with the distribution of the target molecule of NSAIDs. Regarding toxicity through the drug target molecule, the toxicity is concerned to develop in various organs if the target molecule is distributed systemically. Accurate investigation of target molecule distribution using percellome normalization would enable us to choose drug target molecules with less toxicity concern and to predict organs where the toxicity develops.

Next, in the compound screening stage, I demonstrated that the toxicogenomics database (TG-GATEs) is applicable to the concept of Drug Repositioning, discovering new efficacy of existing drugs for novel indications, by identifying PPARα agonist activity of benzbromarone and NSAIDs (chapter 1). In the case of development of an existing drug for a new indication, Phase II trial normally requiring 2 years and 17 million USD (DiMasi *et al*., 2003) can be conducted in a simplified form and shorter period because the safety and pharmacokinetics in humans were already studied. In addition, majority of toxicity and metabolism studies required for the development of medicines can be omitted, allowing us to reduce 40% of overall cost according to DiMasi *et al*. (2003). Although the toxicogenomics database (TG-GATEs) was constructed for solving toxicity issues, application of this database to Drug Repositioning will lead to streamlining of medical product R&D.

In the following non-clinical stage of medical product R&D, I indicated the possibility that profiling of disease model animals using transcriptome analysis would be useful for right choice of disease model animals for drug efficacy evaluation. When the phase of clinical trial proceeds, problem in efficacy that drug efficacy confirmed in

disease model animals is not reproduced in humans becomes leading cause of attrition (52% and 72% in Phase II and III trials, respectively) (Suter *et al*., 2004). Use of model animals accurately reflecting human diseases to obtain drug efficacy data will improve extrapolation of drug efficacy to humans. In chapter 3, I clarified through transcriptome analysis that remarkably low expression of *C1s* gene is related with onset of nephrotic syndrome in ICGN mice. Clarification of pathology in disease model animals through transcriptome analysis allows us to scientifically select disease model animals in drug efficacy evaluation. Because mutation of C1s gene in humans is related with lupus nephritis, use of ICGN mice in the evaluation of drugs for lupus nephritis will enable us to accurately predict the efficacy in clinical practices.

So far, I have discussed the utilization of transcriptome analysis at each stage of medical product R&D. Additionally, we can effectively utilize transcriptome analysis across stages. In chapter 4, transcriptome analysis of ICGN mice kidney identified biomarkers for the diagnosis of disease progression as well as the causative genes of nephrotic syndrome in ICGN mice. These disease-related genes identified in the non-clinical stage would be used in the clinical stage as biomarkers for patient selection (personalized medicine) or as diagnostic and prognostic biomarkers. Moreover, I demonstrated that lectin staining that recognizes a cell surface carbohydrate structure would be also useful as biomarkers for diagnosis and prognosis of nephrotic syndrome (chapter 3). The importance of these biomarkers is indicated by the aforementioned Critical Path Opportunities List（U.S. Department of Health and Human Services, FDA, 2006) by FDA. Novel biomarkers of drug efficacy will facilitate the development of a new type of clinical trial in which better data of drug efficacy can be obtained more promptly than we do currently. Moreover, novel biomarkers which sensitively predict safety are helpful for understanding safety issue of drugs before clinical trials or placing the products on market.

Another opportunity for utilizing transcriptome analysis across the stages of medical product R&D is to input the knowledge obtained by transcriptome analysis in the non-clinical stage into the stage of compound screening. As a trial, I searched in the toxicogenomics database (TG-GATEs) for drugs that improve low expression of *C1s* gene, a causative factor of nephrotic syndrome in ICGN mice, and it was clarified that several NSAIDs induce expression of *C1s* gene in a dose-dependent manner (Fig. GD-2).

By integrating results from chapter 1, 2 and 4, I can propose a development plan of drug for lupus nephritis based on transcriptome analysis. Recently it has been reported that PPARα agonists protect kidney from proteinuria-associated tubular toxicity, in which albumin serves as a carrier of fatty acid and increased fatty acid causes the toxicity (Kamijo *et al.*, 2007a). In chapter 1, it was indicated that some NSAIDs (aspirin, diclophenac sodium and indomethacin) have PPARα agonist activity, and we confirmed that diclophenac sodium and indomethacin have PPARα binding activity by *in vitro* PPARα binding assay (Ohno and Urushidani, 2012). In chapter 4, I identified low expression level of *C1s* genes, whose human homologue has been reorted to associate with lupus nephritis, as an associative factor for nephrotic syndrome in ICGN mice, and I confirmed that some NSAIDs could increase *C1s* gene expression in rat liver (Fig. GD-2). Consequently, it is suggested that drug candidates with strong PPARα agonist activity and C1s gene induction potential would be obtained by structural modification using NSAIDs as a basic compound, and that they would become treatment for lupus nephritis. Because proteinurea and decreased *C1s* gene expression were observed in ICGN mice, evaluation of these drug candidates using ICGN mice will help us to accurately predict the efficacies in clinical practices. Regarding toxicity, these drug candidates derived from NSAIDs are expected to cause toxicity in renal papilla, because papilla-specific gene expressions of cyclooxygenase

(*ptgs1* and *ptgs2*), target molecules of NSAIDs, were identified in chapter 2. Recently, useful biomarkers of renal papillary necrosis have been reported (Sasaki *et al*., 2011). The drug-induced toxicity in renal papilla should be carefully monitored with these biomarkes.

The series of studies have also indicated several important notes in the use of transcriptome analysis in medical product R&D. One is the limited reflection of the *in vivo* system by *in vitro*. In chapter 1, I compared transcriptomic data between rat liver (*in vivo)* and rat primary hepatocytes (*in vitro*) treated with PPARα agonist, and found that a number of genes related with β-oxidation of fatty acids were induced both *in vitro* and *in vivo*. On the other hand, the expression changes of genes related with cellular proliferation, apoptosis, immune response, coagulation, and stress reaction were observed only *in vivo*. PPARα agonist is a rat nongenotoxic carcinogen, and the most likely mechanism is that hepatic parenthymal cells are activated to proliferate while their apoptosis is suppressed (Boitier *et al*., 2003; Michalik *et al*., 2004). In addition, many articles have reported that Kupffer cells or TNFα produced by Kupffer cells are required for the activation of the cellular proliferation by PPARα agnonist (Decker, 1990; Parzefall *et al*., 2001; Rolfe *et al*., 1997; Rose *et al*., 1997). In our results, expression levels of genes related with cellular proliferation or apoptosis were not altered *in vitro*, and it could be due to the fact that the numbers of non-parenchymal cells, including Kupffer cells, in the culture were much less than that for *in vivo* liver. The biggest advantage of *in vitro* assay system in medical product R&D is that efficacy and toxicity of candidate compounds can be evaluated with a small amount of the compounds. However, as shown here, we must keep in mind that reflection of *in vivo* systems by *in vitro* assay systems has limitations.

Another note is important while conducting transcriptome analysis of organs with anatomically complicated structure. The transcriptomic data of kidneys stored in

the national toxicogenomics database (TG-GATEs) were obtained from kidney slices containing papilla, medulla, and cortex. The data strongly reflect transcriptomes of cortex and medulla, but not sufficiently that of papilla. This is due to the difference in the proportion of the regions in the whole slice, cortex > medulla >> papilla. Therefore, while the correlation coefficients of transcriptomic data between whole slice and cortex and medulla were above 0.98 and above 0.95, respectively, that of papilla was approximately 0.8. In addition, the number of genes with present call in all samples of papilla but absent in all of medulla and cortex, papilla-specific genes, were 488, and only 27 (6%) were all present in the whole slice (present call: indicator showing that the gene expression level is trustworthy). From these results, when conducting transcriptome analysis of organs with anatomically complicated structure, it is considered to be preferable to obtain transcriptomic data after separating the target region of the investigation. However, taking into consideration the cost of microarray, in TG-GATEs, the transcriptomic data of kidneys were obtained from whole slice containing papilla, medulla, and cortex. Therefore, when we use TG-GATEs as a reference database, we should keep in mind that we may miss the actually occurring gene expression changes in renal papilla. In the current medical product R&D, we have to obtain truly-valuable knowledge from vast data such as TG-GATEs. The important notes on transcriptome analysis mentioned here would reduce misleading in medical product R&D and help to improve productivity.

In this thesis, I have presented the effective utilization of transcriptome analysis at each stage and across stages of medical product R&D with important notes. Moreover, I proposed a development plan of drug for lupus nephritis based on transcriptome analysis. This knowledge is expected to contribute in improving the productivity of medical product R&D and development of medicine in the future.

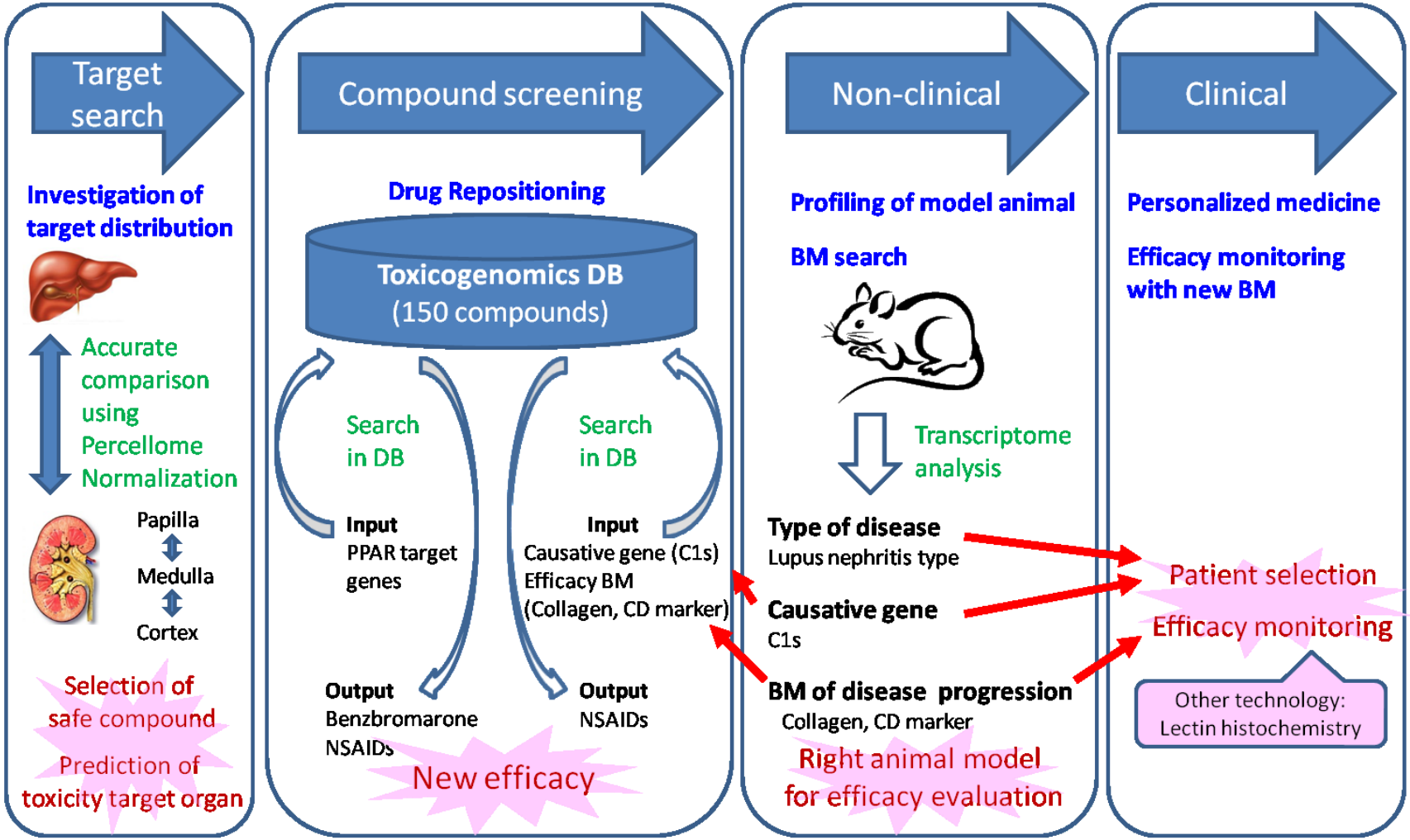

Fig. GD-1.
Techniques and usage of transcriptome analysis for improving the productivity of medical product R&D

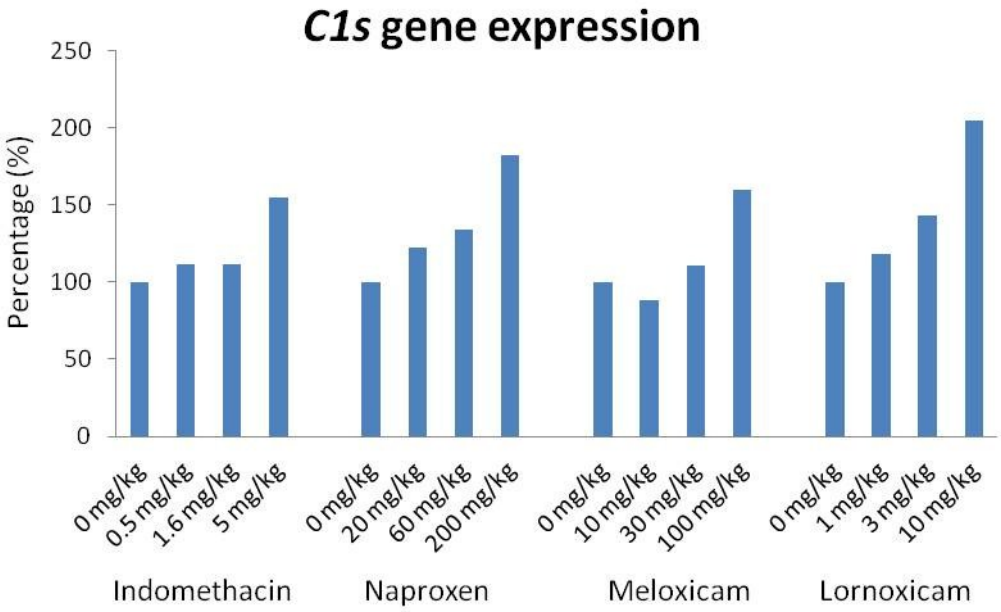

Fig. GD-2.

Expression level of *C1s* gene in rats after 4-day repeated dosing of indomethacin, naproxen, Meloxicam or lornoxicam. The data was extracted from the national toxicogenomics database (TG-GATEs).

References

Amano, M.T., Ferriani, V.P., Florido, M.P., Reis, E.S., Delcolli, M.I., Azzolini, A.E., Assis-Pandochi, A.I., Sjoholm, A.G., Farah, C.S., Jensenius, J.C., *et al.* (2008). Genetic analysis of complement C1s deficiency associated with systemic lupus erythematosus highlights alternative splicing of normal C1s gene. Mol Immunol *45*, 1693-1702.

Arab, M.R., Salari, S., Karimi, M., and Mofidpour, H. (2010). Lectin histochemical study of cell surface glycoconjugate in gastric carcinoma using helix pomatia agglutinin. Acta Med Iran *48*, 209-213.

Ashburn, T.T., and Thor, K.B. (2004). Drug repositioning: identifying and developing new uses for existing drugs. Nat Rev Drug Discov *3*, 673-683.

Baltimore, D. (2001). Our genome unveiled. Nature *409*, 814-816.

Barrero, M.J., Camarero, N., Marrero, P.F., and Haro, D. (2003). Control of human carnitine palmitoyltransferase II gene transcription by peroxisome proliferator-activated receptor through a partially conserved peroxisome proliferator-responsive element. Biochem J *369*, 721-729.

Beers, C., Honey, K., Fink, S., Forbush, K., and Rudensky, A. (2003). Differential regulation of cathepsin S and cathepsin L in interferon gamma-treated macrophages. J Exp Med *197*, 169-179.

Bichet, N., Cahard, D., Fabre, G., Remandet, B., Gouy, D., and Cano, J.P. (1990). Toxicological studies on a benzofuran derivative. III. Comparison of peroxisome proliferation in rat and human hepatocytes in primary culture. Toxicol Appl Pharmacol *106*, 509-517.

Bienaime, F., Quartier, P., Dragon-Durey, M.A., Fremeaux-Bacchi, V., Bader-Meunier, B., Patey, N., Salomon, R., and Noel, L.H. (2010). Lupus nephritis associated with complete C1s deficiency efficiently treated with rituximab: a case report. Arthritis Care Res (Hoboken) *62*, 1346-1350.

Boitier, E., Gautier, J.C., and Roberts, R. (2003). Advances in understanding the regulation of apoptosis and mitosis by peroxisome-proliferator activated receptors in non-clinical models: relevance for human health and disease. Comp Hepatol *2*, 3.

Bradford, M.M. (1976). A rapid and sensitive method for the quantitation of microgram quantities of protein utilizing the principle of protein-dye binding. Anal Biochem *72*, 248-254.

Brandt, J.M., Djouadi, F., and Kelly, D.P. (1998). Fatty acids activate transcription of the muscle carnitine palmitoyltransferase I gene in cardiac myocytes via the peroxisome proliferator-activated receptor alpha. J Biol Chem *273*, 23786-23792.

Brumell, J.H., Howard, J.C., Craig, K., Grinstein, S., Schreiber, A.D., and Tyers, M. (1999). Expression of the protein kinase C substrate pleckstrin in macrophages: association with phagosomal membranes. J Immunol *163*, 3388-3395.

Castelein, H., Gulick, T., Declercq, P.E., Mannaerts, G.P., Moore, D.D., and Baes, M.I. (1994). The peroxisome proliferator activated receptor regulates malic enzyme gene expression. J Biol Chem *269*, 26754-26758.

Cho, A.R., Uchio-Yamada, K., Torigai, T., Miyamoto, T., Miyoshi, I., Matsuda, J., Kurosawa, T., Kon, Y., Asano, A., Sasaki, N.*, et al.* (2006). Deficiency of the tensin2 gene in the ICGN mouse: an animal model for congenital nephrotic syndrome. Mamm Genome *17*, 407-416.

Chong, C.R., and Sullivan, D.J., Jr. (2007). New uses for old drugs. Nature *448*, 645-646.

Corton, J.C., Fan, L.Q., Brown, S., Anderson, S.P., Bocos, C., Cattley, R.C., Mode, A., and Gustafsson, J.A. (1998). Down-regulation of cytochrome P450 2C family members and positive acute-phase response gene expression by peroxisome proliferator chemicals. Mol Pharmacol *54*, 463-473.

Decker, K. (1990). Biologically active products of stimulated liver macrophages (Kupffer cells). Eur J Biochem *192*, 245-261.

Degrandi, D., Konermann, C., Beuter-Gunia, C., Kresse, A., Wurthner, J., Kurig, S., Beer, S., and Pfeffer, K. (2007). Extensive characterization of IFN-induced GTPases mGBP1 to mGBP10 involved in host defense. J Immunol *179*, 7729-7740.

de Melo-Junior, M.R., de Lima-Neto, R.G., Lacerda, A.M., and Beltrao, E.I. (2011). Comparative analysis of extracellular matrix and cellular carbohydrate expression in the sporotrichosis and chromoblastomycosis. Mycopathologia *171*, 403-409.

DiMasi, J.A., Hansen, R.W., and Grabowski, H.G. (2003). The price of innovation: new estimates of drug development costs. J Health Econ *22*, 151-185.

Dragon-Durey, M.A., Quartier, P., Fremeaux-Bacchi, V., Blouin, J., de Barace, C., Prieur, A.M., Weiss, L., and Fridman, W.H. (2001). Molecular basis of a selective C1s deficiency associated with early onset multiple autoimmune diseases. J Immunol *166*, 7612-7616.

Echevarria, M., Windhager, E.E., Tate, S.S., and Frindt, G. (1994). Cloning and expression of AQP3, a water channel from the medullary collecting duct of rat kidney. Proc Natl Acad Sci U S A *91*, 10997-11001.

Fernandez-Suarez, X.M., and Galperin, M.Y. (2013). The 2013 Nucleic Acids Research Database Issue and the online molecular biology database collection. Nucleic Acids Res *41*, D1-7.

Gatsios, P., Haubeck, H.D., Van de Leur, E., Frisch, W., Apte, S.S., Greiling, H., Heinrich, P.C., and Graeve, L. (1996). Oncostatin M differentially regulates tissue inhibitors of metalloproteinases TIMP-1 and TIMP-3 gene expression in human synovial lining cells. Eur J Biochem *241*, 56-63.

Gervois, P., Vu-Dac, N., Kleemann, R., Kockx, M., Dubois, G., Laine, B., Kosykh, V., Fruchart, J.C., Kooistra, T., and Staels, B. (2001). Negative regulation of human fibrinogen gene expression by peroxisome proliferator-activated receptor alpha agonists via inhibition of CCAAT box/enhancer-binding protein beta. J Biol Chem *276*, 33471-33477.

Gu, S., Villegas, C.J., and Jiang, J.X. (2005). Differential regulation of amino acid transporter SNAT3 by insulin in hepatocytes. J Biol Chem *280*, 26055-26062.

Harris, R.C., McKanna, J.A., Akai, Y., Jacobson, H.R., Dubois, R.N., and Breyer, M.D. (1994). Cyclooxygenase-2 is associated with the macula densa of rat kidney and increases with salt restriction. J Clin Invest *94*, 2504-2510.

Hawkins, N.J., Ward, R.L., and Wakefield, D. (1994). Cytokine-mediated induction of HLA antigen expression on human glomerular mesangial cells. Cell Immunol *155*, 493-500.

Horie, S., and Suga, T. (1985). Enhancement of peroxisomal beta-oxidation in the liver of rats and mice treated with valproic acid. Biochem Pharmacol *34*, 1357-1362.

Hsu, S.M., and Raine, L. (1982). Versatility of biotin-labeled lectins and avidin-biotin-peroxidase complex for localization of carbohydrate in tissue sections. J Histochem Cytochem *30*, 157-161.

Ibarra, F., Crambert, S., Eklof, A.C., Lundquist, A., Hansell, P., and Holtback, U. (2005). Prolactin, a natriuretic hormone, interacting with the renal dopamine system. Kidney Int *68*, 1700-1707.

Ichimura, T., Bonventre, J.V., Bailly, V., Wei, H., Hession, C.A., Cate, R.L., and Sanicola, M. (1998). Kidney injury molecule-1 (KIM-1), a putative epithelial cell adhesion molecule containing a novel immunoglobulin domain, is up-regulated in renal cells after injury. J Biol Chem *273*, 4135-4142.

Ikeda, M., Minota, S., and Kano, S. (1997). Regulation of MHC class I expression by inflammatory cytokines in rat mesangial cells. Nephron *76*, 90-95.

Inoue, N., Saito, T., Masuda, R., Suzuki, Y., Ohtomi, M., and Sakiyama, H. (1998). Selective complement C1s deficiency caused by homozygous four-base deletion in the C1s gene. Hum Genet *103*, 415-418.

Jo, I., Nielsen, S., and Harris, H.W. (1997). The 17 kDa band identified by multiple anti-aquaporin 2 antisera in rat kidney medulla is a histone. Biochim Biophys Acta *1324*, 91-101.

Kamijo, Y., Hora, K., Kono, K., Takahashi, K., Higuchi, M., Ehara, T., Kiyosawa, K., Shigematsu, H., Gonzalez, F.J., and Aoyama, T. (2007a). PPARalpha protects proximal tubular cells from acute fatty acid toxicity. J Am Soc Nephrol *18*, 3089-3100.

Kamijo, Y., Hora, K., Nakajima, T., Kono, K., Takahashi, K., Ito, Y., Higuchi, M., Kiyosawa, K., Shigematsu, H., Gonzalez, F.J.*, et al.* (2007b). Peroxisome proliferator-activated receptor alpha protects against glomerulonephritis induced by long-term exposure to the plasticizer di-(2-ethylhexyl)phthalate. J Am Soc Nephrol *18*, 176-188.

Kamijo, Y., Hora, K., Tanaka, N., Usuda, N., Kiyosawa, K., Nakajima, T., Gonzalez, F.J., and Aoyama, T. (2002). Identification of functions of peroxisome proliferator-activated receptor alpha in proximal tubules. J Am Soc Nephrol *13*, 1691-1702.

Kanno, J., Aisaki, K., Igarashi, K., Nakatsu, N., Ono, A., Kodama, Y., and Nagao, T. (2006). "Per cell" normalization method for mRNA measurement by quantitative PCR and microarrays. BMC Genomics *7*, 64.

Karakashian, A., Timmer, R.T., Klein, J.D., Gunn, R.B., Sands, J.M., and Bagnasco, S.M. (1999). Cloning and characterization of two new isoforms of the rat kidney urea transporter: UT-A3 and UT-A4. J Am Soc Nephrol *10*, 230-237.

Kavanaugh, A.F., and Solomon, D.H. (2002). Guidelines for immunologic laboratory testing in the rheumatic diseases: anti-DNA antibody tests. Arthritis Rheum *47*, 546-555.

Kimura, Y., Manabe, N., Nishihara, S., Matsushita, H., Tajima, C., Wada, S., and Miyamoto, H. (1999). Up-regulation of the alpha2,6-sialyltransferase messenger ribonucleic acid increases glycoconjugates containing alpha2, 6-linked sialic acid residues in granulosa cells during follicular atresia of porcine ovaries. Biol Reprod *60*, 1475-1482.

Kockx, M., Gervois, P.P., Poulain, P., Derudas, B., Peters, J.M., Gonzalez, F.J., Princen, H.M., Kooistra, T., and Staels, B. (1999). Fibrates suppress fibrinogen gene expression in rodents via activation of the peroxisome proliferator-activated receptor-alpha. Blood *93*, 2991-2998.

Kono, K., Kamijo, Y., Hora, K., Takahashi, K., Higuchi, M., Kiyosawa, K., Shigematsu, H., Gonzalez, F.J., and Aoyama, T. (2009). PPAR{alpha} attenuates the proinflammatory response in activated mesangial cells. Am J Physiol Renal Physiol *296*, F328-336.

Korzus, E., Nagase, H., Rydell, R., and Travis, J. (1997). The mitogen-activated protein kinase and JAK-STAT signaling pathways are required for an oncostatin M-responsive element-mediated activation of matrix metalloproteinase 1 gene expression. J Biol Chem *272*, 1188-1196.

Kuroki, T., Kubota, A., Miki, Y., Yamamura, T., and Utsunomiya, J. (1991). Lectin staining of neoplastic and normal background colorectal mucosa in nonpolyposis and polyposis patients. Dis Colon Rectum *34*, 679-684.

Lee, E.G., Boone, D.L., Chai, S., Libby, S.L., Chien, M., Lodolce, J.P., and Ma, A. (2000). Failure to regulate TNF-induced NF-kappaB and cell death responses in A20-deficient mice. Science *289*, 2350-2354.

Lehmann, J.M., Lenhard, J.M., Oliver, B.B., Ringold, G.M., and Kliewer, S.A. (1997). Peroxisome proliferator-activated receptors alpha and gamma are activated by indomethacin and other non-steroidal anti-inflammatory drugs. Journal of Biological

Chemistry *272*, 3406-3410.

Li, S., Mo, C., Peng, Q., Kang, X., Sun, C., Jiang, K., Huang, L., Lu, Y., Sui, J., Qin, X.*, et al.* (2013). Cell surface glycan alterations in epithelial mesenchymal transition process of huh7 hepatocellular carcinoma cell. PLoS One *8*, e71273.

Li, W.Q., and Zafarullah, M. (1998). Oncostatin M up-regulates tissue inhibitor of metalloproteinases-3 gene expression in articular chondrocytes via de novo transcription, protein synthesis, and tyrosine kinase- and mitogen-activated protein kinase-dependent mechanisms. J Immunol *161*, 5000-5007.

Lis, H., and Sharon, N. (1986). Lectins as molecules and as tools. Annu Rev Biochem *55*, 35-67.

Londhe, P., and Davie, J.K. (2011). Gamma Interferon Modulates Myogenesis through the Major Histocompatibility Complex Class II Transactivator, CIITA. Molecular and Cellular Biology *31*, 2854-2866.

Maeda, K., Okubo, K., Shimomura, I., Funahashi, T., Matsuzawa, Y., and Matsubara, K. (1996). cDNA cloning and expression of a novel adipose specific collagen-like factor, apM1 (AdiPose Most abundant Gene transcript 1). Biochem Biophys Res Commun *221*, 286-289.

Manabe, N., Chevallier, M., Chossegros, P., Causse, X., Guerret, S., Trepo, C., and Grimaud, J.A. (1993). Interferon-alpha 2b therapy reduces liver fibrosis in chronic non-A, non-B hepatitis: a quantitative histological evaluation. Hepatology *18*, 1344-1349.

Manabe, N., Furuya, Y., Nagano, N., and Miyamoto, H. (1994). Immunohistochemical microquantitation method for type I collagen in kidney histological section of the rats. J Vet Med Sci *56*, 147-150.

Manabe, N., Furuya, Y., Nagano, N., Yagi, M., Kuramitsu, K., and Miyamoto, H. (1995). Immunohistochemical quantitation for extracellular matrix proteins in rats with glomerulonephritis induced by monoclonal anti-Thy-1.1 antibody. Nephron *71*, 79-86.

Maxwell, P.H., Ferguson, D.J., Nicholls, L.G., Iredale, J.P., Pugh, C.W., Johnson, M.H., and Ratcliffe, P.J. (1997). Sites of erythropoietin production. Kidney Int *51*, 393-401.

Mazumder, B., Mukhopadhyay, C.K., Prok, A., Cathcart, M.K., and Fox, P.L. (1997).

Induction of ceruloplasmin synthesis by IFN-gamma in human monocytic cells. J Immunol *159*, 1938-1944.

McGowan, S.E., Jackson, S.K., Doro, M.M., and Olson, P.J. (1997). Peroxisome proliferators alter lipid acquisition and elastin gene expression in neonatal rat lung fibroblasts. Am J Physiol *273*, L1249-1257.

Michalik, L., Desvergne, B., and Wahli, W. (2004). Peroxisome-proliferator-activated receptors and cancers: complex stories. Nat Rev Cancer *4*, 61-70.

Miyamoto, M., Manabe, N., Kuramitsu, K., Kuribayashi, Y., Tamura, K., Furuya, Y., Nagano, N., Fukumoto, M., and Miyamoto, H. (1997). Lectin histochemistry in rat liver fibrosis induced by heterologous serum sensitization. J Vet Med Sci *59*, 681-687.

Miyamoto, M., Manabe, N., Uchio, K., Kuramitsu, K., Tamura, K., Furuya, Y., Nagano, N., and Miyamoto, H. (1998). Characteristics of lectin staining patterns assessed by a modified sensitive thermo-method in rat livers with heterologous serum-induced fibrosis. J Vet Med Sci *60*, 953-960.

Mizuno, S., Horikawa, Y., Okamoto, M., and Kurosawa, T. (1998a). Preventive effect of ACE inhibitor on interstitial myofibroblast formation and matrix deposition in a nephrotic model. Ren Fail *20*, 481-491.

Mizuno, S., Kurosawa, T., Matsumoto, K., Mizuno-Horikawa, Y., Okamoto, M., and Nakamura, T. (1998b). Hepatocyte growth factor prevents renal fibrosis and dysfunction in a mouse model of chronic renal disease. J Clin Invest *101*, 1827-1834.

Mizuno, S., Mizuno-Horikawa, Y., Yue, B.F., Okamoto, M., and Kurosawa, T. (1999). Nephrotic mice (ICGN strain): a model of diffuse mesangial sclerosis in infantile nephrotic syndrome. Am J Nephrol *19*, 73-82.

Mizuno, S., Yue, B.F., Okamoto, M., Horikawa, Y., and Kurosawa, T. (1997). Diffuse glomerulosclerosis without tubular injury does not directly manifest renal dysfunction in nephrotic mice (ICGN strain). Exp Nephrol *5*, 498-507.

Modur, V., Feldhaus, M.J., Weyrich, A.S., Jicha, D.L., Prescott, S.M., Zimmerman, G.A., and McIntyre, T.M. (1997). Oncostatin M is a proinflammatory mediator. In vivo effects correlate with endothelial cell expression of inflammatory cytokines and adhesion molecules. J Clin Invest *100*, 158-168.

Mullard, A. (2011). 2010 FDA drug approvals. Nat Rev Drug Discov *10*, 82-85.

Muramatsu, T. (1988). Alterations of cell-surface carbohydrates during differentiation and development. Biochimie *70*, 1587-1596.

Murphy, L.A., and Goldstein, I.J. (1977). Five alpha-D-galactopyranosyl-binding isolectins from Bandeiraea simplicifolia seeds. J Biol Chem *252*, 4739-4742.

Nakamura, T., Ebihara, I., Tomino, Y., and Koide, H. (1995). Effect of a specific endothelin A receptor antagonist on murine lupus nephritis. Kidney Int *47*, 481-489.

Nejsum, L.N., Elkjaer, M., Hager, H., Frokiaer, J., Kwon, T.H., and Nielsen, S. (2000). Localization of aquaporin-7 in rat and mouse kidney using RT-PCR, immunoblotting, and immunocytochemistry. Biochem Biophys Res Commun *277*, 164-170.

Nishino, T., Sasaki, N., Nagasaki, K., Ahmad, Z., and Agui, T. (2010). Genetic background strongly influences the severity of glomerulosclerosis in mice. J Vet Med Sci *72*, 1313-1318.

Nishino, T., Sasaki, N., Nagasaki, K., Ichii, O., Kon, Y., and Agui, T. (2012). The 129 genetic background affects susceptibility to glomerulosclerosis in tensin2-deficient mice. Biomed Res *33*, 53-56.

Ogata, T., Miyauchi, T., Irukayama-Tomobe, Y., Takanashi, M., Goto, K., and Yamaguchi, I. (2004). The peroxisome proliferator-activated receptor alpha activator fenofibrate inhibits endothelin-1-induced cardiac fibroblast proliferation. J Cardiovasc Pharmacol *44 Suppl 1*, S279-282.

Ogata, T., Miyauchi, T., Sakai, S., Irukayama-Tomobe, Y., Goto, K., and Yamaguchi, I. (2002). Stimulation of peroxisome-proliferator-activated receptor alpha (PPAR alpha) attenuates cardiac fibrosis and endothelin-1 production in pressure-overloaded rat hearts. Clin Sci (Lond) *103 Suppl 48*, 284S-288S.

Ogura, A., Asano, T., Matsuda, J., and Fujimura, H. (1991). Evolution of glomerular lesions in nephrotic ICGN mice: serial biopsy study with electron microscopy. J Vet Med Sci *53*, 513-515.

Ogura, A., Asano, T., Matsuda, J., Koura, M., Nakagawa, M., Kawaguchi, H., and Yamaguchi, Y. (1990). An electron microscopic study of glomerular lesions in hereditary nephrotic mice (ICGN strain). Virchows Arch A Pathol Anat Histopathol

417, 223-228.

Ogura, A., Asano, T., Matsuda, J., Noguchi, Y., Yamamoto, Y., Takano, K., and Nakagawa, M. (1989a). Development of nephrotic ICGN mice--the origin, reproductive ability, and incidence of glomerulonephritis. Jikken Dobutsu *38*, 349-352.

Ogura, A., Asano, T., Matsuda, J., Takano, K., Nakagawa, M., and Fukui, M. (1989b). Characteristics of mutant mice (ICGN) with spontaneous renal lesions: a new model for human nephrotic syndrome. Lab Anim *23*, 169-174.

Ogura, A., Asano, T., Suzuki, O., Yamamoto, Y., Noguchi, Y., Kawaguchi, H., and Yamaguchi, Y. (1994). Hereditary nephrotic syndrome with progression to renal failure in a mouse model (ICGN strain): clinical study. Nephron *68*, 239-244.

Ogura, A., Fujimura, H., Asano, T., Koura, M., Naito, I., and Kobayashi, Y. (1995). Early ultrastructural glomerular alterations in neonatal nephrotic mice (ICGN strain). Vet Pathol *32*, 321-323.

Ohno, Y., Urushidani, T. (2012). Final Business Report of Toxicogenomics Informatics Project. Volume I, 207-220.(Written in Japanese)

Okamoto, M., Yokoi, N., Serikawa, T., Tajima, M., and Kurosawa, T. (2001). Linkage mapping of the mouse nephrosis (nep) gene to chromosome 15. J Vet Med Sci *63*, 1347-1350.

Parzefall, W., Berger, W., Kainzbauer, E., Teufelhofer, O., Schulte-Hermann, R., and Thurman, R.G. (2001). Peroxisome proliferators do not increase DNA synthesis in purified rat hepatocytes. Carcinogenesis *22*, 519-523.

Peters, B.P., and Goldstein, I.J. (1979). The use of fluorescein-conjugated Bandeiraea simplicifolia B4-isolectin as a histochemical reagent for the detection of alpha-D-galactopyranosyl groups. Their occurrence in basement membranes. Exp Cell Res *120*, 321-334.

PricewaterhouseCoopers. (2012). From vision to decision – Pharma 2020. http://www.pwc.com/gx/en/pharma-life-sciences/pharma2020/vision-to-decision.jhtml

Raij, L., Azar, S., and Keane, W. (1984). Mesangial immune injury, hypertension, and progressive glomerular damage in Dahl rats. Kidney Int *26*, 137-143.

Rego, M.J., Vieira-De-Mello, G.S., Araujo, C.W., Cavalcanti Mdo, S., and Beltrao, E.I. (2013). Evaluation of WGA and Concanavalin A (Con A) lectin as biomarkers of hepatosplenic schistosomiasis in human biopsies with no evidence of egg-granuloma system. Rev Inst Med Trop Sao Paulo *55*.

Rohn, W.M., Lee, Y.J., and Benveniste, E.N. (1996). Regulation of class II MHC expression. Crit Rev Immunol *16*, 311-330.

Rolfe, M., James, N.H., and Roberts, R.A. (1997). Tumour necrosis factor alpha (TNF alpha) suppresses apoptosis and induces DNA synthesis in rodent hepatocytes: a mediator of the hepatocarcinogenicity of peroxisome proliferators? Carcinogenesis *18*, 2277-2280.

Rose, M.L., Germolec, D.R., Schoonhoven, R., and Thurman, R.G. (1997). Kupffer cells are causally responsible for the mitogenic effect of peroxisome proliferators. Carcinogenesis *18*, 1453-1456.

Ruan, Y., Le Ber, P., Ng, H.H., and Liu, E.T. (2004). Interrogating the transcriptome. Trends Biotechnol *22*, 23-30.

Rubio, N., and Torres, C. (1999). Interferon-gamma induces proliferation but not apoptosis in murine astrocytes through the differential expression of the myc proto-oncogene family. Brain Res Mol Brain Res *71*, 104-110.

Sasaki, D., Yamada, A., Umeno, H., Kurihara, H., Nakatsuji, S., Fujihira, S., Tsubota, K., Ono, M., Moriguchi, A., Watanabe, K.*, et al.* (2011). Comparison of the course of biomarker changes and kidney injury in a rat model of drug-induced acute kidney injury. Biomarkers *16*, 553-566.

Schnellmann, R.G. (2001): Toxic responses of the kidney. In Casarett & Doull's Toxicology, 6th ed.(Klaassen, C.D., ed.), pp.491-514. McGraw-Hill.

Segerer, S., Mac, K.M., Regele, H., Kerjaschki, D., and Schlondorff, D. (1999). Expression of the C-C chemokine receptor 5 in human kidney diseases. Kidney Int *56*, 52-64.

Shih, W., Hines, W.H., and Neilson, E.G. (1988). Effects of cyclosporin A on the development of immune-mediated interstitial nephritis. Kidney Int *33*, 1113-1118.

Snedecor, G.W. and Cochran, W.G. (1989): Statistical Methods, 8th ed., Iowa State

University Press.

Suter, L., Babiss, L.E., and Wheeldon, E.B. (2004). Toxicogenomics in predictive toxicology in drug development. Chem Biol *11*, 161-171.

Suzuki, Y., Ogura, Y., Otsubo, O., Akagi, K., and Fujita, T. (1992). Selective deficiency of C1s associated with a systemic lupus erythematosus-like syndrome. Report of a case. Arthritis Rheum *35*, 576-579.

Tamura, S., Morikawa, Y., Tanaka, M., Miyajima, A., and Senba, E. (2002). Developmental expression pattern of oncostatin M receptor beta in mice. Mech Dev *115*, 127-131.

Tanaka, Y., Nouchi, T., Yamane, M., Irie, T., Miyakawa, H., Sato, C., and Marumo, F. (1991). Phenotypic modulation in lipocytes in experimental liver fibrosis. J Pathol *164*, 273-278.

Tang, C., Cho, H.P., Nakamura, M.T., and Clarke, S.D. (2003). Regulation of human delta-6 desaturase gene transcription: identification of a functional direct repeat-1 element. J Lipid Res *44*, 686-695.

Tatsumi, H., Satoh, S., Okamoto, M., Nakamura, M., Asano, T., and Kurosawa, T. (1995). Morphological studies on the kidney of the spontaneous nephrotic (ICGN) mice in the late stage. Kaibogaku Zasshi *70*, 96-106.

Teramoto, K., Negoro, N., Kitamoto, K., Iwai, T., Iwao, H., Okamura, M., and Miura, K. (2008). Microarray analysis of glomerular gene expression in murine lupus nephritis. J Pharmacol Sci *106*, 56-67.

Tucker-Burden, C., Chappa, P., Krishnamoorthy, M., Gerwe, B.A., Scharer, C.D., Heimburg-Molinaro, J., Harris, W., Usta, S.N., Eilertson, C.D., Hadjipanayis, C.G*., et al.* (2012). Lectins identify glycan biomarkers on glioblastoma-derived cancer stem cells. Stem Cells Dev *21*, 2374-2386.

Tugwood, J.D., Issemann, I., Anderson, R.G., Bundell, K.R., McPheat, W.L., and Green, S. (1992). The mouse peroxisome proliferator activated receptor recognizes a response element in the 5' flanking sequence of the rat acyl CoA oxidase gene. EMBO J *11*, 433-439.

Uchio-Yamada, K., Manabe, N., Goto, Y., Anann, S., Yamamoto, Y., Takano, K., Ogura,

A., and Matsuda, J. (2005). Decreased expression of matrix metalloproteinases and tissue inhibitors of metalloproteinase in the kidneys of hereditary nephrotic (ICGN) mice. J Vet Med Sci *67*, 35-41.

Uchio-Yamada, K., Manabe, N., Yamaguchi, M., Akashi, N., Goto, Y., Yamamoto, Y., Ogura, A., and Miyamoto, H. (2001). Localization of extracellular matrix receptors in ICGN mice, a strain of mice with hereditary nephrotic syndrome. J Vet Med Sci *63*, 1171-1178.

Uchio, K., Manabe, N., Kinoshita, A., Tamura, K., Miyamoto, M., Ogura, A., Yamamoto, Y., and Miyamoto, H. (1999). Abnormalities of extracellular matrices and transforming growth factor beta1 localization in the kidney of the hereditary nephrotic mice (ICGN strain). J Vet Med Sci *61*, 769-776.

Uchio, K., Manabe, N., Tamura, K., Miyamoto, M., Yamaguchi, M., Ogura, A., Yamamoto, Y., and Miyamoto, H. (2000). Decreased matrix metalloproteinase activity in the kidneys of hereditary nephrotic mice (ICGN strain). Nephron *86*, 145-151.

Uchio, K., Sawada, K., and Manabe, N. (2009). Expression of macrophage metalloelastase (MMP-12) in podocytes of hereditary nephrotic mice (ICGN strain). J Vet Med Sci *71*, 305-312.

Urushidani, T. and Nagao, T. (2005): Toxicogenomics: The Japanese initiative. In Handbook of Toxicogenomics - Strategies and Applications (Borlak, J., ed.), pp. 623-631. Wiley - VCH.

U.S. Department of Health and Human Services, Food and Drug Administration. (2004). Innovation or Stagnation: Challenge and Opportunity on the Critical Path to New Medical Products
http://www.fda.gov/ScienceResearch/SpecialTopics/CriticalPathInitiative/CriticalPathOpportunitiesReports/ucm077262.htm

U.S. Department of Health and Human Services, Food and Drug Administration. (2006a). Innovation or Stagnation: Critical Path Opportunities List.
http://www.fda.gov/downloads/scienceresearch/specialtopics/criticalpathinitiative/criticalpathopportunitiesreports/UCM077258.pdf

U.S. Department of Health and Human Services, Food and Drug Administration. (2006b). Innovation or Stagnation: Critical Path Opportunities Report.
http://www.fda.gov/downloads/ScienceResearch/SpecialTopics/CriticalPathInitiative/C

riticalPathOpportunitiesReports/UCM077254.pdf

van de Water, B., de Graauw, M., Le Devedec, S., and Alderliesten, M. (2006). Cellular stress responses and molecular mechanisms of nephrotoxicity. Toxicol Lett *162*, 83-93.

Venter, J.C., Adams, M.D., Myers, E.W., Li, P.W., Mural, R.J., Sutton, G.G., Smith, H.O., Yandell, M., Evans, C.A., Holt, R.A.*, et al.* (2001). The sequence of the human genome. Science *291*, 1304-1351.

Wallace, P.M., MacMaster, J.F., Rouleau, K.A., Brown, T.J., Loy, J.K., Donaldson, K.L., and Wahl, A.F. (1999). Regulation of inflammatory responses by oncostatin M. J Immunol *162*, 5547-5555.

Walport, M.J. (2001a). Complement. First of two parts. N Engl J Med *344*, 1058-1066.

Walport, M.J. (2001b). Complement. Second of two parts. N Engl J Med *344*, 1140-1144.

Walport, M.J., and Davies, K.A. (1996). Complement and immune complexes. Res Immunol *147*, 103-109.

Weigt, C., Gaertner, A., Wegner, A., Korte, H., and Meyer, H.E. (1992). Occurrence of an actin-inserting domain in tensin. J Mol Biol *227*, 593-595.

Xiong, W., Chao, L., and Chao, J. (1989). Renal kallikrein mRNA localization by in situ hybridization. Kidney Int *35*, 1324-1329.

Yamamoto, K., Makino, Y., Yoshioka, T., Kobashi, H., Tomita, M., and Tsuji, T. (1992). Quantitative analysis of activated Kupffer cells in viral hepatitis: application of computer image analysis for lectin histochemistry. Liver *12*, 199-204.

Yonezawa, S., Irisa, S., Nakamura, T., Uemura, S., Otsuji, Y., Ohi, Y., and Sato, E. (1983a). Deposition of alpha 1-antitrypsin and loss of glycoconjugate carrying Ulex europaeus agglutinin-I binding sites in the glomerular sclerotic process. Phenomena common to chronic pyelonephritis and chronic diffuse proliferative glomerulonephritis. Nephron *33*, 38-43.

Yonezawa, S., Nakamura, T., Irisa, S., Otsuji, Y., and Sato, E. (1983b). Ulex europaeus agglutinin I staining of human glomerular lesions using a highly sensitive immunoperoxidase method in paraffin sections. Nephron *35*, 187-189.

Yonezawa, S., Shibata, M., Shimizu, T., Nakamura, T., and Sato, E. (1986). Griffonia simplicifolia I-A4 staining of mice glomerular tufts and its alteration in diabetic mice. Acta Pathol Jpn *36*, 1653-1658.

Acknowledgement

本論文作成にあたり，多大なる御指導と御鞭撻を賜りました東京大学大学院農学生命科学研究科高等動物教育研究センター（付属牧場）眞鍋昇教授に謹んで感謝の意を表し，厚く御礼申し上げます。

本論文の研究を遂行するにあたり懇切なる御指導と御鞭撻を賜りました同志社女子大学薬学部　漆谷徹郎教授，国立医薬品食品衛生研究所安全性生物試験研究センター　小野敦博士，東京理科大学薬学部 DDS 研究センター　宮城島利一博士，並びに長尾拓博士に深く感謝致します。

本論文の研究において，有益な御助言と御援助を頂きましたアステラス製薬株式会社安全性研究所　能登貴久博士，西原久美子博士，並びにアステラスリサーチテクノロジー株式会社安全性研究部中野健二氏に深く感謝致します。

本研究を遂行し，本論文を作成する機会を与えて下さり，御理解と御鞭撻を賜りましたアステラス製薬株式会社研究本部長　塚本紳一博士，同安全性研究所長　宮前陽一博士，同安全性研究所　関二郎博士，宇波明博士，廣田里香博士，並びに同薬事部　渡部浩治博士に深く感謝致します。

本研究の遂行に理解を示し，暖かく見守って下さったアステラス製薬株式会社安全性研究所分子毒性室の皆様に深く感謝致します。

最後に，研究の道へ進む機会を与えてくれた父 秀三郎，母 和子，著者の良き理解者であり,長年にわたり研究を支えてくれた妻 真由子に心から感謝致します。